TÉCNICO LISBOA

A Sensor Based on Nanoantennas

Ricardo Alexandre Marques Lameirinhas

Thesis to obtain the Master of Science Degree in

Electrical and Computer Engineering

Supervisors: Professor João Paulo Neto Torres
Professor António Carlos De Campos Simões Baptista

Examination Committee

Chairperson: Professor Francisco André Corrêa Alegria
Supervisor: Professor João Paulo Neto Torres
Member of the Committee: Professor Carlos Alberto Ferreira Fernandes

June 2020

I declare that this document is an original work of my own authorship and that it fulfills all the requirements of the Code of Conduct and Good Practices of the Universidade de Lisboa.

Declaro que o presente documento é um trabalho original da minha autoria e que cumpre todos os requisitos do Código de Conduta e Boas Práticas da Universidade de Lisboa.

First of all, I would like to express my most sincere thanks to all the people who helped me on my university journey in Instituto Superior Técnico.

To all the professors, who with their own knowledge and experience, allow my scientific evolution and progress. Specially to professor João Torres and to professor António Baptista, not only for their guidance, advice and support, but also for all the opportunities given to me, during all my academic course. Their attitude makes possible the success of this work.

On the other hand, to my family and friends, those who always heard me about my difficulties and concerns and always had some advises in order to successfully overcome them. Specially to my mother and to my father, that every day support me on my choices, helping me on the bad ones and congratulating me on the good ones. Also, to my girlfriend, Mariana Maldonado, who always stood on my side, day every day, though the best and the worst moments. Without them, I would never be who I am.

Although it is impossible to express my gratitude merely in words, to all of them, a big *thank you...*

Abstract

Nanoscience and nanotechnology are emerging fields where new phenomena, applications and devices are being discovered and developed. In 1998, Ebbesen reported an extraordinary optical transmission - EOT -, when a beam of light was incident on a metallic film with a subwavelength hole array. He associated this behaviour with metal surface plasmon polaritons, and suggested that new devices, such as optical sensors, could be designed based on this phenomenon.

The surface plasmon-polaritons theory was the first theoretical approach to EOT. Subsequently, other approaches were developed to explain the EOT, namely the composite diffracted evanescent wave model - CDEW -. Both theories are presented and discussed, covering an important topic on the theoretical foundations.

Nanoantennas, which are structures that support EOT, can act as a sensor. Several nanoantennas structures were created and simulated, using the software *COMSOL Multiphysics*, proving EOT occurrence, verifying the surface plasmon-polaritons propagation, and the feasibility of developing optical sensors. Some experiences were done to verify how its parameters and topologies affect the output responses.

In the following, a sensor of temperature, as well as a sensor to differentiate cells and human tissues were simulated. Regarding their results, we concluded that nanoantennas could be an essential part of sensors to detect events or changes in different environments.

Keywords

Nanoantennas; Optoelectronic devices; Sensors; Subwavelength structures; Surface plasmons polaritons.

Resumo

As nanociências e nanotecnologias são áreas emergentes onde novos fenómenos, aplicações e dispositivos foram descobertos e desenvolvidos recentemente. Em 1998, Ebbesen reportou a descoberta da transmissão ótica extraordinária, do inglês *extraordinary optical transmission* - EOT -, na qual um raio de luz incidia numa estrutura metálica de aberturas de diâmetro inferior ao comprimento de luz incidente. Ele associou este comportamento aos polaritões dos plamões superficiais, e sugeriu que novos dispositivos, como os sensores óticos, pudessem ser desenvolvidos tendo por base este fenómeno.

A teoria dos polaritões dos plasmões superficiais foi a primeira abordagem teórica ao EOT. Seguiram-se outras explicações que tentaram explicar este fenómeno, nomeadamente o modelo CDEW, do inglês *composite diffracted evanescent waves*. Ambas as teorias são apresentadas e discutidas, cobrindo os tópicos mais importantes dos fundamentos teóricos.

Nanoantenas, estruturas que suportam o EOT, podem funcionar como sensores. Várias destas estruturas foram criadas e simuladas utilizando o *software COMSOL Multiphysics*. Os resultados obtidos permitem provar a ocorrência do EOT, verificar a propagação dos polaritões dos plasmões superficiais e demonstrar a viabilidade do desenvolvimento de sensores óticos. Realizaram-se simulações para verificar como é que os parâmetros e a topologia da estrutura afetam a resposta destes dispositivos.

Neste trabalho, é simulado o funcionamento de estruturas como sensores de temperatura e como sensores que permitem a deteção e diferenciação de células e tecidos do corpo humano. Com base nos resultados obtidos, é possível concluir que as nanoantenas podem ser partes essenciais de sensores que permitem detetar alterações ou eventos em diferentes ambientes.

Palavras Chave

Dispositivos ópticos; Nano-antenas; Nano-estruturas; Polaritões dos plasmões superfíciais; Sensores.

Contents

List of Figures

Acronyms

CDEW Composite Diffracted Evanescent Waves Model

EOT Extraordinary Optical Transmission

LASER Light Amplification by Stimulated Emission of Radiation

LED Light Emitter Diode

SPP Surface Plasmons Polaritons

Nomenclature

$\bar{\epsilon}$	Complex dielectric function
$\bar{n}$	Complex refractive index
ϵ'	Real part of the complex dielectric function
ϵ"	Imaginary part of the complex dielectric function
$\hat{z}$	Penetration depth
λ	Wavelength
λ_{max}	Maximum intensity peak wavelength
ω	Angular frequency
ω_p	Plasma angular frequency
$\bar{\boldsymbol{E}}$	Complex electric field vector
$\bar{\boldsymbol{H}}$	Complex magnetic field vector
$\bar{\boldsymbol{k}}$	Wavevector
$\bar{\boldsymbol{M}}$	Complex magnetic dipole vector
$\bar{\boldsymbol{P}}$	Complex electric dipole vector
$\bar{\boldsymbol{S}}$	Complex electromagnetic power vector
c	Velocity of light in the vacuum
L_x	Propagation length
f	Frequency
k	Wavevector norm (propagation purposes) or extinction factor (optical properties purposes)
n	Refractive index

1

Introduction

Contents

1.1 Motivation

In the last decades, a huge progress in electronics and photonics allowed the development of some new devices, with a large number of applications in the fields of energy, medicine, information, defence, environment and industry. Furthermore, in parallel with these technological developments, nanotechnology and nanoscience are emerging, which contributes to the miniaturization of these devices, such as medical, chemical or biological sensors, antennas for a communication system and components to photonic integrated circuits.

There is a high social and scientific recognition for those doing research or developing nanodevices and nanotechnologies. The evolution of nanotechnology has lead to the discovery of some new phenomena and to the development of new devices and applications. However, it is dependent on several factors, such as the improvement of computational methods and the nanostructures techniques of synthesis and fabrication.

Over the years, light behaviour and its interactions with matter are inducing curiosity to the scientific community, who is trying to understand these phenomena. One of these phenomena is the Extraordinary Optical Transmission - EOT -, which was discovered by Ebbesen in 1998. Ebbesen experimentally showed that a metallic array with nanoholes - which is called nanoarray or nanoantenna -, can support optical transmission resonances. As it is suggested by the phenomenon designation, in certain conditions these transmission resonances can lead to light amplification and confinement - allowing the devices' miniaturisation -. Even more, this phenomenon can not be predicted by classical theories.

In the same report, Ebbesen and his colleagues also advanced the hypothesis that surface plasmons were the main agents of this phenomenon, pointing out some evidence of it. Although over the years some models, as the Composite Diffracted Evanescent Waves - CDEW -, model have been proposed, it was verified that a theory that includes the propagation of Surface Plasmons Polaritons - SPP -, and of a creeping wave, is the most correct theory until these days, being the polaritons the main agents of EOT, at least for the visible spectral region.

Nowadays, EOT is used for many applications, using for example nanoantennas to exploit the aforementioned resonances. Depending on the characteristics of the material or content where the nanoantenna is placed on, the resonance behaviour is going to be different, which is the main principle to have a good sensor. This property is critical to the creation of medical, chemical or biological sensors, providing the ability to manipulate and amplify the fluorescent behaviour of some molecules. Therefore, analysis and studies about this kind of sensors, based on EOT and nanoantennas, are an attractive research theme. In this innovative research field, the sensors of the future are being developed for applications, in early detection of diseases or real-time checking of diseases and chemical tests.

1.2 Objectives

The main objectives of this master thesis are the modelling, simulation and design of a sensor based on nanoantennas. For these purposes the interaction between light and metallic surfaces with nano slits will be analysed. The development of the classical diffraction theories due to Bethe and Bouwkamp will be helpful to understand light propagation through subwavelength holes.

The design of the sensor demands the knowledge of the control, geometrical and electrical parameters of the sensor structure. To verify the influence of these parameters on the output response and to create the necessary nanostructures, *COMSOL Multiphysics* software was used to simulate their optical response. Moreover, considering this analysis, 3D structures of sensors based on nanoantennas were created and simulated.

1.3 Outline

This document is divided into six chapters. The first one is the introductory chapter 1, where the motivation is presented and the objectives are declared. Chapter 2 cover the theoretical review, starting with classical diffraction theories, going through the surface plasmon polaritons theory and the Drude-Lorentz model, as well as the Composite Diffraction Evanescent Wave (CDEW) model. On chapter 3, the state-of-art devices are presented as well as their fundamentals. On chapter 4 the created simulation environment is presented and the parameters study is performed in order to know their influence on the structure optical response. Using this study, structures are developed thinking in real applications as sensors, showing that it is possible to develop sensors based on nanoantennas on chapter 5, exemplifying two different applications. Finally, on chapter 6 the overall conclusions are taken and the some future work topics are pointed out.

2

Evolution of the Theoretical Foundations

Contents

2.1 Classical Diffraction Theories

2.1.1 Huygens' Principle and Young's Experiment

On the XVII century, Huygens proved that every unobstructed point of a wave front behaves as a punctual source of a new spherical wave with the same characteristics of the incident one [1,2]. In particular, for the case of a plane wave that has normal incidence to an array of slits, each slit behaves as a punctual source. As a result of that, after the array, there are as many waves as the number of slits. However, if necessary a more detailed analysis is possible, considering each slit as a combination of more than one punctual source [1,2].

One century later, Fresnel reformulated the Huygens' principle for a curve wave front, which is used to determine the near-field regime, since near the slits, the wave is not plane. The assumption of plane waves is only valid when the target and the array are enough distanced so that, $D \gg \lambda, a$ and the wave propagation can be analysed through geometrical optics methods [1].

In 1803, Thomas Young experimentally proved the wave characteristic of light by double slit experiments [1,2]. As illustrated on figure 2.1, light is normally incident on a perfect conductive plane where there are two slits of width a and spaced by d. Also, a target is placed in parallel with the plane distanced of D.

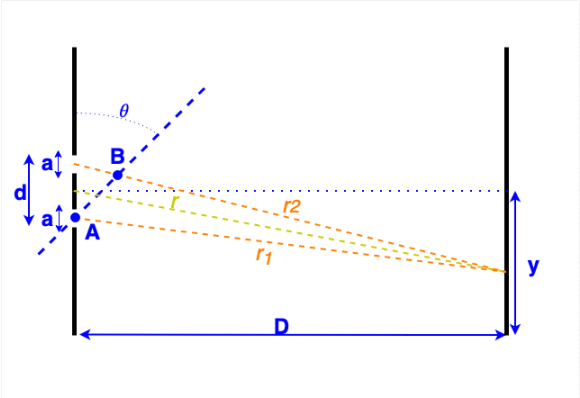

Figure 2.1: Young's experiments geometry (Adapted from [1])

Using Huygens' principle, each slit transmits one ray and since $D \gg d$, the small angle approximation is valid. Thus, $\tan(\theta) = \frac{y}{D} \approx \sin(\theta) \approx \theta$ and both rays can be considered parallels near the array, such as expressed in expression 2.1, where x is the difference between both optical paths near the slits [1].

$$r_2 - r_1 = x = d\,sin(\theta) \approx d\,\theta \tag{2.1}$$

If the optical path length difference of the two rays is a multiple, m, of $\lambda/2$, they interfere destructively, as they are in phase-opposition, expression 2.2 [1]. Likewise, maxima positions can be determined using expression 2.3 and they are related with constructive interference and in-phase waves, such that the

optical path length difference of the two rays is a multiple m of the wavelength λ [1].

$$m\lambda + \frac{\lambda}{2} = d\,sin(\theta) \rightarrow m\lambda + \frac{\lambda}{2} \approx d\,\theta \rightarrow y_{min} \approx (2m+1)\,\frac{\lambda D}{2d} \tag{2.2}$$

$$m\lambda = d\,sin(\theta) \rightarrow m\lambda \approx \theta\,d \rightarrow y_{max} \approx \frac{m\lambda D}{d} \tag{2.3}$$

However, it is possible to extrapolate Young's experiment to an array of $N+1$ slits, such that expressions 2.2 and 2.3 can be respectively rewritten into expressions 2.4 and 2.5 [1, 2].

$$Nm\lambda + \lambda = Nd\,sin(\theta) \approx Nd\,\theta \tag{2.4}$$

$$Nm\lambda = Nd\,sin(\theta) \approx Nd\,\theta \tag{2.5}$$

At this point, it is very important to distinguish what is diffraction from what is interference. The main difference between these two phenomena is the number of coherent waves in the process. Waves are classified as coherent when their frequency and direction are the same, such that their phase difference is invariant. Then, as illustrated on figure 2.2, for a small number of waves interacting the phenomenon is called interference otherwise, for a huge number of waves, it is called diffraction. However, as it is very difficult to say what is a huge or a small number of waves, it is not usual to distinguish these terms, since they are quite similar. Nonetheless, analysing patterns it is possible to differentiate them, since the diffraction pattern is the envelope of the interference one [1].

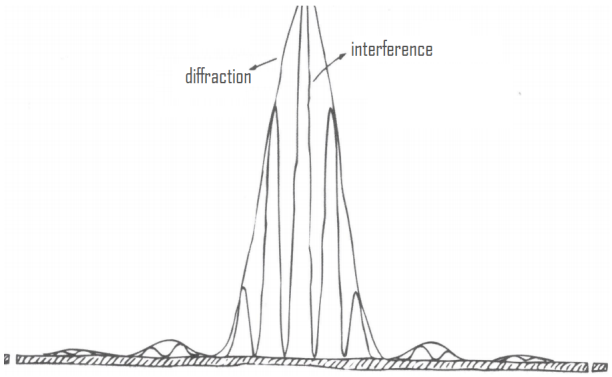

Figure 2.2: Relation between diffraction and interference patterns (Adapted from [1])

2.1.2 Fraunhofer Diffraction Theory

Assuming a plane and monochromatic wave with perpendicular incidence to a perfect conductive metal, as is illustrated in figure 2.3, where there is only one slit of size a - on the order of the wavelength of the light -, distanced of D from a target, the ratio between the irradiance at a certain angle of diffraction θ and the main lobe one - $\theta = 0°$ -, is given by Fraunhofer diffraction theory, which is mathematically presented

in expression 2.6, where λ corresponds to the incident wavelength such as $k = \frac{2\pi}{\lambda}$ and $\beta = \frac{ka}{2}\sin\theta$ [2,3].

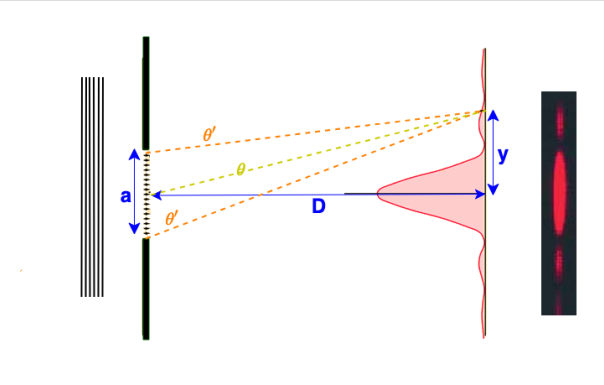

Figure 2.3: Representation of Fraunhofer's ideology.

According to Huygens' principle, any wave front can be replaced by a collection of punctual sources distributed uniformly over this wave front. This principle is used in Fraunhofer theory in order to divide the wave front in many sources emitting rays in phase and the maxima and minima positions along y axis can be determined using the analysis explained on section 2.1.1, based on constructive and destructive interference. Under small angle conditions - which is equivalent to state that the distance of all punctual sources to the target point is the same -, it is possible to relate y, D and θ, such as $\tan(\theta) = \frac{y}{D} \approx \sin(\theta) \approx \theta \approx \theta'$ and thus, $\beta = \frac{ay\pi}{\lambda D}$ [1–3].

$$\frac{I(\theta)}{I(0)} = \left(\frac{sin(\beta)}{\beta}\right)^2 \tag{2.6}$$

As presented on figure 2.3 and verified on expression 2.6, the pattern in the target is related to a *sinc* function. Nonetheless, under the same conditions, there is also a Fraunhofer diffraction theory of an array of N slits, equally spaced by d, which is mathematically formulated as expression 2.7 and the relations 2.8 and 2.9, where I_0 is the contribution of each equal slit for the overall irradiance [1]. Thus, the pattern at the target will depend on two *sinc* functions, one related to the size of each slit and the other associated to the distance between slits. In particular, if $N = 1$ and consequently $d = 0$, expression 2.7 degenerates in expression 2.6.

$$I(\theta) = I_0\left(\frac{sin(\beta)}{\beta}\right)^2\left(\frac{sin(N\alpha)}{\alpha}\right)^2 = I_0N^2\left(\frac{sin(\beta)}{\beta}\right)^2\left(\frac{sin(N\alpha)}{N\alpha}\right)^2 \tag{2.7}$$

$$\beta = \frac{ka}{2}sin(\theta) = \frac{\pi a}{\lambda}sin(\theta) = \frac{\pi ay}{\lambda D} \tag{2.8}$$

$$\alpha = \frac{kd}{2}sin(\theta) = \frac{\pi d}{\lambda}sin(\theta) = \frac{\pi dy}{\lambda D} \tag{2.9}$$

2.1.3 Kirchhoff Diffraction Theory

Kirchhoff considered a plane wave incident to an opaque plane, propagating along the x axis, so that an aperture on this plane origin a transmitted wave determined by expression 2.10 [4]. Even more, Kirchhoff's theory includes as limit cases the Fresnel and Fraunhofer's theories.

$$\nabla^2 \bar{u} + k_0^2 \bar{u} = 0 \tag{2.10}$$

Using Green's theorem, it is possible to find the solution of expression 2.10, where the integration is based on the surface coordinates y' and z', being x', y' and z' the coordinates of a point $\boldsymbol{r'}$ before or over the metal surface and $\boldsymbol{\phi}$ is the Green's function, for a monochromatic wave at a point $\boldsymbol{r}$ after the plane, given by $r^2 = x^2 + y^2 + z^2$ [3, 4]. The solution is presented in expression 2.11 and it is based on the assumptions that $\bar{u}$ is a scalar wave and $\bar{u}$ and $\frac{\partial \bar{u}}{\partial x'}$ are null after the surface, such that near the slit $u = \bar{u} = u_0$, considering u_0 as the field intensity of the incident wave, without disturbances [3, 4].

$$u(\boldsymbol{r}) = \frac{1}{4\pi} \int \left[-\frac{\partial u}{\partial x'}(\boldsymbol{r'})\, \boldsymbol{\phi}(|\boldsymbol{r} - \boldsymbol{r'}|) + u(\boldsymbol{r'}) \frac{\partial \boldsymbol{\phi}}{\partial x'} \right] d\sigma \tag{2.11}$$

Most of all, the previous results are the base to analyse wave propagation for an aperture dimension greater than the incident wavelength. Then, theory extension for subwavelength apertures is expressed in 2.12, only valid for $ka \ll 1$ where a is the aperture diameter and A its area [3, 4].

$$u(\boldsymbol{r}) = -A \left[\frac{\partial u_0}{\partial x'} \boldsymbol{\phi}(\boldsymbol{r}) + u_0 \frac{\partial \boldsymbol{\phi}(\boldsymbol{r})}{\partial x} \right] \tag{2.12}$$

2.1.4 Bethe Diffraction Theory

Kirchhoff's theory assumes an opaque and finite plane and consequently, boundary conditions are not satisfied at the metal surface, namely at the slit limits, such that both incident and reflected waves did not exist over the surface. However, when considering subwavelength slits, this approximation does not guarantee correct results. Thus, in 1944, Hans Albrecht Bethe amended Kirchhoff's theory, assuming a plane wave normally incident to an infinite, perfect conductive metal surface, propagating along z and polarized along x direction. A subwavelength circular hole on the metal surface is studied as a cavity upon oscillation, making three main assumptions [4]: (1) incident and reflected waves coexist over the metal surface; (2) the electromagnetic wave does not penetrate the surface, due to the infinity metal conductivity; (3) The complex electric field vector, $\bar{\boldsymbol{E}}$, is tangential to the surface and the complex magnetic field vector, $\bar{\boldsymbol{H}}$, is perpendicular to it.

Since the considered hole is circular, Bethe's theory is presented in cylindrical coordinates, considering $\boldsymbol{r}$ as the analysed point after the metal surface - $r^2 = x^2 + y^2 + z^2$ -, $\boldsymbol{r'}$ a point before the surface - $(r')^2 = (x')^2 + (y')^2 + (z')^2$ and $\boldsymbol{r'} = \boldsymbol{0}$ is the source coordinates -, a as the hole radius, $\boldsymbol{\kappa}$ as the unity

vector pointed to $\boldsymbol{r}$, as well as $\bar{\boldsymbol{E}}_{\mathbf{0}}$ and $\bar{\boldsymbol{H}}_{\mathbf{0}}$ the electric and magnetic field complex vectors before the metal surface, if there is no hole [4].

Then, according to Bethe, Maxwell's equations and boundary conditions are satisfied since it is assumed an integration at large distance, *i.e.*, far from the metal screen, $kr \gg 1$, where k is the wave vector given by expression 2.13 [4]. Thus, a punctual source is considered, leading to the approximation presented on expression 2.14 and to the Green's function of expression 2.15. Consequently, Maxwell's equations will degenerate on expressions 2.16 and 2.17 [4].

$$k = \frac{\omega}{c} = \frac{2\pi}{\lambda} \tag{2.13}$$

$$\boldsymbol{\nabla\phi} = ik\boldsymbol{\kappa r} \xrightarrow{linear\ aproximation} \boldsymbol{\phi} = \boldsymbol{\phi_0}\left(1 - ik\boldsymbol{\kappa r'}\right) \tag{2.14}$$

$$\phi_0 = \phi(\boldsymbol{r'} = \mathbf{0}) = \frac{e^{ikr}}{r} \tag{2.15}$$

$$\bar{\boldsymbol{E}} = \frac{1}{3\pi}k^2a^3\boldsymbol{\phi_0\kappa} \times \left(2\bar{\boldsymbol{H}}_{\mathbf{0}} + \bar{\boldsymbol{E}}_{\mathbf{0}} \times \boldsymbol{\kappa}\right) \tag{2.16}$$

$$\bar{\boldsymbol{H}} = -\frac{1}{3\pi}k^2a^3\boldsymbol{\phi_0\kappa} \times \left(2\bar{\boldsymbol{H}}_{\mathbf{0}} \times \boldsymbol{\kappa} - \bar{\boldsymbol{E}}_{\mathbf{0}}\right) \tag{2.17}$$

Applying the Poynting's theorem at expressions 2.16 and 2.17 it is possible to determine the complex radiation power per squared meter as presented on expression 2.18 for a certain direction to the point $\boldsymbol{r}$ [4]. Moreover, the total power transmitted for the hole is the result of an integration of expression 2.18 among all the diffracted angles - equivalent to all $\boldsymbol{\kappa}$ directions -, resulting on expression 2.19.

$$\bar{\boldsymbol{S}} = \frac{c}{4\pi}\bar{\boldsymbol{E}} \times \bar{\boldsymbol{H}} = \frac{c}{36\pi^3}\frac{k^4a^6}{\boldsymbol{r}^2}\boldsymbol{\kappa}\left(2\boldsymbol{\kappa} \times \bar{\boldsymbol{H}}_{\mathbf{0}} - \boldsymbol{\kappa} \times \boldsymbol{\kappa} \times \bar{\boldsymbol{E}}_{\mathbf{0}}\right)^2 \tag{2.18}$$

$$\bar{\boldsymbol{S}}_{\boldsymbol{tot}} = \frac{c}{27\pi^2}k^2a^6\boldsymbol{\kappa}\left(4{\bar{\boldsymbol{H}}_{\mathbf{0}}}^2 + {\bar{\boldsymbol{E}}_{\mathbf{0}}}^2\right) \tag{2.19}$$

Therefore, the electric and magnetic field are proportional to k^2a^3 and, consequently, the radiation power is proportional to k^4a^6. However, if it is considered a subwavelength hole, such as $ka \ll 1$, the radiation power is going to be proportional to $(a/\lambda)^4$ [4]. Comparing Bethe's theory with Kirchhoff's one, it can be shown that Kirchhoff's intensity drop with λ^{-2}, comparing to the λ^{-4} deduced by Bethe.

Another important conclusion took by Bethe is that the aperture can be modelled as an electric and a magnetic dipole, $\boldsymbol{P}$ and $\boldsymbol{M}$ respectively. As an electric dipole, the relation to the electromagnetic field given by 2.16 and 2.17 is presented on expressions 2.20 and 2.21, as well as a magnetic dipole, the relation is detailed on expressions 2.23 and 2.21 [4–6].

$$\bar{\boldsymbol{E}} = k^2\boldsymbol{\phi_0\kappa} \times \left(\bar{\boldsymbol{P}} \times \boldsymbol{\kappa}\right) \tag{2.20}$$

$$\bar{\boldsymbol{H}} = k^2\boldsymbol{\phi_0\kappa} \times \bar{\boldsymbol{P}} \tag{2.21}$$

$$\bar{\boldsymbol{H}} = k^2 \boldsymbol{\phi_0 \kappa} \times \left(\bar{\boldsymbol{M}} \times \boldsymbol{\kappa} \right) \tag{2.22}$$

$$\bar{\boldsymbol{E}} = -k^2 \boldsymbol{\phi_0 \kappa} \times \bar{\boldsymbol{M}} \tag{2.23}$$

Replacing the electromagnetic field expressions 2.16 and 2.17 on expressions 2.20 to 2.23, it is possible to deduce expressions 2.24 and 2.25, where the electric and magnetic dipoles are written in terms of the incident field and to the aperture radius.

$$\bar{\boldsymbol{P}} = -\frac{1}{3\pi} a^3 \bar{\boldsymbol{E}}_{\boldsymbol{0}} \tag{2.24}$$

$$\bar{\boldsymbol{M}} = -\frac{2}{3\pi} a^3 \bar{\boldsymbol{H}}_{\boldsymbol{0}} \tag{2.25}$$

On top of that, Bethe analysed the electromagnetic field near the aperture, determining equations 2.26 and 2.27, which are only valid up to a distance of the same order than the wavelength [4–6]. However, they are presented in cartesian coordinates, that is useful to analyse boundary conditions.

$$\bar{\boldsymbol{E}}(\boldsymbol{r}) \Rightarrow \begin{cases} \bar{E}_x = -\dfrac{4}{\pi} jk \sqrt{a^2 - x^2 - y^2} \\ \bar{E}_y = 0 \\ \bar{E}_z = jkx \end{cases} \tag{2.26}$$

$$\bar{\boldsymbol{H}}(\boldsymbol{r}) \Rightarrow \begin{cases} \bar{H}_x = 0 \\ \bar{H}_y = \dfrac{1}{\mu_0 c} \\ \bar{H}_z = -\dfrac{4}{\mu_0 c \pi} \dfrac{y}{\sqrt{a^2 - x^2 - y^2}} \end{cases} \tag{2.27}$$

Analysing expressions 2.26 and 2.27, it is possible to observe that boundary conditions are not totally satisfied, since $\bar{E}_z \neq 0$, due to the fact the Bethe neglected terms of the same order than ka [5, 6].

2.1.5 Bouwkamp Diffraction Theory

In 1950, Bouwkamp proposed the rectification of Bethe's theory, in order to guarantee the satisfaction of the boundary conditions [5, 6]. Bouwkamp's approach is based on the Babinet's principle, so that he assumed a disk - instead of an aperture or a hole -, in order to obtain the magnetic currents for the disk's hole and to deduce the electromagnetic field relations presented on expressions 2.28 and 2.29 [5, 6]. Comparing these expressions with Bethe's ones, it is possible to observe that the magnetic

field expression did not change.

$$\bar{\boldsymbol{E}}(\boldsymbol{r}) \Rightarrow \begin{cases} \bar{E}_x = -\dfrac{4ik}{3\pi} \dfrac{2a^2 - x^2 - 2y^2}{\sqrt{a^2 - x^2 - y^2}} \\ \bar{E}_y = -\dfrac{4ik}{3\pi} \dfrac{xy}{\sqrt{a^2 - x^2 - y^2}} \\ \bar{E}_z = 0 \end{cases} \tag{2.28}$$

$$\bar{\boldsymbol{H}}(\boldsymbol{r}) \Rightarrow \begin{cases} \bar{H}_x = 0 \\ \bar{H}_y = \dfrac{1}{\mu_0 c} \\ \bar{H}_z = -\dfrac{4}{\mu_0 c\pi} \dfrac{y}{\sqrt{a^2 - x^2 - y^2}} \end{cases} \tag{2.29}$$

Due to differences in the electric field the total radiation power transmitted by the hole, determined by Bouwkamp and presented on expression 2.30, is different from the determined by Bethe [5, 6].

$$\bar{\boldsymbol{S}}_{\boldsymbol{tot}} = \frac{64}{27\pi} k^4 a^6 \bar{\boldsymbol{S}}_{\mathbf{0}} = \frac{64}{27\pi} k^4 a^6 \frac{1}{2} c\epsilon_0 \bar{\boldsymbol{E}}_{\mathbf{0}}{}^2 \tag{2.30}$$

In the same way of Bethe, results for the electromagnetic field may be explained due to the simultaneous existence of an electric dipole and a magnetic dipole. The expression for the field of the magnetic dipole is the same of Bethe, but the expression for the field of the electric dipole is of course different, as it is possible to observe on expressions 2.31 and 2.32, respectively for the electric and magnetic dipole [5, 6].

$$\bar{\boldsymbol{P}} = \frac{1}{3\pi} a^3 \bar{\boldsymbol{E}}_{\mathbf{0}} \tag{2.31}$$

$$\bar{\boldsymbol{M}} = -\frac{2}{3\pi} a^3 \bar{\boldsymbol{H}}_{\mathbf{0}} \tag{2.32}$$

2.2 Surface Plasmons Polaritons

In the 1950's the interest in plasmons receive a great impulse with the works of Pines and Bohm. Later, in 1956 Fano introduces the concept of polariton and in in 1957 Ritchie presented the first theoretical description of surface plasmons [7–9]. Thereafter Ritchie explained the anomalous behaviour of metal gratings through surface plasmons resonances and Kretschmann and Raether proposed the optical excitation in metal films of surface plasmons, followed in 1988 by a book of Raether [7–9].

A plasmon is a quasiparticle, a quantum of a plasma oscillation - redistribution of plasma's free electrons -, just as light is the optical oscillation of photons. Therefore, plasmons are collective oscillations that can be coupled with photons, creating another quasiparticle called (plasmon) polariton. A polariton is the result of a strong coupling between electromagnetic waves and an electric or magnetic dipole. So,

a surface plasmon and a surface plasmon polariton are not the same, despite the fact that they have a straight relation [7–9].

Surface plasmon polaritons are electromagnetic waves, propagating at the interface, between a metal/plasma and a dielectric. Assuming a dipole structure - for example an array of slits, grooves, holes, apertures or even a corrugation on the surface -, where light is incident on, the photons can excite coherent fluctuations of free electron charges at the metal boundary, creating plasmon oscillations. Then, these oscillations can couple with the incident light and consequently, polaritons are created and they will propagate at the interface [7–9]. The coupling is a resonant behaviour capable of amplifying and of concentrating light near the surface, due to polariton generation. This resonant behaviour is the consequence of the energy transference between incident light, surface plasmons and the propagation of its polaritons.

As presented in figure 2.4, it is assumed a surface at $z = 0$, so that there is metal/plasma for $z < 0$ and dielectric for $z > 0$. Thus, the non-null components of the electromagnetic field are presented on expression 2.33 - "+" for $z > 0$ and "-" for $z < 0$ -, where m is the indication of the material: 1 for the metal/plasma with a relative dielectric function given by $\bar{\epsilon}_1$ and 2 for the dielectric characterised by a relative dielectric function of $\bar{\epsilon}_2$ [9]. In this case, it is studied the most common and easier excitation of surface plasmon, which is due to the electric field normal incidence, exciting a TM polariton [9]. However, there is also the possibility of a surface plasmon excitation due to a perpendicular magnetic field where the polariton will be a TE wave.

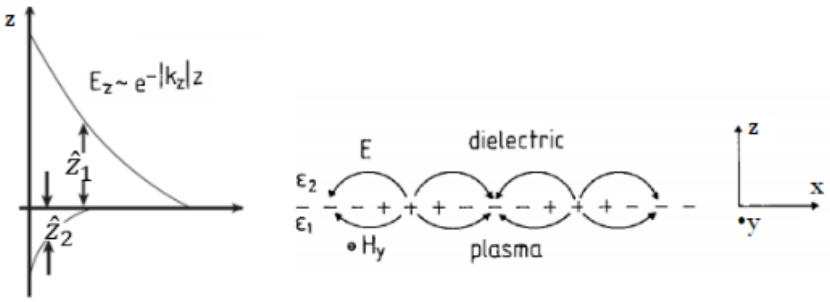

Figure 2.4: Charges and electromagnetic field of surface plasmons propagation in x direction and $\bar{E}_z$ dependence with z (Adapted from [9])

$$\begin{cases} \bar{E}_{x,m}(x,y,z,t) = E_0 e^{j(\bar{k}_x x + \bar{k}_{z,m}|z| - \omega t)} \\ \bar{E}_{z,m}(x,y,z,t) = \pm \dfrac{\bar{k}_x}{\bar{k}_{z,m}} E_0 e^{j(\bar{k}_x x + \bar{k}_{z,m}|z| - \omega t)} \\ \bar{H}_{y,m}(x,y,z,t) = H_0 e^{j(\bar{k}_x x + \bar{k}_{z,m}|z| - \omega t)} \end{cases} \tag{2.33}$$

Thus, there are oscillations along x and an exponential decay over z direction. Another consideration that have to be done is the fact that $\bar{k}_z$ have different values for each material, but $\bar{k}_x$ will be the same for both of them, such as $|\bar{k}_x| = \frac{2\pi}{\lambda_{sp}}$, where λ_{sp} is the wavelength of the plasma oscillation. Above all,

Maxwell's equations and boundary conditions - at $z = 0$: $\bar{E}_{x,1} = \bar{E}_{x,2}$ and $\bar{H}_{y,1} = \bar{H}_{y,2}$ -, impose relations presented on expressions 2.34, leading to the determination of $\bar{k}_x$ [3, 9].

$$\boldsymbol{\nabla} \times \bar{\boldsymbol{H}} = \bar{\epsilon}\frac{\partial \bar{\boldsymbol{E}}}{\partial t} \Rightarrow \begin{cases} \dfrac{E_0}{H_0} = -\dfrac{\bar{k}_{z,1}c}{\bar{\epsilon}_1\omega} \\ \dfrac{E_0}{H_0} = \dfrac{\bar{k}_{z,2}c}{\bar{\epsilon}_2\omega} \\ k^2 = k_x^2 + k_z^2 \end{cases} \Rightarrow \begin{cases} \dfrac{\bar{k}_{z,1}}{\bar{\epsilon}_1} + \dfrac{\bar{k}_{z,2}}{\bar{\epsilon}_2} = 0 \\ k_x^2 + k_{z,m}^2 = \epsilon_m \left(\dfrac{\omega}{c}\right)^2 \end{cases} \Rightarrow \bar{k}_x = \frac{\omega}{c}\left(\frac{\epsilon_1\epsilon_2}{\epsilon_1+\epsilon_2}\right)^{1/2} \tag{2.34}$$

Electromagnetic waves propagating near a metal suffer from a damping effect caused by Ohmic losses and so, it is better to consider an imaginary dielectric function $\bar{\epsilon}_1 = \epsilon_1' + j\epsilon_1''$ as well as, $\bar{k}_x = k_x' + jk_x''$, using the relations 2.34. Then, it is possible to determine the formulas of k_x', k_x'' and k_z, as presented on expressions 2.35, 2.36 and 2.37, respectively [3, 7–9].

$$k_x' = \frac{\omega}{c}\left(\frac{\epsilon_1'\epsilon_2}{\epsilon_1'+\epsilon_2}\right)^{1/2} \tag{2.35}$$

$$k_x'' = \frac{\omega}{c}\left(\frac{\epsilon_1'\epsilon_2}{\epsilon_1'+\epsilon_2}\right)^{3/2}\frac{\epsilon_1''}{2(\epsilon_1')^2} \tag{2.36}$$

$$k_{z,m} = \left[\epsilon_m\left(\frac{\omega}{c}\right) - k_x^2\right]^{1/2} \tag{2.37}$$

However, it is also assumed a real ω and ϵ_2 and also that $|\epsilon_1'| \gg \epsilon_1''$, in order to determine independently k_x' and k_x''. Nonetheless, for a given incident wavelength, these expressions and assumptions lead to two important conditions for surface plasmon excitation: (1) $\epsilon_1' < 0$ and $|\epsilon_1'| > \epsilon_2$; (2) The wave vector component of the incident light, that is parallel to the interface metal-dielectric have to match with the wave vector of the surface plasmon polariton [3, 9]. Thus, only materials with a dielectric function with negative real part and small imaginary part can support this kind of excitation [9]. The appearance of metamaterials enables the use of surface plasmons in several applications, because previously only doped semiconductors and some noble metals could fulfil these conditions. Nowadays, it is possible to design metamaterials in order to check these conditions and to reach some remarkable properties, by adjusting not only their dielectric function but also their shape, size, orientation and arrangement.

The dielectric function is dependent on the incident angular frequency ω and on the plasma bulk frequency ω_p. Thus, the dispersion relation is presented on figure 2.5, where the light-green dashed straight line is the light line. On its left, is the dispersion curve of a free-space wave and on its right, the dispersion curve of a surface plasmon polariton. Furthermore, it is possible to observe that for small values of k_x the surface plasmon polariton behaviour is similar to the light one, but as k_x increase its behaviour tends to an asymptotic limit called surface plasmon frequency given by $\omega_{SP} = \frac{\omega_p}{\sqrt{1+\epsilon_2}}$, presenting a resonant behaviour for $\epsilon_1' \to -\epsilon_2$, as predicted by the $\bar{k}_x$ expression presented on 2.34.

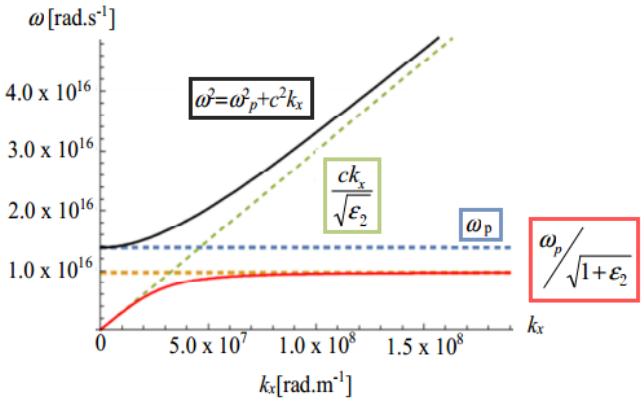

Figure 2.5: Numerical example for an interface between air (dielectric) and gold (metal/plasma), presenting the surface plasmons polariton dispersion relation (red solid-curve), the free-space dispersion curve (black solid-curve) and the limits, as dashed-lines, for the light propagation relation (light-green), for the plasma bulk frequency (blue) and for the surface plasmon frequency (orange) (Adapted from [3]).

Therefore, as the dispersion curve is on the right side of the line one, the surface plasmon polaritons have a smaller wavelength than a free-space wave and consequently, their modes are evanescent [3, 9]. Moreover, it is very important to evaluate the propagation distance, along x and z, supported by this kind of wave. Calling penetration depth to the value of z for which the electric field along this axis decays $1/e$, it is possible to conclude that this value is given by $z = \hat{z} = |\bar{k}_{z,m}|^{-1}$, as explicitly presented on expressions 2.38 and 2.39 for each material, because $E_z \approx e^{-|\bar{k}_z|z}$, as shown on figure 2.4 [3, 9].

$$\hat{z}_1 = \frac{\lambda}{2\pi}\left(\frac{\epsilon_1' + \epsilon_2}{(\epsilon_1')^2}\right)^{1/2} \tag{2.38}$$

$$\hat{z}_2 = \frac{\lambda}{2\pi}\left(\frac{\epsilon_1' + \epsilon_2}{(\epsilon_2)^2}\right)^{1/2} \tag{2.39}$$

In the same way, it is defined the propagation length L_i as the x distance where the electric field decays $1/e$. The electric field is given by $\bar{E}_x \approx e^{-jk_x'' x}$, and so that $L_i = (2k_x'')^{-1}$ or in the explicit form as in expression 2.40 [3, 9]. Moreover, knowing the group velocity v_g, the propagation time, until the wave arrive to $x = L_i$, is given by $T_i = \frac{L_i}{v_g}$ [9].

$$L_i = \frac{1}{2k_x''} = \frac{c}{\omega}\frac{(\epsilon_1')^2}{\epsilon_1''}\left(\frac{\epsilon_1'\epsilon_2}{\epsilon_1' + \epsilon_2}\right)^{2/3} \tag{2.40}$$

Finally, it remains to explain how it is possible to excite surface plasmons and consequently their polaritons. One way is to use electron beams in order to exploit the electrons scattering energy, that is transferred to the plasma's bulk, to origin a wave vector parallel to the surface [9]. A surface plasmon is created with this wave vector. The other possibility is to use photons to excite a surface plasmon polariton, which is going to have the same frequency and linear momentum [9]. An incident photon can excite a free electron on the surface. As the free-space photon has more momentum than the surface

plasmon, they cannot couple and so that, a surface plasmon was created but the polariton will not [9]. Thus, the momentum of the free-space photon must decrease, which can be done using a grating or a more complex structure with prisms. Talking about the grating - that can be an array of slits, grooves, apertures, holes or a rough surface -, if light is incident on, photons will scatter at the surface, creating a surface plasmon with the same wave vector of the parallel component of the scattered wave, but the surface plasmon also interacts with the scattered wave, originating the polariton [9]. In other words, momentum and energy conservation must be verified, allowing a resonant interaction between incident light and surface plasmons, creating the polaritons which are revealed as intense radiation maxima. Also, minima are predicted by what is called Wood's anomaly [9].

2.3 Optical Properties and Drude-Lorentz Model

In Maxwell's equations, the permittivity ϵ and the permeability μ are parameters that relate the properties of matter and the electromagnetic field. When considering the propagation of electromagnetic waves, namely in optics, the refractive index n is frequently used. If ϵ_0 is the permittivity of the vacuum, the refractive index is related to the permittivity by expression 2.41.

$$n = \sqrt{\frac{\epsilon}{\epsilon_0}} \tag{2.41}$$

Considering monochromatic fields, with frequency ω, and if the fields $\bar{\boldsymbol{E}}$ and $\bar{\boldsymbol{H}}$ have components of the form $E = E_0 e^{-j\omega t}$ and $H = H_0 e^{-j\omega t}$, then the complex permittivity and the complex refractive index can be related by expression 2.42. Whereas the refractive index n is related with the phase velocity and the dispersion losses, k, is the extinction factor, that describes the material electromagnetic attenuation. The extinction factor is related with the absorption coefficient and the Ohmic losses. In this case, if $k > 0$ there is a lossy medium, if $k = 0$ there are no losses, and if $k < 0$ there is light amplification. The real and imaginary parts of each complex quantity can be related by expressions 2.43 and 2.44.

$$\bar{\epsilon} = \epsilon' + j\epsilon'' = \bar{n}^2 = (n + ik)^2 \tag{2.42}$$

$$\epsilon' = n^2 - k^2 \tag{2.43}$$

$$\epsilon'' = 2nk \tag{2.44}$$

Since the main focus is to reach an optical resonant peak, possibly with gain, using nanoantennas, it is quite important to know the optical properties of regular materials, specially these electromagnetic parameters, in order to design structures to fulfil specifications. However, this electromagnetic properties have frequency dependence. The Drude-Lorentz model relates the complex dielectric function with the

incident wavelength or frequency. Analysing the value of $\bar{\epsilon}(\omega)$ or $\bar{\epsilon}_r(\omega)$, we can look for the wavelengths associated to the excitation of surface plasmons polaritons and consequently, to the creation of a spectral resonant peak [3, 10–12]. On appendix A are presented the complex permittivity - also called complex dielectric functions -, for all the materials used in the simulations, some of them are Drude-Lorentz fittings, others are experimental fittings.

In the XX century, the classical Drude model was combined with the quantum mechanical statistics of Fermi-Dirac, by Arnold Sommerfeld. The Drude-Sommerfeld model describes the electric current created by an incident electromagnetic field in a metal [10–13]. This model assumes a neutral metal, since the total positive ions charge is equal to the total negative charge of electrons [10–12]. Moreover, it assumes that, when a oscillating electric field is applied, the positive nuclei do not move and the electrons oscillate with the electric field. This approximation is justified, due to the difference of masses: the electron mass is much lower than the nuclei one. Expression 2.45 describes the movement of an electron at a point $\boldsymbol{r}$, where m_e is the electron mass, q is its charge, $\overline{\boldsymbol{E}}_{\mathbf{0}}$ is the complex amplitude of the incident electric field at a given angular frequency ω and the damping constant is defined as $\Gamma = \frac{v_F}{l}$, where v_F is the Fermi velocity and l is the average distance that one electron can travel between collisions [10–13].

$$m_e \frac{\partial^2 \boldsymbol{r}}{\partial t^2} + m_e \Gamma \frac{\partial \boldsymbol{r}}{\partial t} = q\overline{\boldsymbol{E}}_{\mathbf{0}} \tag{2.45}$$

Using Maxwell's equations and field definitions, it is possible to solve expression 2.45 in order to get the relative dielectric function. This solution is presented on expression 2.46, where ω_p is the previously mentioned plasma angular frequency, which is given by $\omega_p = \sqrt{\frac{\tilde{n}q^2}{m_e \epsilon_0}}$, being $\tilde{n}$ the free electrons density [3, 10–14].

$$\bar{\epsilon}_{Drude}(\omega) = 1 - \frac{\omega_p^2}{\omega^2 + i\Gamma\omega} = 1 - \frac{\omega_p^2}{\omega^2 + \Gamma^2} + i\frac{\Gamma\omega_p^2}{\omega\left(\omega^2 + \Gamma^2\right)} \tag{2.46}$$

This model is very accurate for infrared band applications, however its use to other spectral regions is not recommended, because there are some processes that can not be neglected. Bound electrons have to be considered to improve the model accuracy for all the spectrum, in special for visible region applications [3, 10–12]. The movement of bound electrons can be described by expression 2.47, where m is the electron effective mass, γ is the damping constant of radiation correlated with the bound electrons and α is the restitution coefficient of the potential force [3, 10–12]. Solving this equation, the relative dielectric function is revealed, which is presented on expression 2.48, being $\tilde{\omega}_p = \sqrt{\frac{\tilde{\tilde{n}}q^2}{m\epsilon}}$ where $\tilde{\tilde{n}}$ is the bound electrons density and $\omega_0 = \sqrt{\frac{\alpha}{m}}$.

$$m\frac{\partial^2 \boldsymbol{r}}{\partial t^2} + m\gamma\frac{\partial \boldsymbol{r}}{\partial t} + \alpha\boldsymbol{r} = q\overline{\boldsymbol{E}}_{\mathbf{0}} \tag{2.47}$$

$$\bar{\epsilon}_{bound}(\omega) = 1 + \frac{\tilde{\omega}_p^2\left(\omega_0^2 - \omega^2\right)}{\left(\omega_0^2 - \omega^2\right)^2 + \gamma^2\omega^2} + i\frac{\gamma\tilde{\omega}_p^2\omega}{\left(\omega_0^2 - \omega^2\right)^2 + \gamma^2\omega^2} \tag{2.48}$$

The Drude-Lorentz model takes into account the free electrons movement and the bound electrons' harmonic oscillations. Thus, the relative dielectric constant is given by expression 2.49, where the value of ϵ for high frequencies is ϵ_∞ [3, 10–12, 14].

$$\overline{\epsilon}_{DL}(\omega) = \epsilon_\infty - \frac{f_0\omega_p^2}{\left(\omega^2 - \omega_0^2\right)^2 + i\omega\gamma_0} - \sum_n \frac{f_n\omega_p^2}{\left(\omega^2 - \omega_n^2\right)^2 + i\omega\gamma_n} \tag{2.49}$$

Thus, in the visible and near-infrared regions, typical metals can be described onto two different sub-regions: the Drude's and the interband regimes [15].

Ohmic losses are proportional to the conductivity of the material, $\sigma(\omega)$, which can be also related to the dielectric function, as $\epsilon''(\omega) = \frac{\sigma(\omega)}{\epsilon_0\omega}$ [15, 16]. This kind of losses influence the field propagation within the penetration depth - near the surface -, and so they also affect the polariton excitation and propagation [15, 16]. To reduce losses, it is possible to choose a metal with a more negative real part of the dielectric function - decreasing the refractive index value and, consequently, the dispersion losses -, leading to a decrease of the penetration depth or, to select a material with low module of the imaginary part of the dielectric function in order to reduce directly Ohmic losses [15, 16].

For typical metals and considering Ohmic losses, only on the Drude regime it is really possible to "catch polaritons". Although, on the interband regime, the real part of the dielectric function can be negative - polariton can be excited -, its value is very small and its imaginary part is very high, leading to huge Ohmic losses on the nanostructures, making almost impossible to propagate the polariton until a structure zone where is possible to use their characteristics.

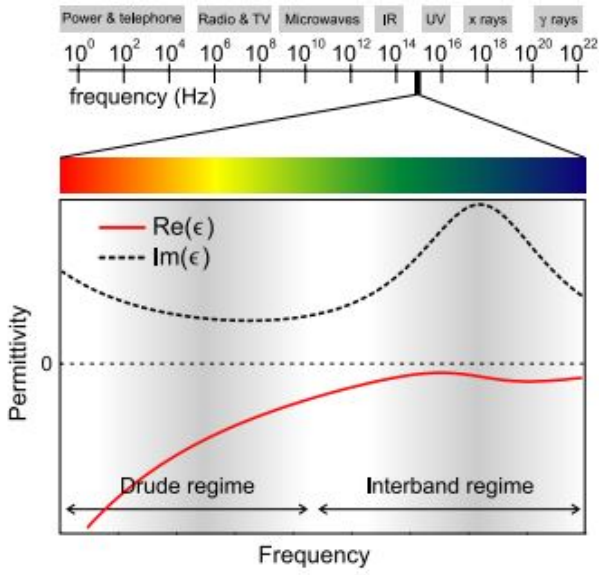

Figure 2.6: Contribution of free and bound electrons model to the complex dielectric function of a typical metal in the visible (and near-infrared) region (Sourced on [15]).

2.4 The First Observation

In 1998, Ebbesen reported an unusual transmission spectrum for a nanostructure where light has normal incidence [17]. This nanostructure is a metallic periodic hole array characterised by a periodicity constant, a hole diameter, and a thickness. Ebbesen shown huge transmission peaks on the spectrum for wavelengths larger than ten times the diameter of each hole [17]. However, these peaks are orders of magnitude greater than the predict ones, using Bouwkamp-Bethe's theory.

The absolute transmission efficiency, which is defined by Ebbesen as the ratio between the transmitted light intensity per unit area and the incident light intensity per unit area, has a value greater than 2 at the maximum, which means that more than twice the light is "transmitted as impinges directly on the holes" [17]. In addition, the experimental results reveal that the transmittivity of the array is linearly proportional to the hole surface area [17]. Then, the array is considered an active element, whose characteristic behaviour can be tuned by changing the hole diameter, the periodicity of the holes, the structure thickness and by changing the material dielectric function [17]. Increasing the array periodicity, the maximum peaks' wavelength - spectrum position -, increased too, without dependence on the type of material, the hole diameter or the film thickness [17]. By changing the relation between the thickness and the hole diameter, the peak width will change too, and for different hole shapes the spectrum will also be completely different [17].

Ebbesen soon suggested that the main responsible agents for this remarkable phenomenon are surface plasmons, because in several tests he observed the same behaviour when surface plasmons were excited in metallic gratings and coupled with incident light, creating polaritons [17]. Thus, extraordinary optical transmission was discovered and Ebbesen predicted that this phenomenon would be the key for the development of several new optical and photonic devices [17].

2.5 Composite Diffracted Evanescent Waves Model

In 2004, Lezec and Thio proposed one model confronting the surface plasmon polaritons theory, named composite diffracted evanescent waves - CDEW -, in which the resonant behaviour is not due to the surface plasmon polaritons mechanism, but is due to the interference of diffracted evanescent waves [18]. They reported that the transmission enhancement factors were not of the orders of 100 to 1000, as presented by Ebbesen, but it should be considered a value around 7 [18, 19].

According to this model, at the slit a huge number of evanescent waves with different wave vectors values are launched. The superposition of these waves is called a composite evanescent wave, which is the sum of all diffracted inhomogeneous modes [18]. This wave propagates with a well-defined wave vector, a finite phase and an amplitude characterised by a decay with the propagation distance [18, 19]. Lezec and Thio reported that their model could be used to characterise the electric field at any frequency along time and space, with or without apertures, by expression 2.50, for a wave vector magnitude equal

to the source $k_0 = \frac{2\pi}{\lambda}$, where $Si(\alpha) = \int_0^\alpha \frac{sin(t)}{t} dt$ [18]. Although Fraunhofer theory is only valid for radiative modes ($0 < k_x < k_0$), they extended his theory for all the range $0 < k_x < \infty$ and proceeded to a numerical integration of the weighted modes spectrum, for $x > a$, leading to expression 2.51. It is possible to verify, based on this expression, that the electric field decays at $1/x$ and it has a phase difference of $\pi/2$ [18].

$$\boldsymbol{E}(x, z = 0) = \begin{cases} -\frac{E_0}{x}\left[Si\left(k_0\left(x + \frac{a}{2}\right)\right) - Si\left(k_0\left(x - \frac{a}{2}\right)\right)\right], |x| > \frac{a}{2} \\ \frac{E_0}{x}\left[\pi - Si\left(k_0\left(x + \frac{a}{2}\right)\right) + Si\left(k_0\left(x - \frac{a}{2}\right)\right)\right], |x| < \frac{a}{2} \end{cases} \tag{2.50}$$

$$\boldsymbol{E}(x) = \frac{E_0}{\pi}\frac{a}{x} cos\left(k_0 x + \frac{\pi}{2}\right) \tag{2.51}$$

This model was experimentally verified not only by Lezec and Thio, but also in the same year by Gay [19]. While Lezec and Thio used tungsten structures Gay used one of silver. Even though tungsten has a real part of the dielectric constant positive, they observed the occurrence of EOT, however with a low enhancement factor [18, 19]. Once that, at least one of the EOT conditions was not verified and these experiments could be used to prove that the field amplification was not due to surface plasmon polaritons in these cases.

Two years later, in 2006, Lalanne and Hugonin developed a study based on Maxwell's equations, showing that the interaction between light and the structures results from two contributions, one from the surface plasmons polaritons and other from a creeping wave [20]. Even more, they demonstrated that the polaritons are the main agents of this interaction, at least for the visible region [20]. Their report refuted the CDEW model, because they show similar results to the surface plasmon polaritons theory and huge differences in comparison to the CDEW model [20]. They suggested that experimental results of Lezec and Thio were spoiled by impurities and that their theoretical model has the same limitations than Kirchhoff's theory [20].

3

State-of-the-Art

The extraordinary optical transmission has been observed along the frequency spectrum, from the audio band until the X rays band. In the near infrared, visible and near ultraviolet part of the spectrum, the antennas used to take advantage of EOT have subwavelength dimensions, on the order of nanometers, nanoantennas [3, 21].

The design of a nanoantenna for sensors can be divided into two different cases: one where the structure is used to improve an existing sensor or measurement system and another where the structure is itself the main agent of the measurement system.

Taking advantage of EOT, an electromagnetic wave can be amplified. In medical imaging, x-rays or magnetic resonance imaging applications, EOT and nanoantennas can be used to diminish the power needed per scan but also to focus radiation, such that, the maximum intensity of the field will be almost confined to the wound or illness area leading to a less intense radiation exposure on the healthy areas. In this way the radiation intensity in the healthy areas decreases, resulting in a decrease of the local heating and the risks of burning. Beyond that, in the case of x-ray and the higher ultra violet radiation - ionising radiations -, there is a minimisation of the damage risks to the healthy tissues, such as cell damage or radiation sickness. In photodetection and light emission, EOT and nanoantennas can be used to improve the system's sensibility - amplifying a certain spectral region and attenuating others - [21].

However, a deep state-of-art review shows that nanoantennas are being used as sensors, rather than as an improvement to a measurement system [14, 17, 21–35]. This recent type of sensors, based on nanoantennas and EOT properties, are allowing to monitor the presence of certain molecules or cell types, for example it is quite common to being used to detect proteins or verify their profile. Furthermore, a sensor based on nanoantennas has been purposed to the detection of cancerous cells.

There is a huge opportunity to create new sensors based on EOT. However, to design a sensor that could enter into the market, it is necessary to guarantee an acceptable fabrication cost and a good reproducibility [24, 25, 36]. Cost minimisation demands a good project. That includes the definition of the specifications, taking into account the trade-off between cost and performance, and a very accurate design, including hand calculations, numerical simulations, circuit layout design and again simulations, taking in consideration the parasitic elements. Then, if necessary, return to improve the device or circuit design layout. All this process is necessary because the problems in the fabrication, demanding a return to the circuit design process, are costly. The importance of the simulation processes implies the development of computational methods and the use of powerful simulation software for the device or circuit project and for the simulation of the layout of the integrated circuit. The fabrication of the integrated circuits - namely with dimensions in the nano order -, is only possible with advanced techniques of synthesis of semiconductors and nanomaterials.

The most common techniques to produce nanoantennas are the top-down methods such as ion

beam milling or electron-beam lithography and the bottom-up self-assembly schemes [21, 24, 25]. If the nanostructures are metal made, they are chemically stable, enduring long duration against ultraviolet irradiation and a high temperature range [26].

Comparing sensors based on nanoantennas with other plasmonic structures its nano-size leads to the miniaturisation of the sensor, the possibility to measure not only *in vitro* but also *in vivo*, the potential for multiplexing and to have low limits of detection [21, 24, 25, 36]. However, researchers are trying to improve some figures of merit such as sensitivity, detection limits, selectivity and dynamic range, as well as to create standalone and portable devices, with the capability of give real-time information to the user [21, 24, 25, 36]. To reach these objectives, new types of nanoantennas are being developed, as well as completed systems composed by the nanoantenna and several other devices, as internal spectrometers, angle scanners, tunable laser or the interfaces and controllers with the processing units [21, 24, 25, 36].

The majority of nanoantennas sensors are based on the wavelength shift of the resonance peak [22, 23]. Depending on the monitored conditions, the resonance peak position will change and consequently the intensity value too. However, the intensity peak value must be detectable in order to determine its position and to conclude about its shift value.

As previously referred, to excite surface plasmons with gratings, momentum and energy conservation must be satisfied, which is mathematically expressed by expression 3.1, for displacement vectors $\hat{e}_1$ and $\hat{e}_2$ and, an incident angle θ [27, 28, 37]. If it is considered a square array - $\hat{e}_1 = \hat{x}$ and $\hat{e}_2 = \hat{y}$ -, with circular holes, the reciprocal array vectors are $G_x = G_y = \frac{2\pi}{a_0}$, expression 3.2 must be satisfied, where m and n are the integers values associated to surface modes [27, 28, 37]. It should be noted that, in order to free-space photons - $\bar{k}_x$ -, couple to plasmons - $\bar{k}_{sp}$ -, their momentum is reduced by the gratings, such that the final momentum should be equal to $\bar{k}_x$ of a surface plasmon - compare expressions 3.2 and 2.34 -.

$$\begin{cases} \bar{\boldsymbol{k}}_{\boldsymbol{sp}} = \bar{\boldsymbol{k}}_{\boldsymbol{x}} + m\boldsymbol{G}_{\boldsymbol{e_1}} + n\boldsymbol{G}_{\boldsymbol{e_2}} \Rightarrow k_{sp} = k_x + mG_x + nG_y \\ k_x = \dfrac{2\pi}{\lambda}\sin\theta \end{cases} \tag{3.1}$$

$$k_{sp} \simeq \Re\{\bar{\boldsymbol{k}}_{\boldsymbol{sp}}\} = \Re\left\{\frac{\omega}{c}\left[\frac{\bar{\epsilon}_1\epsilon_2}{\bar{\epsilon}_1+\epsilon_2}\right]^{1/2}\right\} = \left[\left(\frac{2\pi}{\lambda}\sin\theta + m\frac{2\pi}{a_0}\right)^2 + \left(n\frac{2\pi}{a_0}\right)^2\right]^{1/2} \tag{3.2}$$

At normal incidence ($\theta = 0°$), the peak position, given by expression 3.3, can be deduced from expression 3.2 [27, 37, 38]. In this expression, a_0 is the slit periodicity, that is linearly related to the wavelength correspondent to the maximum intensity. A similar deduction can be done for a triangular array - also called hexagonal or diagonal square centred -, resulting expression 3.4 [27, 37, 38].

$$\lambda_{max_{square}} = \Re\left\{\left[\frac{\bar{\epsilon}_1\epsilon_2}{\bar{\epsilon}_1+\epsilon_2}\right]^{1/2}\right\} \times \frac{a_0}{|m\hat{x}+n\hat{y}|} = a_0\left(m^2+n^2\right)^{-1/2}\left[\frac{\epsilon_1'\epsilon_2}{\epsilon_1'+\epsilon_2}\right]^{1/2} \tag{3.3}$$

$$\lambda_{max_{tri}} = \Re\left\{\left[\frac{\bar{\epsilon}_1\epsilon_2}{\bar{\epsilon}_1+\epsilon_2}\right]^{1/2}\right\} \times \frac{a_0}{|m\hat{e}_1 + n\hat{e}_2|} = a_0\left(\frac{4}{3}\left(m^2+mn+n^2\right)\right)^{-1/2}\left[\frac{\epsilon_1'\epsilon_2}{\epsilon_1'+\epsilon_2}\right]^{1/2} \tag{3.4}$$

Whichever the geometry of the array and the value of θ, an expression for λ_{max} can be written as presented on expression 3.5, where b is a parameter that depends on the array geometry [27, 37, 38].

$$\lambda_{max} = \frac{a_0}{b}\left[\left(\frac{\epsilon_1'\epsilon_2}{\epsilon_1'+\epsilon_2}\right)^{1/2} - \sin\theta\right] \tag{3.5}$$

Moreover, the transmission intensity peak value, for circular holes, is given by expression 3.6, where C is a constant, h is the hole depth and a is the hole diameter. Thus, it is possible to relate expressions 3.3 or 3.4, with expression 3.6, such that increasing the periodicity, the peak intensity will increase too, until saturate in a value given by C [39, 40]. In order to consider expression 3.6 it must be assumed that surface plasmon modes are just on one side of the nanoantenna or, if they are on both sides they should be uncoupled.

$$I(h,\lambda_p,a) = C\,exp\left\{-\frac{4\pi h}{\lambda_{max}}\sqrt{\left(\frac{\lambda_{max}}{1.7a}\right)^2 - 1}\right\} \tag{3.6}$$

The transmission spectrum presents dips or minima, that are related to the Wood's anomaly, which was reported by Wood in 1902 [7, 8, 22, 27, 37]. The wavelength value associated to the intensity minimum occurs when the diffracted light arises parallel to the metal surface, which is equivalent to say that the wave vector component perpendicular to the surface, k_z, must be considered null, resulting in expression 3.7. Comparing minimum and maximum expressions, it is possible to verify that the wavelength value for the maximum should be higher than the minimum one.

$$\lambda_{min} = a_0\sqrt{\epsilon_2} \tag{3.7}$$

However, comparing theoretical values, expressions 3.3 and 3.4, with experimental values, the expressions are a valid first approximation, but a phase term imposed by the grating is neglected. This phase term depends on the hole shape or geometry leading to $k_{sp} = k_x + xG_x + yG_y + \frac{\arg(\tau)}{a}$ and to the general peak wavelength given by $\lambda_{max} = \Re\left\{\left[\frac{\bar{\epsilon}_1\epsilon_2}{\bar{\epsilon}_1+\epsilon_2}\right]^{1/2}\right\} \times \frac{a_0}{|x\hat{x}+y\hat{y}|+\frac{\arg(\tau)}{2\pi}}$ [22, 27, 37, 41]. This phase term, $\arg(\tau)$, describes the effect of the hole geometry on the effective dielectric function at the surface between the dielectric and the metal. According to experimental results, the peak value is higher for holes with higher area [41]. Of course, if it is compared a circular and a square hole, having both a characteristic dimension equal to a - diameter, on the case of the circular hole and the width, for the square -, the square has a greater area and peak intensity will be greater.

The change of the refractive index, associate to the dielectric constant, corresponds to a shift on the peak position, or in other words, the incident wavelength that corresponds to the maximum value of light intensity changes.

The most common way to design a biomedical or biological sensor based on EOT is illustrated on figure 3.1, where each side of the nanoantenna is in contact with a different material. One of these materials should be solid and will be the sensors substrate - with a dielectric function $\bar{\epsilon}_3$ -, where the metal nanoantenna is placed on the top - $\bar{\epsilon}_1$ -. Thus, samples in any physical state can be placed on the top and inside the nanoantenna's holes - $\bar{\epsilon}_2$ -. The transmission spectrum can have two different resonances - peaks -, corresponding to different surface plasmon polaritons modes, because each side of the metal surface has a different dielectric constant, the solid substrate and the sample.

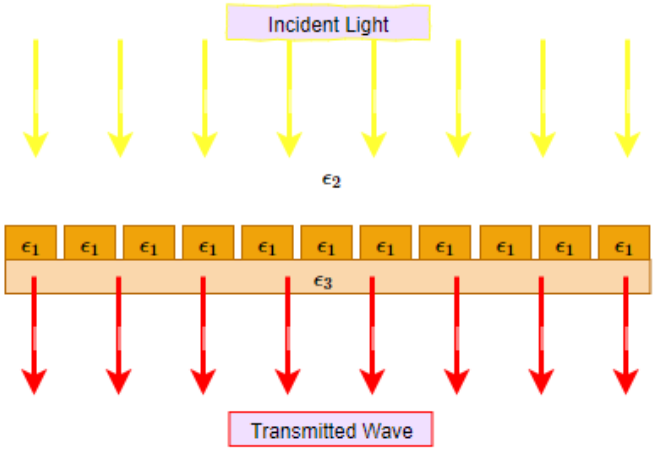

Figure 3.1: Topology of the EOT peak shift sensor.

The process to detect a biological identity in a biological sample begins with the placement of the sample on the sensor, followed by the immobilisation process, by the illumination of the sample with a perpendicular beam of light and the measurement of the transmission spectrum on the substrate side, using a spectrometer.

The type of light emitter depends on the application and namely on the wavelength band of the desired measurement, If the application demands a small wavelength band, a LASER - Light Amplification by Stimulated Emission of Radiation -, is usually a good choice. In some cases for a greater wavelength, if coherent light is not necessary, a LED - Light Emitter Diode -, or other types of emitters, as halogen lamps, can be good choices. The emitter should have an objective lens in order to adjust the incident power and to focus light into the sensor's active area and a polariser in order to guarantee that the incident electric field is parallel to the sensor.

Due to molecular absorption, the relative dielectric function value ($\bar{\epsilon}_1$) changes and its value can be determined by a weighted average of $\bar{\epsilon}(z)$, within the extension $\hat{z}$, as presented on expression 3.8 [22, 23].

$$\bar{\epsilon}_1 = \frac{2}{\hat{z}} \int_0^\infty \bar{\epsilon}(z) e^{-\frac{2z}{\hat{z}}} dz \tag{3.8}$$

If it is considered an effective absorption layer thickness of t_d, the aforementioned integral is only valid until this value. Thus, the modulus of dielectric constant variation can be associated to a variation of the complex refractive index $\Delta\bar{n}$, such that $\bar{\epsilon} = \bar{n}^2 = (n+ik)^2 \Leftrightarrow n = \Re\{\sqrt{\bar{\epsilon}}\}$, where n is the refractive index and k is the extinction coefficient (and not the wave number, here). When for $k > 0$ light is absorbed and there are losses, $k = 0$ there are no losses and when $k < 0$ there is the possibility of field amplification (when it is referred to the wave propagation k is the wave number however, when describing the material optical properties k is the extinction factor). Expression 3.9 shows the relation between a variation of the refractive index and the peak wavelength shift, where s_n is the sensitivity of the wavelength shift to the variation of the refractive index [23, 28].

$$\Delta\lambda_{max} = s_n \Delta n \left[1 - e^{-\frac{2t_d}{z}}\right] \tag{3.9}$$

Despite the fact that the previous formulation does not take into consideration medium properties as temperature or pressure, the variation of these properties has influence on the peak position and intensity. Thus, it is also possible to design a sensor to monitor this kind of variables [30]. Its topology remains the same, as presented on figure 3.1. The following formulation is done considering a region where the nanoantenna dielectric function is almost constant, leading simple analytical models. Nonetheless, in most devices the variation of both dielectric functions - dielectric and metallic -, should be considered, leading to a more complex formulation.

A model for the dependence of temperature and pressure of nanoantennas transmission spectrum was proposed by Kowalski, including a set of thermodynamic equations that were related to the Lorentz-Lorentz law, where the (effective) dielectric function of the dielectric, ϵ_2, changes [29, 30, 38], according to expression 3.10, where T is the temperature, P the pressure and C the material concentration.

According to Lorentz-Lorentz law, the refractive index and the dielectric function are related by expression 3.11, being C_0 a constant reference value calculated by expression 3.12, where ρ is the material density and, n_0 and ρ_0 are the reference values for a certain temperature and pressure [29, 30, 38]. The material's concentrations will remain constant, for the same sensor and consequently, the last term of expression 3.10 is null.

$$d\epsilon_2 = \frac{\partial\epsilon_2}{\partial T}|_{P,C}\, dT + \frac{\partial\epsilon_2}{\partial P}|_{T,C}\, dP + \frac{\partial\epsilon_2}{\partial C}|_{P,T}\, dC \tag{3.10}$$

$$\left[\frac{\epsilon_2 - 1}{\epsilon_2 + 2}\right] = \left[\frac{n_2^2 - 1}{n_2^2 + 2}\right] = C_0\, \rho \tag{3.11}$$

$$C_0 = \left[\frac{n_{2_0}^2 - 1}{n_{2_0}^2 + 2}\right] \left(\frac{1}{\rho_0}\right) \tag{3.12}$$

Likewise, the dependence of the density with pressure and temperature takes into account two tabulated values: the volumetric expansion coefficient, β, and the isothermal compressibility factor, k_T. Thus, the

density variation factor, $\phi = \frac{\rho}{\rho_0}$, expression 3.13, can be replaced on expression 3.11, leading to the relation expressed on 3.14 [29, 30, 38].

$$\phi = exp\left\{-\left[\beta(T - T_0) - k_T(P - P_0)\right]\right\} \tag{3.13}$$

$$n_2^2 = \epsilon_2 = \left[\frac{1 + 2C_0\rho_0\phi}{1 - C_0\rho_0\phi}\right] \tag{3.14}$$

Considering the overall transmission spectrum of the nanoantenna, it is possible to determine the position of the intensity peak by the expression 3.15, where θ is the incidence angle, a_0 the slit periodicity and b is a value related to the surface plasmon modes and array geometry [29, 30, 38]. In fact, this expression is very similar to expression 3.5, by replacing ϵ_2 for the expression that presents its variation with temperature and pressure.

$$\lambda_{max} = \frac{a_0}{b}\left[\frac{\epsilon_1'\left[\frac{1+2C_0\rho_0\phi}{1-C_0\rho_0\phi}\right]}{\epsilon_1' + \left[\frac{1+2C_0\rho_0\phi}{1-C_0\rho_0\phi}\right]} - sin(\theta)\right] \tag{3.15}$$

4

Structure Parameters Evaluation

Contents

4.1 Geometry Selection

In this chapter, 3D simulations of several nanostructures, using *COMSOL Multiphysics*, are going to be presented, using *COMSOL Multiphysics*.

Firstly, it is quite important to set a configuration that works as reference, in order to confront the obtained results with the reference ones. Thus, a nanostructure defined a dielectric, a nanoantenna and the substrate, as illustrated on figure 4.1 is taken as the reference. All the materials used on simulations have their dielectric functions presented on appendix A.

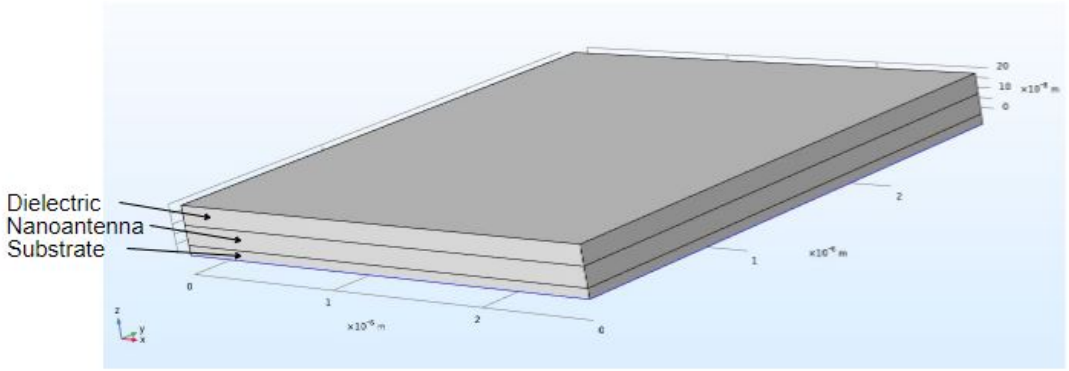

Figure 4.1: Topology of the simulated structure (axis framework on lower left corner).

In the simulated structure, the dielectric is always air, modelled by the Ciddor model stated on 1996. In this model, the extinction coefficient is null. The thickness of this layer is $200\,\mathrm{nm}$ counting from the substrate, and the air fills the holes, as illustrated on figure 4.2.

The nanoantenna is square arrayed and it is composed by circular holes, having a periodicity a_0 equal to $0.5\,\mu\mathrm{m}$, a thickness of $100\,\mathrm{nm}$ and a total number of 9 holes, forming a 3x3 array. Furthermore, the circular holes have a diameter of $d = 150\,\mathrm{nm}$.

The substrate is below the nanoantenna and its thickness has a reference value of $50\,\mathrm{nm}$.

Furthermore, all the external boundaries are totally absorbent, meaning that there is no reflection.

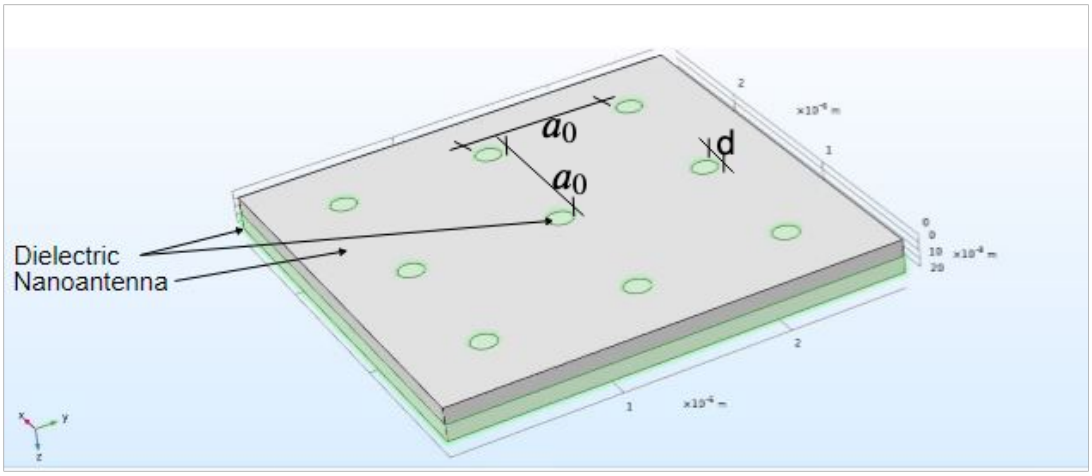

Figure 4.2: Observation of the nanoantenna dielectric holes (axis framework on lower left corner).

An electromagnetic wave with the electric field components, defined by a norm of $|E_0| = 1\,\mu\text{V m}^{-1}$, is generated on the top of the structure presented on figure 4.1 - that is on the external boundary of the dielectric medium -, and it is perpendicular incident on the nanoantenna, having the z axis opposite direction. Thus, on the generation port, this electric field was defined as $|E_x| = |E_y| = \frac{1}{\sqrt{2}}\,\mu\text{V m}^{-1}$ and $|E_z| = 0\,\mu\text{V m}^{-1}$.

All the simulations are done for 250 equidistant wavelength points, from $250\,\text{nm}$ to $1200\,\text{nm}$. The wavelength analysis is done using 4 probes. These probes analyse the square of the module of the maximum ratio between the electric field and the incident electric field, $|\frac{E}{E_0}|^2$. There is one domain probe for each material and one boundary probe to analyse the output radiation spectrum, which is the main goal of these simulations. The domain probes are useful to find the points on the domain where the aforementioned ratio is higher than one. Thus, even if the output spectrum - determined from the boundary probe results -, do not allow us to observe field amplification, it can be possible to verify the polaritons propagation, due to the field amplification, concluded by the domain probes. Although it is impossible to present all the results taken from the created simulation environment, it must be noted that for all the following simulations, after the nanoantenna screen, the data from the domains probes confirms the existence of field amplification, mainly on the interface dielectric-metal. One example of what can be seen is in figure 4.3. This is a good example, illustrative of the referred cases, with points presenting impressive gain values.

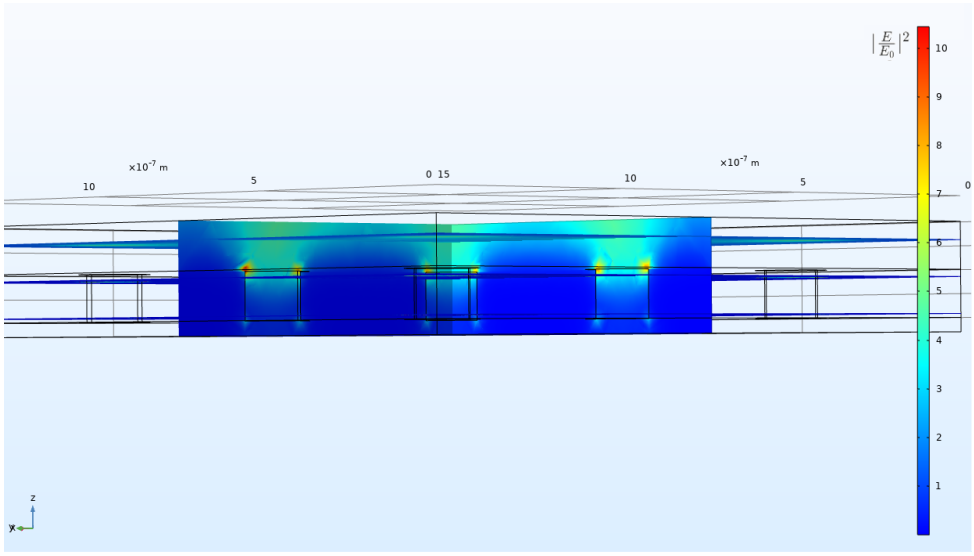

Figure 4.3: Observation of the generation and propagation of surface plasmon polaritons (axis framework on lower left corner).

Gold, silver, aluminium and copper are the chosen materials to the nanoantenna. Their dielectric functions are presented on appendix A. Gold and copper have very similar complex dielectric functions. The transition between the Drude and the interband regimes appears at approximately $2\,eV \sim 2.3\,eV$, *i.e.*, $530\,\text{nm} \sim 600\,\text{nm}$, and consequently these materials are used on applications on the red and near-infrared regions, according to the explanation provided on section 2.3. Silver is expected to be better than copper or gold on the optical region between $600\,\text{nm} \sim 800\,\text{nm}$, because its transition is above $3\,eV$ *i.e.*, at wavelengths smaller than $400\,\text{nm}$. But aluminium is considered the best among these materials if it is desired gain along all the visible region. In this region, aluminium has a dielectric function with a large negative real part, and it is used for wavelengths between $400\,\text{nm}$ and $650\,\text{nm}$. Gold and copper have a small imaginary part of its dielectric function along the visible and near-infrared regions, but their interband maximum makes them bad materials to be used on this region, due to the linear relation between Ohmic losses and dielectric imaginary part. Nonetheless, silver has higher dielectric function imaginary part module, being its interband maximum the way to diminish its relative value and, consequently, Ohmic losses. The aluminium case is pretty different. Aluminium has an almost null dielectric function imaginary part until $500\,\text{nm}$. After it, its value increases until a maximum located around $800\,\text{nm}$, making this material the worst one to be used on the red and near-infrared region applications [15, 16].

The selection of a metal does not depend uniquely on the optical properties. It is also important to consider the chemical stability of these metals, in order to know if the metal maintains the optical properties and consequently, the output spectrum, along time. In silver and copper oxides and sulfites can quickly be formed under ambient conditions [15, 16]. In aluminium, surface oxidation results in Al_2O_3. Considering the chemical stability, gold is known to have an excellent stability [15, 16].

On the following sections, the simulations are presented and analysed. In section 4.2, the substrate is air. The behaviour of the antenna made with each one of the four metals discussed above is observed. In order to test the parameter influence on the output spectrum, periodicity, hole diameter, thickness and the number of holes will be swept. In section 4.3, some of the simulations of section 4.2 are repeated, with a substrate formed by a solid dielectric, silicon dioxide - SiO_2 -.

The solid dielectric SiO_2, commonly known as quartz, has a great advantage, because it does not influence the output spectrum, since its transition between the Drude and the interband regime is around $0.15\,eV$ - $8000\,\text{nm}$ -, as it is observable on appendix A. Furthermore, it is a stable material, even at high temperatures, suitable to guarantee some protection and robustness to the structure.

The complex dielectric function of quartz has a null imaginary part along all the simulated range and a real part with small variations. Thus, this substrate will not create a new resonant peak in the simulated range. However, comparing the results of structures in sections 4.2 and 4.3, it is expected a decrease of the intensity in section 4.3, due to the increase of the dispersion losses, resulted from the substitution of air by quartz.

On figure 4.4 is illustrated a simulated output spectrum. As expected the spectrum presents a resonant peak. The gain region is defined as a wavelength band or a union of wavelength bands where the module of the ratio between the electric field and the incident electric field is higher than one. In figure 4.4 is shown the square of the field gain or in other words the radiation intensity gain. The peak maximum is called maximum gain only if this peak corresponds to a gain situation. Some sensors need a gain region, others do not. Thus, the gain region is not a necessary condition to develop a sensor. Each application has its own specifications that can be accomplished tuning the nanostructure parameters.

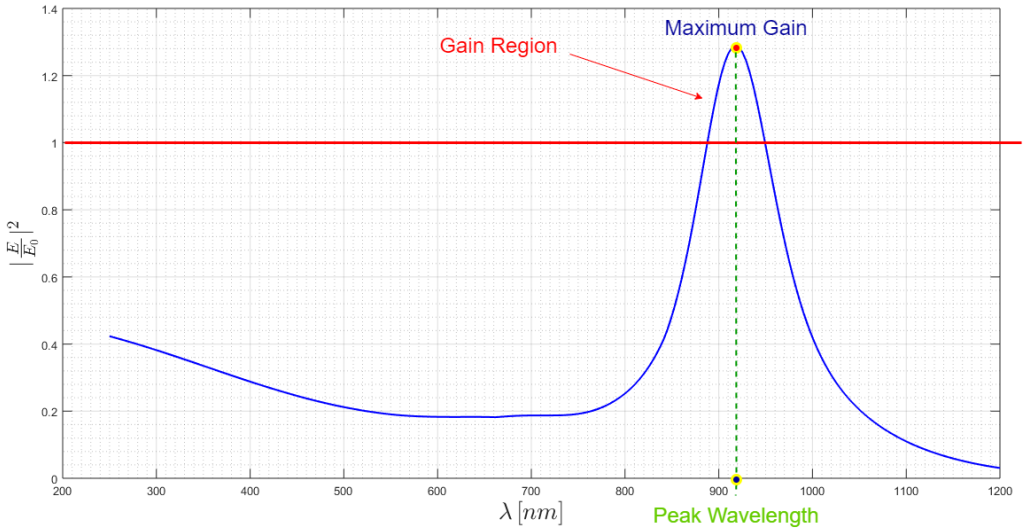

Figure 4.4: Example of a simulated optical response.

4.2 Air-Metal-Air

In this section, the influence of each structure parameter on the output spectrum is analysed, when the nanoantenna dielectric substrate is air.

The simulations results are divided by the parameter variation. The first parameter analysed is the periodicity, a_0. This variation considers four different values: $0.3\,\mu m$, $0.5\,\mu m$, $0.7\,\mu m$ and $0.9\,\mu m$. Then, the hole diameter is varied however, considering that the nanostructure periodicity remains constant and equal to $0.5\,\mu m$, and that the hole diameter will not be higher than the periodicity. As observed on figure 4.2, if it happen the structure will not be correctly defined, because $d < a_0$ should be satisfied. Thus, the hole diameter varies between $50\,nm$ and $200\,nm$, with a variation step equal to $50\,nm$, leading to the extraction of four different results. After that, the nanoantenna thickness will be swept, taking three different values: $50\,nm$, $100\,nm$ and $150\,nm$. The last parameter evaluated in this section is the number of holes. As the nanoantenna is square arrayed, six different arrays topologies will be tested, sweeping the number of lines and columns of the array: 3x3, 5x3, 7x3, 7x5, 5x5 and 7x7.

4.2.1 Periodicity Sweep

The first structure parameter that is swept is its periodicity. The first simulation results are presented on figure 4.5, for a silver nanoantenna. It is possible to observe that despite this variation, the maximum peak remains more or less at the same wavelengths. According to expression 3.5, the maximum peak wavelength should have a linear dependence with the structure periodicity. Although expression 3.5 is spread across the literature, it was already shown that it is a rough approximation. The main fault is the fact that dielectric function does not vary with the frequency or wavelength. Thus, an estimation of the peak intensity can be done using expression 3.6, however this expression should not be used on periodicity sweeps, regarding the previously statement.

In figure 4.5 it is observed that the peak intensity value decreases as the periodicity increase, having reached a maximum intensity peak for $a_0 = 0.3\,\mu m$, where the output optical gain is approximately 3.33 - for an incident wavelength of $807\,nm$ -. Even though, the minimum value of the gain maximum is 1.31 - for an incident wavelength of $827\,nm$ and a periodicity $a_0 = 0.9\,\mu m$ -.

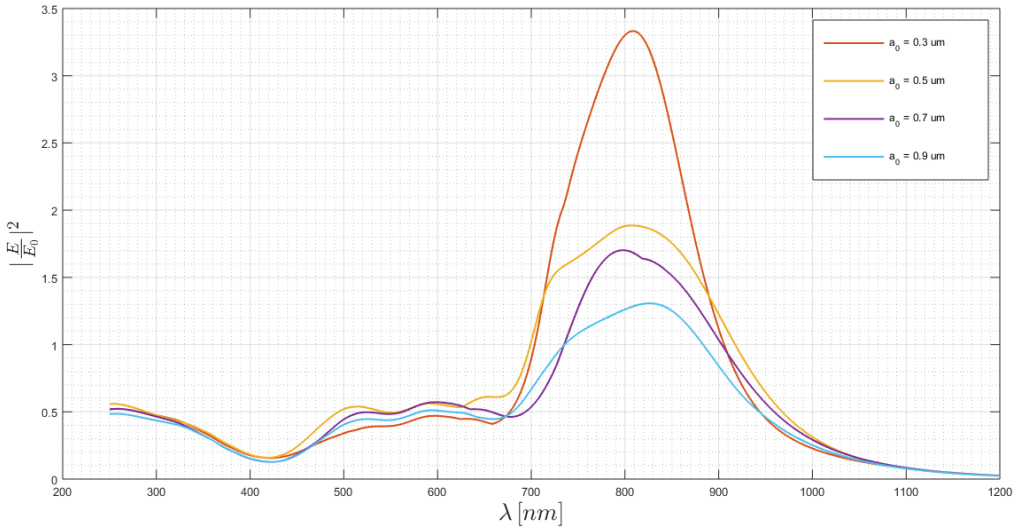

Figure 4.5: Periodicity sweep on a silver nanostructure with an air substrate.

After it, a gold nanoantenna is simulated and its results are illustrated on figure 4.6. Here, it is possible to take the same conclusion as it was taken for the silver simulations: when the periodicity increases, the peak intensity diminish and the peak wavelength keeps around the same value. In this case, when $a_0 = 0.3\,\mu\text{m}$ the maximum optical gain is 1.28 - for an incident wavelength of $918\,\text{nm}$ -, and for $a_0 = 0.9\,\mu\text{m}$, but the minimum value of the maximum gain is 0.88 - for an incident wavelength of $929\,\text{nm}$ -. In this case, $a_0 = 0.9\,\mu\text{m}$, leads already to a response without any gain region. However the existence of an output resonant spectrum reveals the propagation of polaritons on the surface.

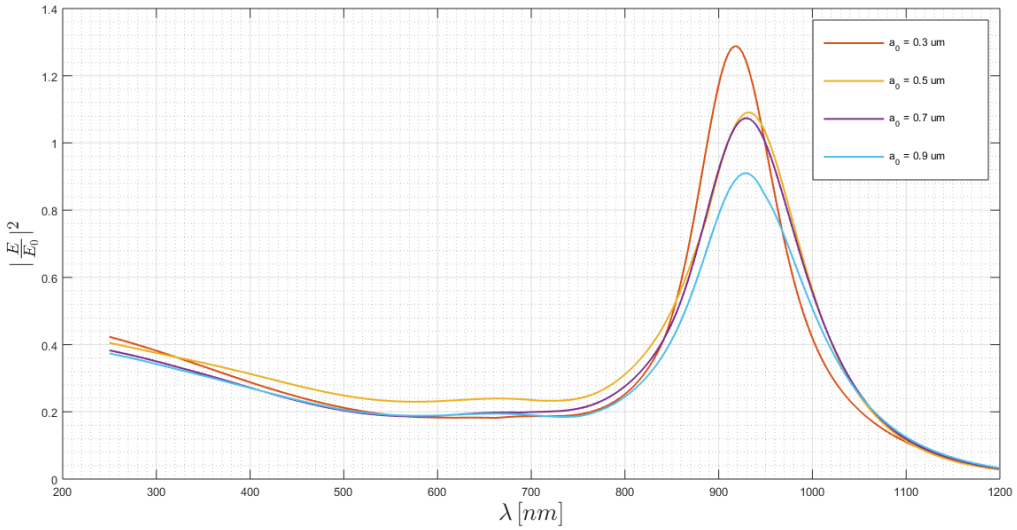

Figure 4.6: Periodicity sweep on a gold nanostructure with an air substrate.

Stepping forward, the next case is the simulation of the copper nanoantenna. The response, presented on figure 4.7, is similar to the gold one. However, none of the simulations presents an optical response with gain. Further tests will allow us to understand that it is possible to have gain regions with a copper nanoantenna. On the other hand, the copper behaviour seems to be different from gold and silver, because there is not a linear dependence between the resonant peak and the periodicity, a_0, in the considered interval for a_0. In the interval between $a_0 = 0.3\,\mu m$ and $a_0 = 0.7\,\mu m$ the maximum gain is almost constant, only for $a_0 = 0.9\,\mu m$ there is a small decrease.

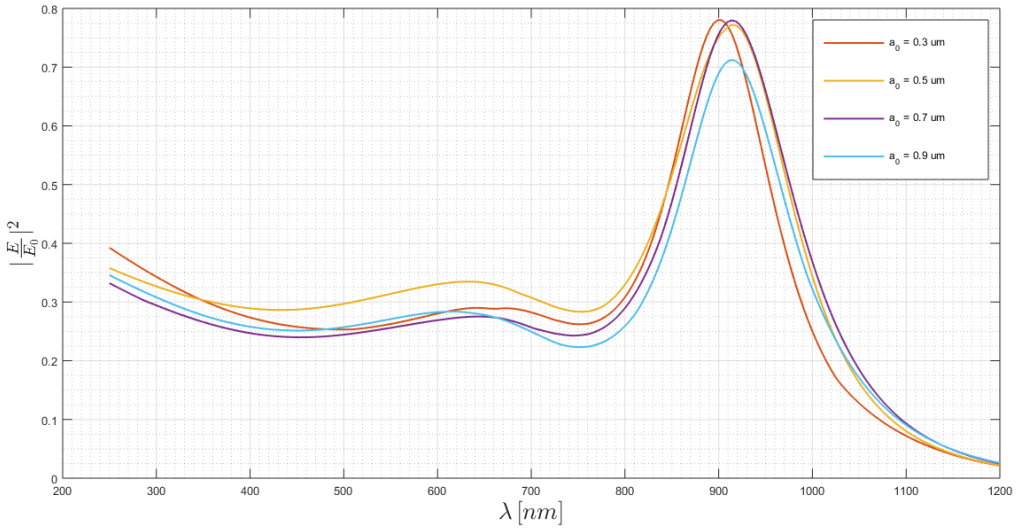

Figure 4.7: Periodicity sweep on a copper nanostructure with an air substrate.

In these simulations, the maximum achieved gain is around 0.78, which is reach both for $a_0 = 0.3\,\mu m$ - for an incident wavelength of $902\,nm$ -, and for $a_0 = 0.7\,\mu m$ - for an incident wavelength of $914\,nm$ -.

Last, but not the least, the simulation results for an aluminium nanoantenna are presented on figure 4.8. As previously referred, due to a completely different complex dielectric function characteristic, the aluminium response is different from the obtained with the other three metals. The aluminium optical response can be tuned to allow amplification in the visible region and to present great attenuation in the infrared wavelengths. It is possible to observe that both $a_0 = 0.3\,\mu m$ and $a_0 = 0.5\,\mu m$ allow to have a gain region capable to amplify almost all the visible region, reaching maximum gain values around 1.23 - for an incident wavelength of $551\,nm$ -, and 1.29 - for an incident wavelength of $391\,nm$ -, respectively. Nonetheless, the aluminium optical response for $a_0 = 0.3\mu m$ seems to have a larger gain region.

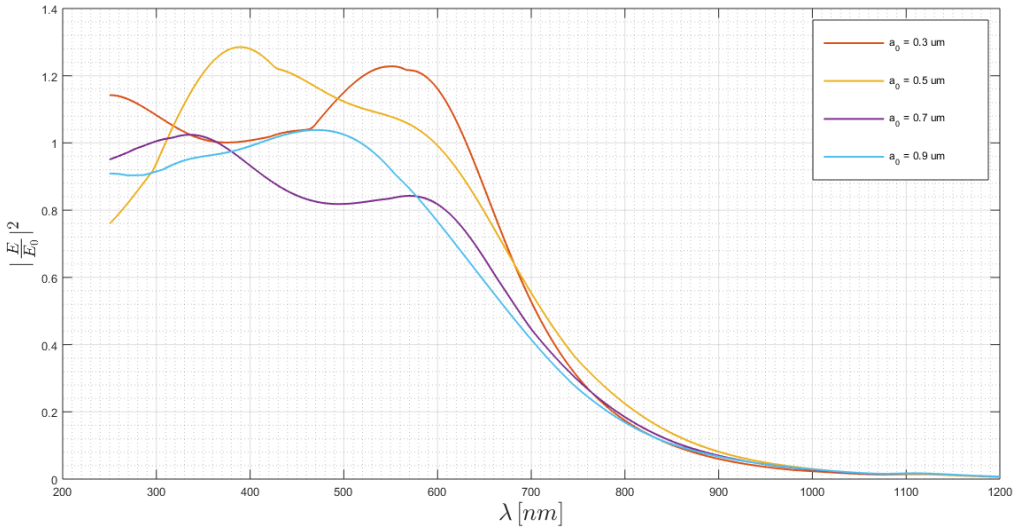

Figure 4.8: Periodicity sweep on an aluminium nanostructure with an air substrate.

The main conclusion from this sweep is that the maximum intensity peak wavelength does not depend linearly on the periodicity. Considering the values of $0.3\,\mu m$, $0.5\,\mu m$, $0.7\,\mu m$ and $0.9\,\mu m$, there are materials where the peak value decreases as the periodicity increase - silver and gold -, and other where no rule seems to be valid - copper -. The aluminium is here on other category, because whereas silver, gold and copper have a well defined peak and bandwidth, working almost as a band-pass filter in this frequency range, aluminium can work as a high-pass filter, for this specific range. Despite its response analysis can be done focusing on the peak values, it is better to do it spotlighting the amplification ripple - response smoothness of the gain region -, and the gain/attenuation difference between the gain region and the other wavelengths that must be attenuated. Depending on the application, these specifications can be given and the structure can be tuned in order to accomplish it.

4.2.2 Hole Diameter Sweep

In this section the defined structure is simulated considering the variation of the hole diameter from $50\,nm$ to $200\,nm$, using a step variation of $50\,nm$. Now, expression 3.6 can be used to compare optical responses, since all the parameters are constant except the hole diameter. According to this expression, when the hole diameter increases the intensity peak increases.

On the silver simulations set, illustrated on figure 4.9, the previous statement is verified. In addition, it is verifiable that the maximum peak wavelength varies. As the hole diameter increases, red-shifts occur.

What is also quite impressive is that the minimum region, at wavelengths around $430\,nm$, for hole diameters of $50\,nm$ and $100\,nm$ is almost constant. However, for hole diameters greater than $100\,nm$ the wavelength of the minimum shifts to a higher wavelength. Beyond that, when the hole diameter

increases, the peak value increases too, the peak wavelength is higher, the wavelength of the minimum is equal or higher and the transition region between the minimum and the maximum intensity peak becomes larger, a consequence of a smaller shift of the minimum than the shift of the peak maximum. The gain region is increased.

A gain of 2.77 is obtained for $d = 200\,\text{nm}$ - for an incident wavelength of $960\,\text{nm}$ -, and a only a ratio of 0.19 is observed for $d = 50\,\text{nm}$ - for an incident wavelength of $502\,\text{nm}$ -. In this last situation, the optical response leads to an attenuation of approximately $12\,\text{dB}$ between intensity values associated to the wavelengths of $960\,\text{nm}$ and $502\,\text{nm}$.

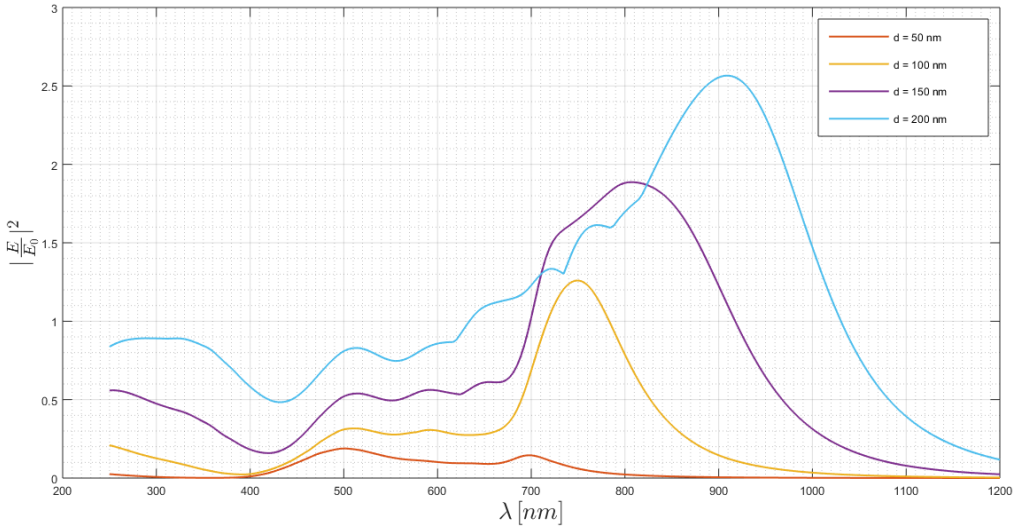

Figure 4.9: Hole diameter sweep on a silver nanostructure with an air substrate.

The same statements are true when analysing the gold and copper behaviour, illustrated, respectively on figures 4.10 and 4.11. Once again, it is obvious that both materials have similar behaviours when the hole diameter changes. However, the copper optical response exhibits lower intensity peaks. For $d = 200\,\text{nm}$, a gold nanoantenna presents a maximum gain of 1.96 - for an incident wavelength of $971\,\text{nm}$ -, whereas a copper one has a response maximum of 1.53 - for an incident wavelength of $956\,\text{nm}$ -.

On the other hand, it is observable that copper response is more sensitive to the hole diameter sweep. For $d = 50\,\text{nm}$ and $d = 100\,\text{nm}$ the output electromagnetic field is practically null, due to higher dispersion and Ohmic losses, in almost all the range for the copper nanoantennas whereas, on the gold nanoantenna it is still possible to see the resonant peak. As previously seen and discussed, for $d = 150\,\text{nm}$ - the reference structure geometry with a gold nanoantenna -, presents a tiny and narrow gain region in comparison with a no gain behaviour obtained for copper. In addition, the peak shift is visible for both materials, the hole diameter increases, the wavelength shift for the red occurs.

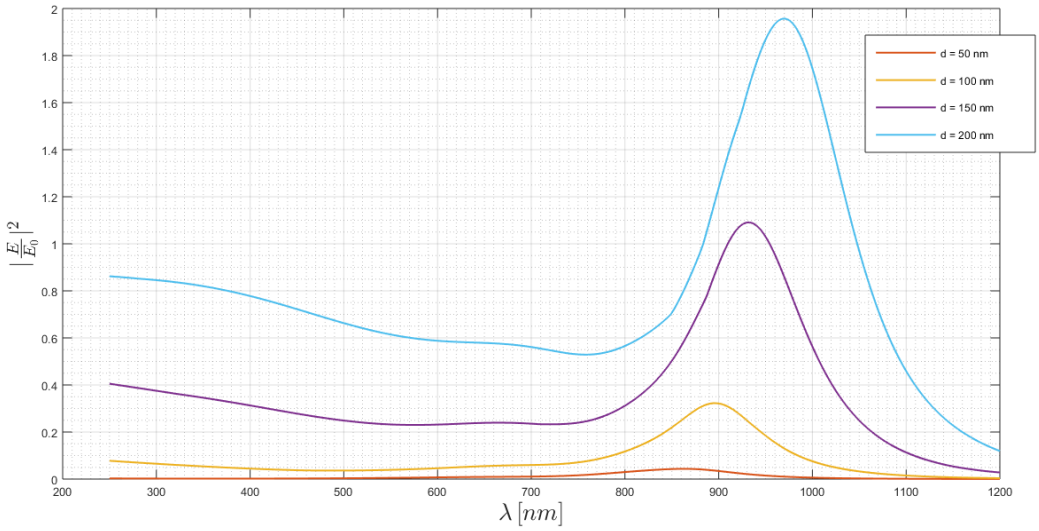

Figure 4.10: Hole diameter sweep on a gold nanostructure with an air substrate.

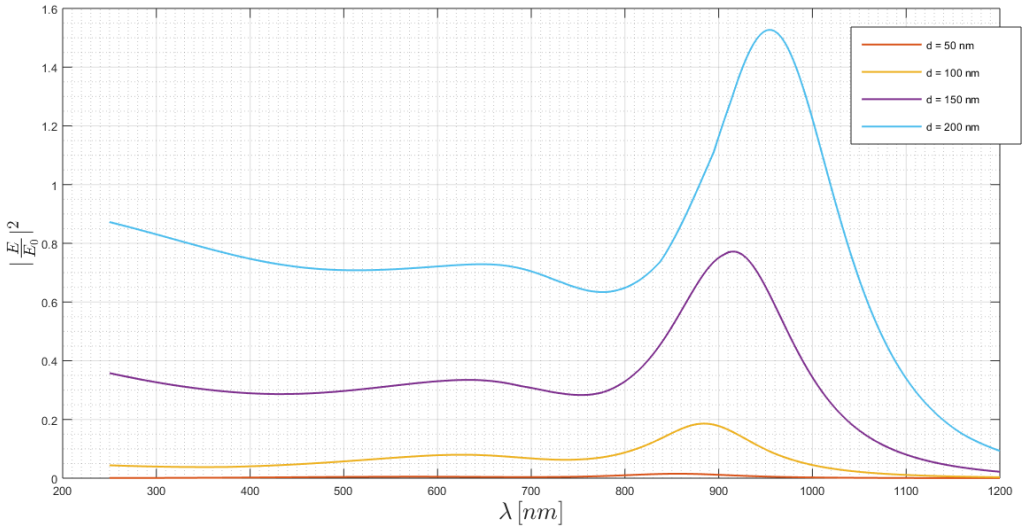

Figure 4.11: Hole diameter sweep on a copper nanostructure with an air substrate.

The aluminium nanoantenna optical response is presented on figure 4.12, where the gain increases with the hole diameter, such as expected. Furthermore, the gain region becomes larger, expanding to both spectral sides, despite it grows more to the red-side, it also stretch to the violet-side. Thus, it is possible to tune the desired wavelength range to amplify. The highest gain, 1.75, was obtained for $d = 200\,\text{nm}$ - for an incident wavelength of $651\,\text{nm}$ -, and for $d = 50\,\text{nm}$ the output electromagnetic field is practically null for the simulated band.

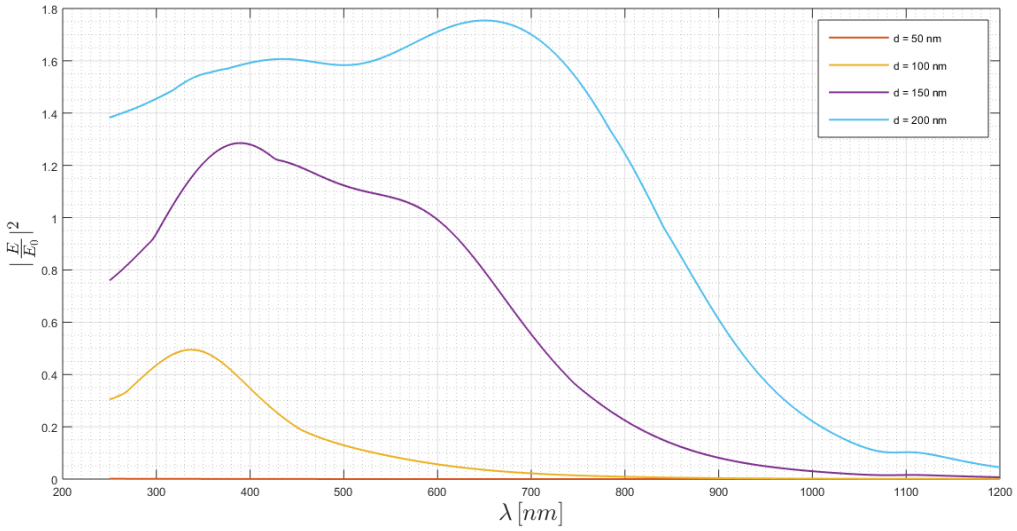

Figure 4.12: Hole diameter sweep on an aluminium nanostructure with an air substrate.

To sum it up, an adjustment done on the hole diameter allows to increase or decrease the output spectrum, within a certain wavelength range. Although the intensity peak can decrease a lot, when varying the hole diameter, it can be adjusted the value of other parameter to rise it. Nonetheless, it is important to note that, due to the computational effort limitation, the maximum value of d was limited to $d = 200\,\text{nm}$. A greater range of values could be useful, to know what is the diameter value for which the intensities start to decrease, with the diameter increase, leaving the condition of subwavelength structure.

4.2.3 Nanoantenna Thickness Sweep

The nanoantenna thickness sweep is analysed in this section. Here, it is very important to refer again that the nanoantenna is inside the dielectric medium. The dielectric medium has a thickness of $200\,\text{nm}$ and so, when the nanoantenna thickness is varying, it is also varying the air thickness. This is an important statement, because all the conclusion that can be taken will continue to be based on the assumption that the distance between the port - where the electromagnetic wave is generated -, and the nanoantenna rear, which is in contact with the ”substrate” remains constant.

On figure 4.13 the silver behaviour is presented. The decrease of the nanoantenna thickness, increases the peak and a red-shift of the peak wavelength occurs. The maximum achieved gain was 2.65 for $t = 50\,\text{nm}$ - for an incident wavelength of $918\,\text{nm}$ -.

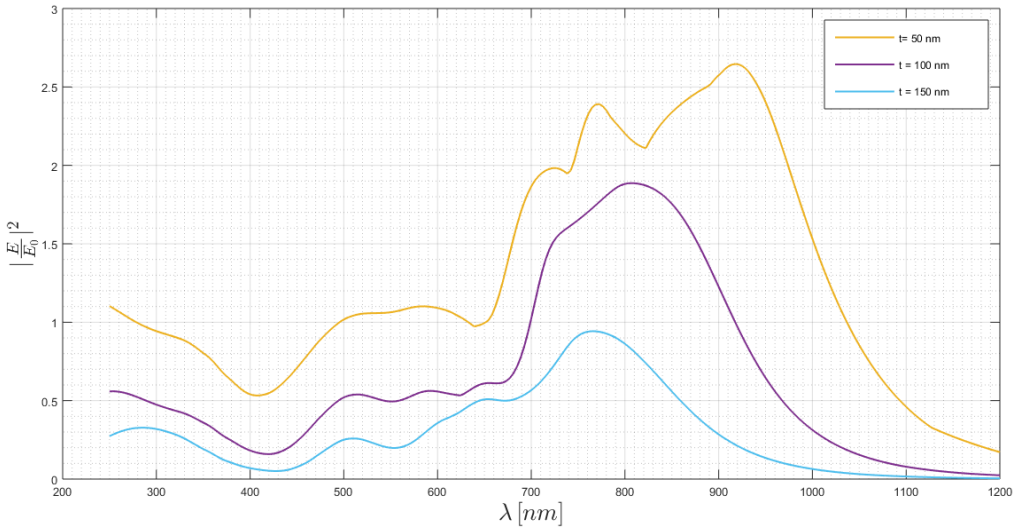

Figure 4.13: Nanoantenna thickness sweep on a silver nanostructure with an air substrate.

The same behaviour is observed in the gold and copper simulations, presented respectively on figures 4.14 and 4.15. Once again, it is suggested that both characteristic responses are similar, in spite of the sweep, registering a maximum gain of 2.18 - for an incident wavelength of $975\,\mathrm{nm}$ -, for the gold nanoantenna in comparison with 1.94 - for an incident wavelength of $956\,\mathrm{nm}$ -, with a copper one.

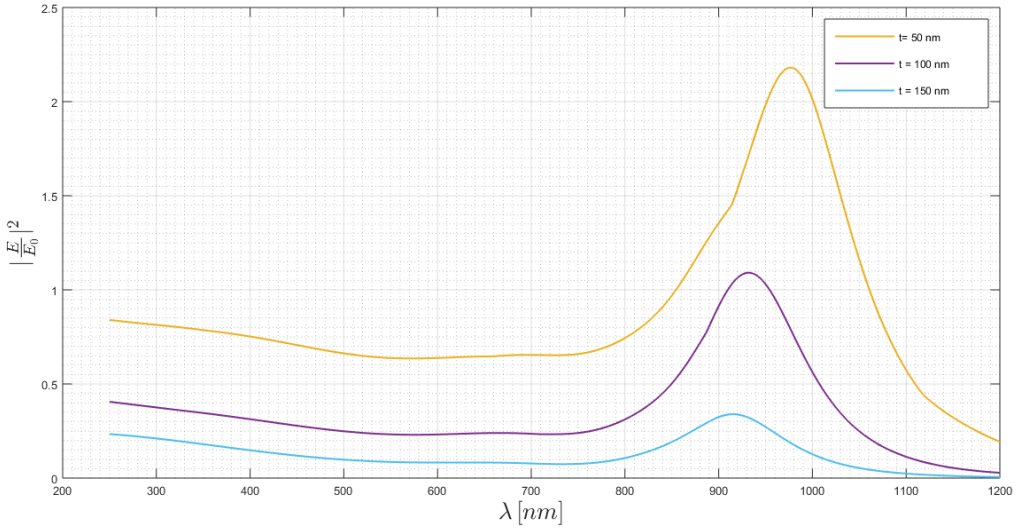

Figure 4.14: Nanoantenna thickness sweep on a gold nanostructure with an air substrate.

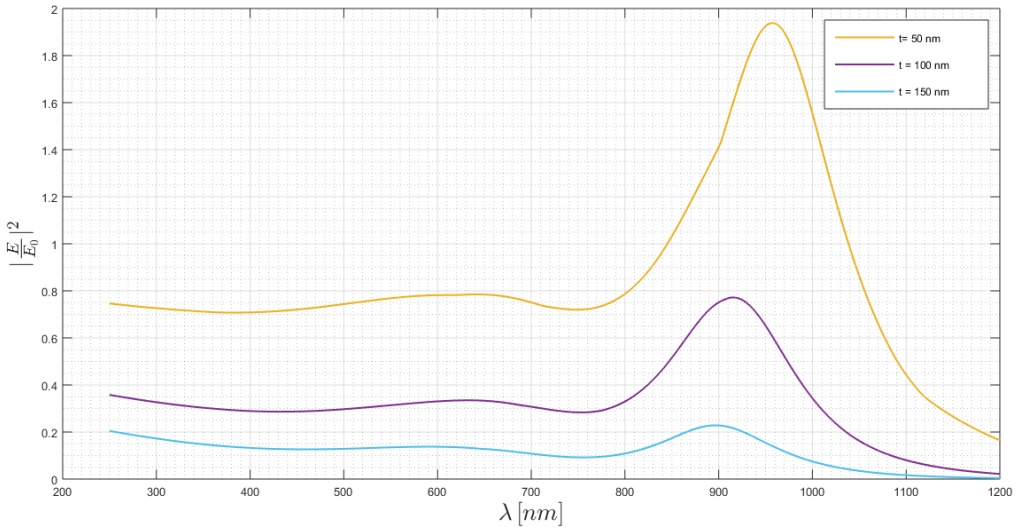

Figure 4.15: Nanoantenna thickness sweep on a copper nanostructure with an air substrate.

On the aluminium spectrum it is quite evident that as increasing the thickness, a flatter gain region will be created. However, it is also obvious that the intensity maximum will be lower. Thus, it is an important advantage the tuning possibility, if it is needed a flatter region, using the variation of other parameters to increase the gain and push this region to a higher intensity peak value. Furthermore, analysing these curves, they seem to reveal a blue-shift when the structure thickness is increased.

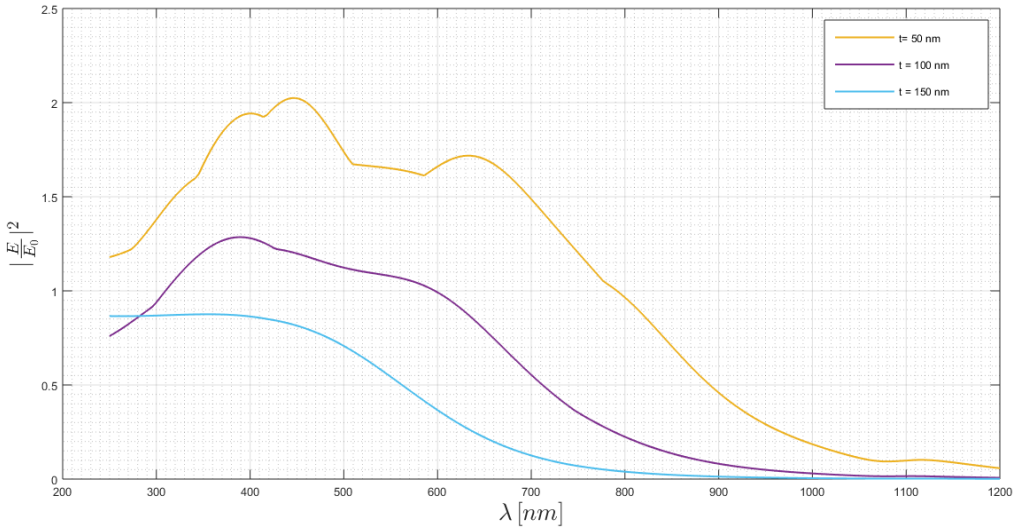

Figure 4.16: Nanoantenna thickness sweep on an aluminium nanostructure with an air substrate.

To conclude the study of this parameter influence on the output spectrum, it is stated that the thicker the nanoantenna is, the lower the maximum intensity peak will be, due to the increasing of dispersion

losses - which are proportional to the propagation length -. Associated to this peak decay is a wavelength shift to the violet and ultra-violet region - a blue-shift -. Moreover, the aluminium optical response becomes flatter, in the gain region, when its thickness increases.

This last conclusion has an enormous importance, because both thickness and hole diameter of an aluminium made nanoantenna can be adjusted together to create a flatter gain region, *i.e.*, use the thickness to smooth it and the hole diameter to improve the gain. Further, the hole diameter increasing mainly leads to a red-shift - or at least a predominant expansion of the gain region to the red-side of the spectrum -, whereas the nanoantenna thickness leads to a blue-shift so that, the band wavelength of the gain can also be adjusted.

Nonetheless, this conclusion is stated assuming that the structure parameters and their influence on the optical response are independent, or in other words if tuning more than one parameter, the result is the sum of the spectrum variations that satisfies each independent tuning .

4.2.4 Number of Holes Sweep

In this section it is considered the variation of the number of holes which composes the nanoantenna. If the holes in the metal are disposed according a squared lattice, it is the number of lines and columns that change. For each metal, six different topologies are simulated, considering arrays of 3x3 - 9 holes -, 5x3 - 15 holes -, 7x3 - 21 holes -, 7x5 - 35 holes -, 5x5 - 25 holes -, and 7x7 - 49 holes -. In these simulations, several other geometrical aspects are imposed to the nanoantenna, such as the different position of the nanoantenna centre - in a 3x3 array the centre is at the centre of a hole -, and the possibility of increasing the number of adjacent holes - in a 3x3 array only the centre one has holes in its front, back, left, right and in all the 4 diagonals directions -.

On figure 4.17 are the simulations results with silver. It is possible to observe that the overall spectrum does not vary a lot. The most visible variation happens on the minimum before the peak - the local minimum due to the Wood's anomaly -, where its value and shape change. However, no rule seems to be able to express this variation, since the spectrum shape changes too.

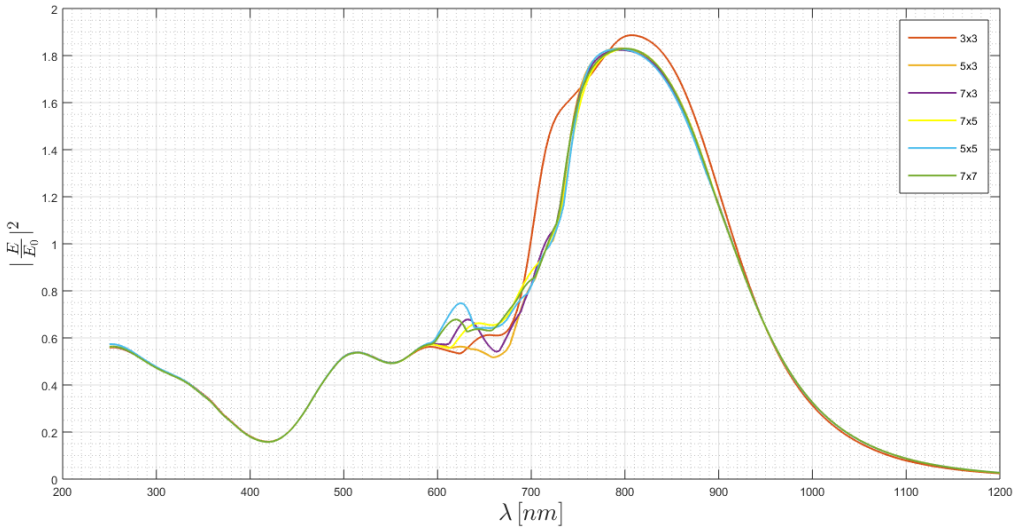

Figure 4.17: Sweep of the number of holes that composes a silver nanostructure with an air substrate.

The nanostructure simulations with gold are presented on figure 4.18. Considering these simulations, it is quite impressive that the optical response with a gold nanoantenna is not modified when the number of holes is varying. Thus, it is possible to conclude, based on these values, that the optical response is almost independent on the number of holes of a squared nanoantenna of gold.

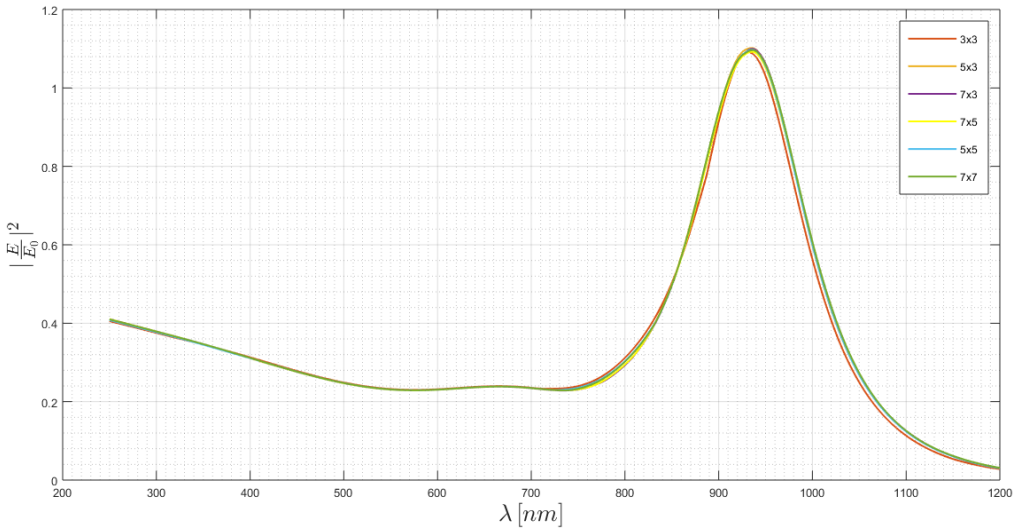

Figure 4.18: Sweep of the number of holes that composes a gold nanostructure with an air substrate.

Although gold and copper have similar optical responses, their behaviour can be different when the parameters values are modified. Whereas the gold response is almost independent on the number of holes, with the copper nanoantenna the value of the resonant peak depends on it, as verified on figure

4.19.

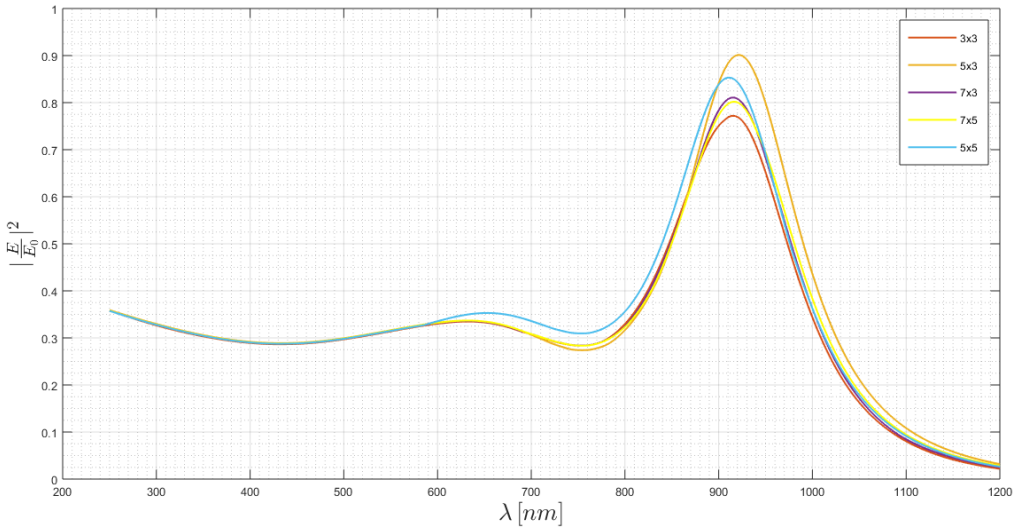

Figure 4.19: Sweep of the number of holes that composes a copper nanostructure with an air substrate.

The behaviour of aluminium nanoantenna is visualised on figure 4.20. Based on this figure, it is possible to conclude that there are not quite significant variations on the aluminium optical response.

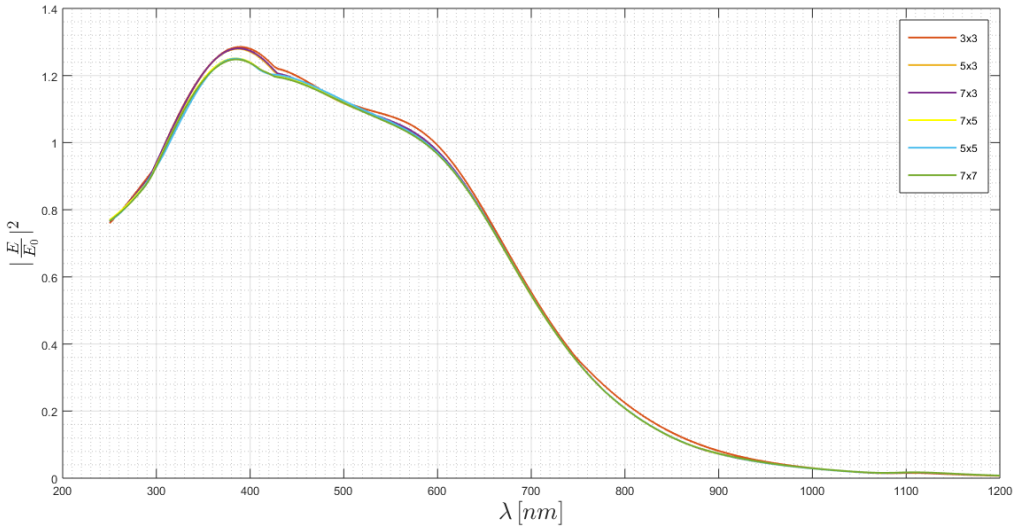

Figure 4.20: Sweep of the number of holes that composes an aluminium nanostructure with an air substrate.

The main conclusion taken based on these data sets is that the gold and the aluminium spectra are almost independent of the number of holes in the nanoantenna, whereas in copper, the resonant peak value and the peak wavelength have a small variation. The silver response differs on the Wood's

minimum region.

When the number of holes increase, the structure dimensions increase too, and so, based on the last statement, if the manufacture can not produce a small device as the ones presented here, on the gold or aluminium structures, the device dimensions can increase, by increasing the number of holes without having a trade-off on the output response.

It is quite important to refer that a 5x3 or a 3x5 array is the same, because the incident electromagnetic field is orthogonal to the structure screen and its magnitude is uniformly distributed for the other components. Thus, only one of these situations is presented on the figure. Furthermore, three numbers are used - 3, 5 and 7 -, in all of their combinations in order to show the optical responses when one or both dimensions - length and width: x and y directions -, are expanded.

4.3 Air-Metal-Substrate

The next step is the placement of a solid substrate underneath the nanoantenna, replacing air by quartz and creating an air-metal-quartz structure.

However, only gold and aluminium will be tested on this topology. First, gold not only because its optical response can be easily tuned in order to reach some specifications, but also due to the fact that it is the only metal that is chemically stable, as previously mentioned. On the other hand, aluminium is also chosen because its optical response is different from the response of the other analysed metals and, therefore an aluminium nanoantenna have different applications.

In order to compare the results of this section with the results of the previous one, the simulations are done by varying the same parameters, in the same ranges. Thus, for both metals, the structure periodicity, the hole diameter and the nanoantenna thickness values are swept. The variation of the number of holes is not tested here, because these two metals are the ones whose spectra seem to be independent on it. This decision is based on the fact that the quartz substrate will not have a huge influence on the spectra - since its transition between the Drude's and the interband regime is far away of the simulated wavelength range -, except on the decrease of the intensity peak value, due to the increase of dispersion losses, associated to a higher refractive index, n, and consequently of the real part of the dielectric function, ϵ'. Then conclusions about the substrate placement can be taken.

In addition, the substrate thickness is also analysed, making a sweep from $20\,\mathrm{nm}$ to $50\,\mathrm{nm}$, with a wavelength step of $10\,\mathrm{nm}$, in order to conclude about this structure parameter.

The optical signal radiation, at the boundary probe will be less intense with the quartz substrate comparing to the case of air, as previously explained. Despite the fact that these nanostructures can exist without a solid substrate - in an dielectric-metal-dielectric topology, for instance having a support frame on the horizontal plan and the nanoantenna orthogonal to it -, the solid substrate must be used

in order to give a better protection to the device. Furthermore, the substrate can be useful to convert the optical signal into an electrical signal. Thus, the substrate would act as part of a photodetector, that converts photons flux into electrons flux.

4.3.1 Periodicity Sweep

First, the gold nanoantenna was simulated and its results are presented on figure 4.21. Comparing this figure with figure 4.6, the peak values decrease, due to greater losses with the quartz substrate. The complex refractive index of quartz has a real part greater than that of air, and both have a null extinction factor. This implies a null imaginary part of the dielectric function of air and quartz, and a real part equal to the square of the refractive index value.

Generically, for each periodicity value, the inclusion of this substrate creates a spectral red-shift and a decay on intensity ratio values, mainly on the maximum gain. Taking as example the situation for a structure periodicity of $a_0 = 0.3\,\mu\text{m}$, where for both structures the highest gain value is reached, the variation of the peak wavelength was around $45\,\text{nm}$ -, $918\,\text{nm}$ with air and $963\,\text{nm}$ with quartz -, and the maximum gain has a relative variation of approximately 49% -, from 1.29 without air to approximately 0.66 considering quartz -.

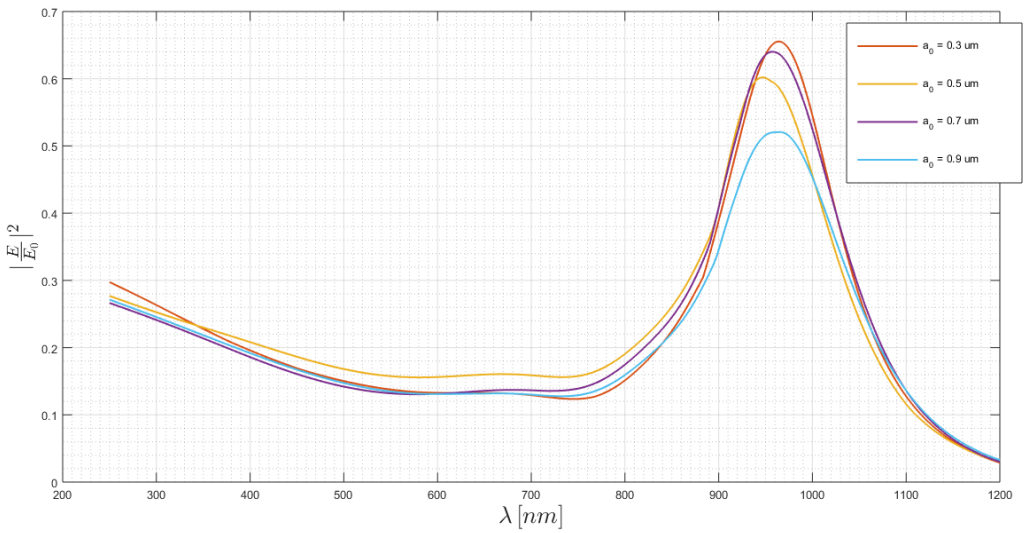

Figure 4.21: Periodicity sweep on a gold nanostructure with a quartz substrate.

The same conclusions can be taken for the aluminium made nanoantenna, whose results are on figure 4.22. Based on the comparison between this figure and figure 4.8, it is possible to observe a drop on the intensity ratio values along all the simulated range, obtaining a spectrum without a gain region.

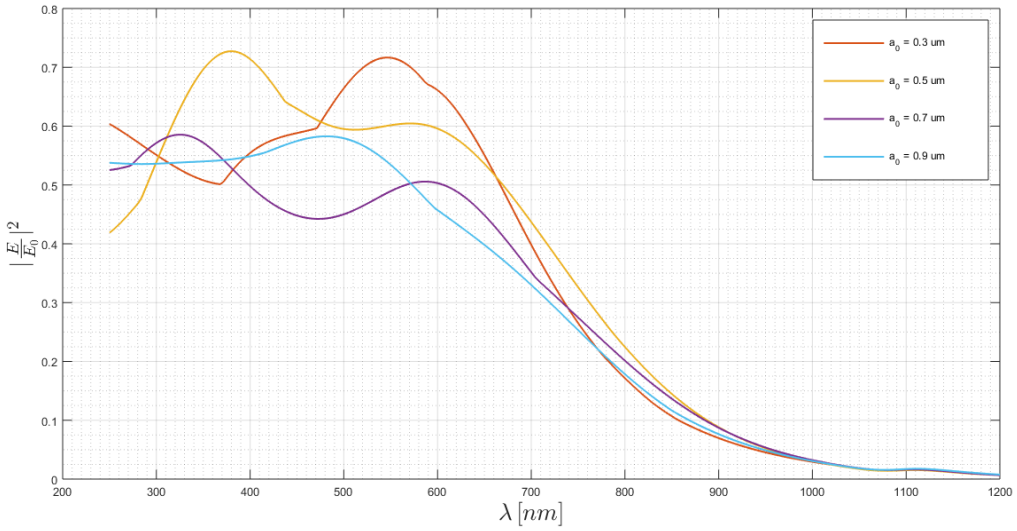

Figure 4.22: Periodicity sweep on an aluminium nanostructure with a quartz substrate.

Considering these results, the inclusion of a quartz substrate imposes a small red-shift and a decrease of the intensity values along all the spectrum, on the gold nanoantenna. On the aluminium nanoantenna, the intensity drop is also verified, but the peak shift seems not to have a specific rule.

4.3.2 Hole Diameter Sweep

The results of the hole diameter sweep are on figures 4.23 and 4.24, respectively for the gold and aluminium nanoantenna. Based on these figures, the decrease on the intensity caused by the quartz substrate in relation to the air substrate is also verified, having the same order of magnitude of the previously analysed structure.

However, on the gold spectra this parameter can be used to shift the output spectrum within a certain wavelength range or to increase the maximum gain, by increasing the hole diameter. On the aluminium structure the intensity values increase too, with the increasing of the hole diameter and, consequently the gain region expands however, more to the red-side than to the blue-side.

In addition, it is also noticeable that for diameters below $d = 100\,\text{nm}$ the spectra values are small in this wavelength band, and for these cases no applications are foreseen.

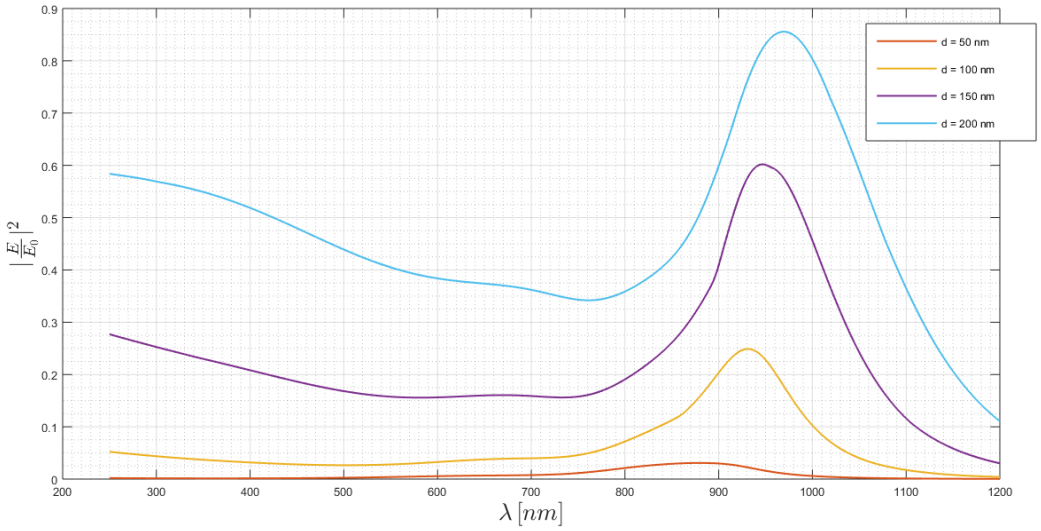

Figure 4.23: Hole diameter sweep on a gold nanostructure with a quartz substrate.

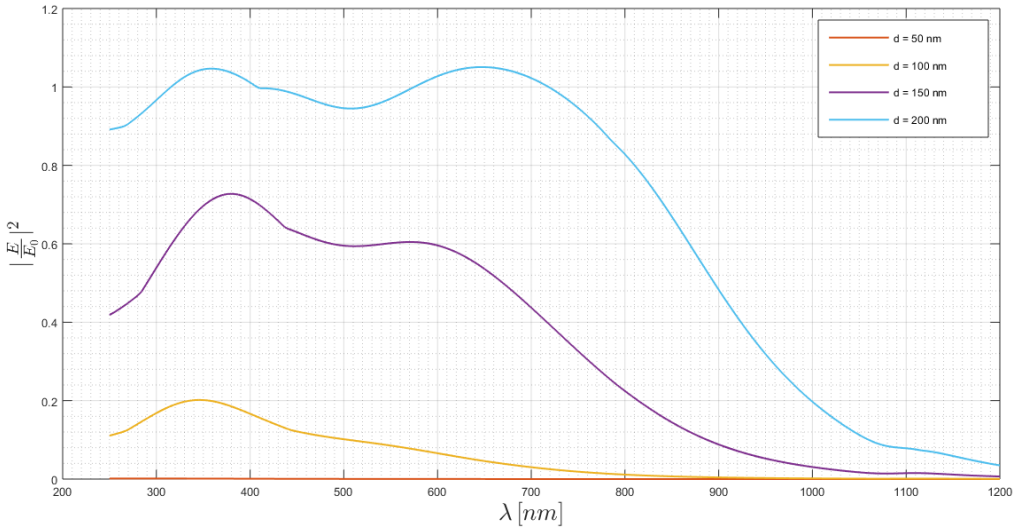

Figure 4.24: Hole diameter sweep on an aluminium nanostructure with a quartz substrate.

4.3.3 Nanoantenna Thickness Sweep

The results obtained when the thickness of the gold and aluminium nanoantennas changes are, respectively, on figures 4.25 and 4.26. Based on these figures it is also quite obvious that the quartz substrate increases the losses and consequently, all the intensity values decrease, including the maximum gain. Similar to the situation with the air substrate, and giving more reliability to these conclusions, it is noted that the thicker the nanoantenna is, the lower the maximum intensity peak will be. Also, a blue-shift of

the gain region will occur. These statements can be observed on both gold and aluminium responses. The aluminium optical response will have a flatter region as the nanoantenna thickness increases.

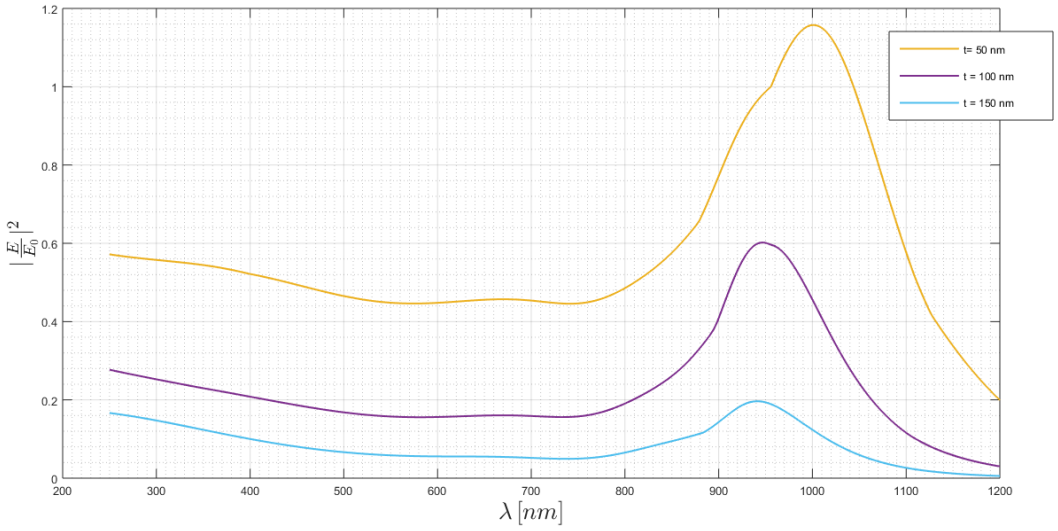

Figure 4.25: Nanoantenna thickness sweep on a gold nanostructure with a quartz substrate.

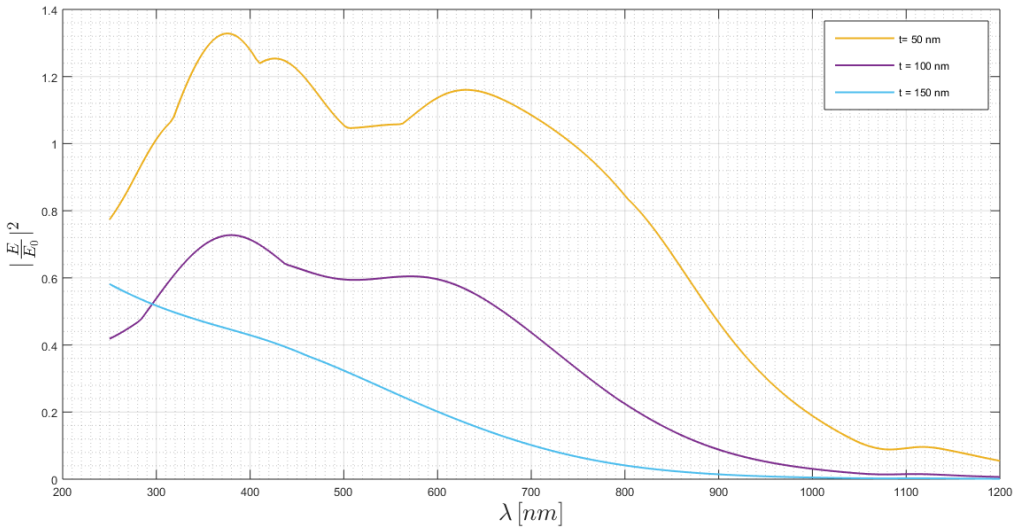

Figure 4.26: Nanoantenna thickness sweep on an aluminium nanostructure with a quartz substrate.

4.3.4 Substrate Thickness Sweep

The last structure parameter that is analysed is the substrate thickness. This dimension is very important, because it is expected that the greater the substrate thickness is, the higher the losses are and the lower the intensity peak value at resonance is.

The results for the gold and the aluminium nanoantennas are on figures 4.27 and 4.28, respectively. Both results suggest the validation of the previous statement, because, based on these figures, it is visible that the optical response shape remains the same, the resonant peak is on the same wavelength and the intensity peak at resonance decreases with the increase of substrate thickness. Nonetheless, it is also possible to verify in the response of the gold nanostructure that if the substrate thickness is small, it also can affect the polaritons propagation.

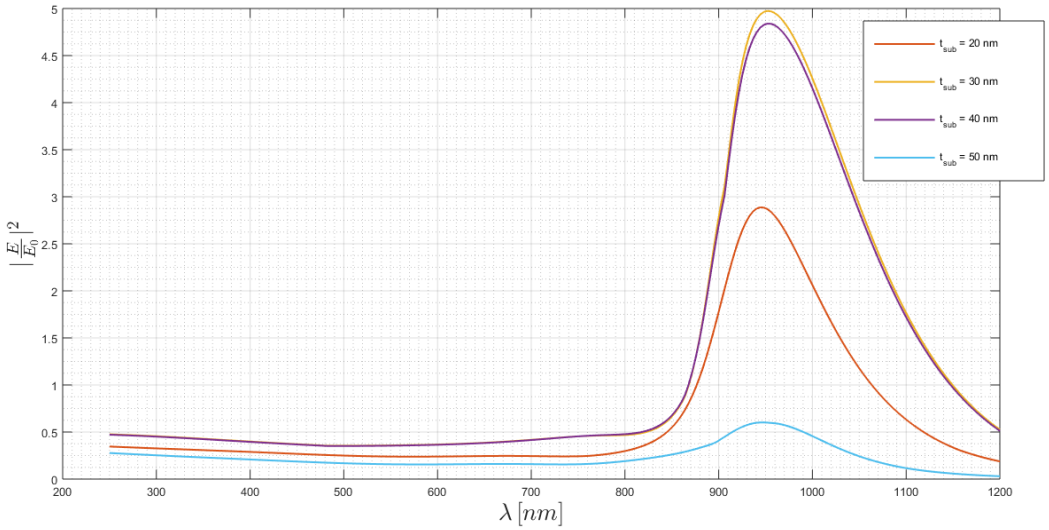

Figure 4.27: Substrate thickness sweep on a gold nanostructure with a quartz substrate.

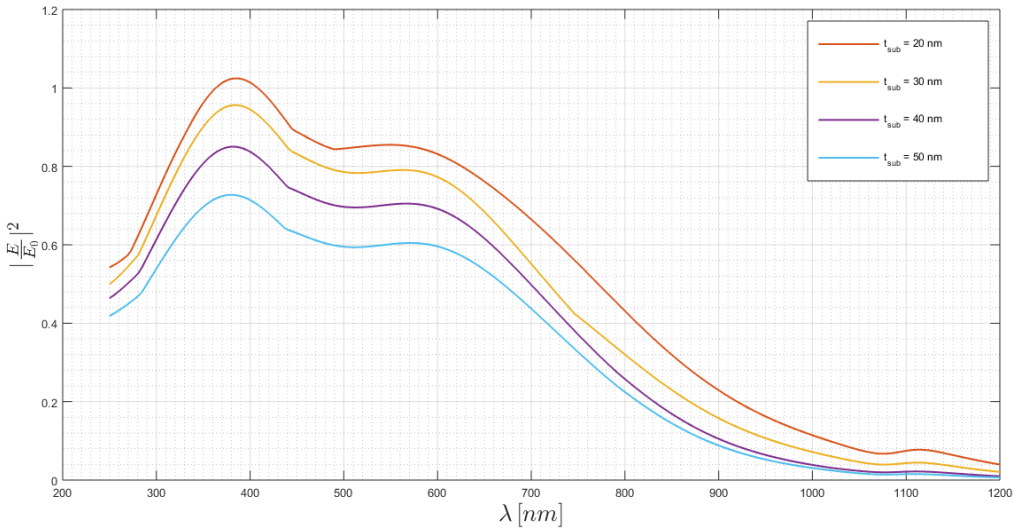

Figure 4.28: Substrate thickness sweep on an aluminium nanostructure with a quartz substrate.

5

Sensors

Contents

5.1 Typology Selection

Based on the appraisal done on the previous chapter, a structure is defined in order to develop a sensor. A sensor is a device which when exposed to physical or chemical phenomena - for example temperature, force, displacement, chemical elements concentration or chemical reaction -, produces a proportional output signal - for example optical, electrical, mechanical or thermal -. However, it is called a sensor because the sensor's input is an optical signal and its output, in this work, is an optical signal too. Nonetheless, several materials, such as the direct band-gap semiconductors, allow us to have an electrical output - voltage or current -, and so that, the device is named a transducer, thanks to its capability to generate an output signal type different from the input one.

An analysis based on neural networks or even on Monte Carlo runs could be done in order to obtain the best result. Even though, some of these simulations were already on the limit of memory and processing capabilities of a "regular" computer and each one takes one day, in average, to generate results. However, as previously mentioned, there is not necessarily a optimal solutions, because to create a sensor more than one specification most be dependently reached, having several trade-offs.

Since there are not specifications and this work aims to show that is possible to tune the parameters in order to obtain a useful sensor, the structures are chosen by selecting the best parameter value, considering the previous sweeps as independents.

Based on the simulations from previous chapter, a structure with an SiO_2 substrate of thickness $t_{sub} = 20\,\text{nm}$, and a nanoantenna of gold defined by a periodicity of $a_0 = 0.3\,\mu\text{m}$, a hole diameter $d = 120\,\text{nm}$ - which is 40% of the periodicity, as the relation between $a_0 = 0.5\mu\text{m}$ and $d = 200\,\text{nm}$ -, and a thickness of $t = 50\,\text{nm}$, is simulated. Results from the previous chapter indicate that, when the substrate thickness decreases, the maximum gain increases. However, previous tests on the proposed structure revealed that, with a substrate thickness $t_{sub} = 20\,\text{nm}$ the optical response presents a lower peak than with $t_{sub} = 30\,\text{nm}$. Thus, the new nanostructure was tested for both combinations and the better one, with $t_{sub} = 20\,\text{nm}$, was the choice.

The result is shown on figure 5.1, where it is obvious that the result of a parameters combination creates a worst case in terms of gain when comparing with some of the previous simulated structures - for example when comparing with figure 4.27 -. Thus, it is possible to conclude that parameters results are not totally independent, and it was demonstrated when the hole diameter have to be scaled based on the periodicity relative percentage - in order not to create an impossible structure where the hole is bigger than its periodicity -. However, all the previous rules remain, *i.e.*, sweeping only one parameter having a reference structure will result the same as previous mentioned. The unpredictable problem occurs when more than one parameter is swept and the solution is to find the equation models for each sweep. The results of figure 5.1, for the defined structure of the gold sensors, show a maximum gain of 4.67 for $983\,\text{nm}$, and a gain region between $860\,\text{nm}$ and $1172\,\text{nm}$.

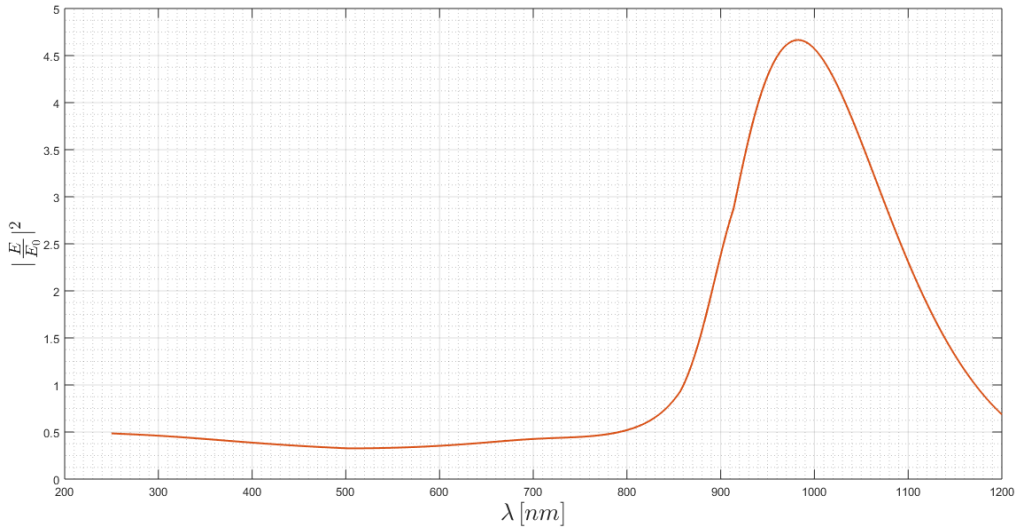

Figure 5.1: Optical response of an air-gold-quartz nanostructure characterised by $a_0 = 0.3$µm, $d = 120$nm, $t = 50$nm and $t_{sub} = 20$nm.

The sensor with the aluminium nanoantenna guarantees gain along all the visible region. The structure is the same of the sensor with gold. In order to create a flatter gain in the visible part of the spectrum two other values of the nanoantenna thickness were tested. However, these results were not satisfactory, and the initial structure was chosen. The corresponding simulation results are presented on figure 5.2. In this case, the final result is better than those resulting from independently varying the different parameters of the structure one by one.

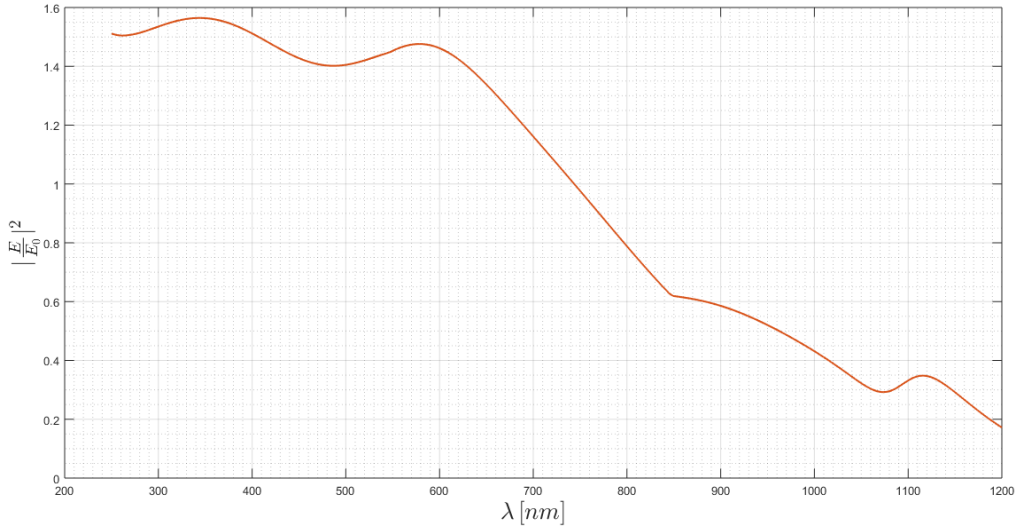

Figure 5.2: Optical response of an air-aluminium-quartz nanostructure characterised by $a_0 = 0.3$µm, $d = 120$nm, $t = 50$nm and $t_{sub} = 20$nm.

5.2 General Purposes

A sensor is characterised by a parameter whose values change with the occurrence of something. The parameter change has to be measured. Nonetheless, simpler applications must be analysed first, in order not to break the reasoning, even that these applications are not defined as sensors. For this reason, some applications are going to be cover, using the lastly presented nanostructures and the responses. Depending on the application the sensor can be optimised. The optimisation process depends on the different parts of the sensor, but in some situations the simple optimisation of the nanoantenna response to optimise the sensor.

An example is a nanoantenna of gold used to improve the sensibility of infrared sensors - for example on medical applications -, since some infrared wavelengths have high amplification and the others have huge attenuation. Then the output of sensor presents an improved sensitivity.

Another example is the oximeter, where the sensor measures the amount of oxygen on blood. There are different types, from the portable to the hospital ones. In both cases, there are LED emitting two distinct signals, for example on the spectral red and blue regions. The optical spectrum of blood varies with the amount of oxygen, because cells can absorb more or less radiation according to the oxygen they transport. Thus, for example using the oximeter on fingers and analysing the output spectrum resulting from the photodetection of the red and blue light after the radiation propagates through cells, it is possible to determine the percentage of oxygen. In this case, nanoantennas can detect and amplify the detected radiation, in the two spectra interval of interest, replacing photodetectors and increasing the device sensibility. In this case, it is suggested that a gold nanoantenna can be used to detect the red signals and a silver one to detect the blues. The overall sensibility will increase, weak signals can be generated and detected, and small devices can be built.

The optical response of the nanostructure with a nanoantenna of gold can be used to improve LED and LASER - used for example in optical communications -, sensibilities in a certain wavelength band. As seen on the previous simulations, changing the material of the nanoantenna, it is possible to place the peak along the frequency/wavelength range. In the case of the spectrum on figure 5.1, a near-infrared region is amplified, specially around $1000\,\mathrm{nm}$. Another example on communications applications is the use these nanoantennas to convert free-space energy into guided energy and *vice-versa*, as it is done by a regular antenna. In this case, in addition to this conversion, the structure can be tuned to filter and amplify, using just one miniaturised device.

Lastly, the aluminium nanostructure, whose spectrum is on figure 5.2, can be used to amplify the visible and ultraviolet regions. An example of this application is on the concentration and amplification of the solar irradiance - which is predominant on the visible region -, incident on the active area of a solar cell, resulting in more incident power and consequently, on more generation of output power. However, it is necessary to guarantee the chemical stability of aluminium for long-term applications.

5.3 Temperature Sensor

The first sensor - in the strict sense of the definition -, is the temperature one, *i.e.*, a thermometer. To simulate this sensor, it is necessary to have experimental results or models for the dependence of the optical properties with the temperature. However, it is very difficult to find available results on literature.

It was impossible to find air and quartz models for different temperatures. However, as these materials do not have interband region on the simulated range, it is not necessary to have its models. On the other hand, the temperature has small influence on the dielectric function real part, in comparison with the imaginary one. Thus, the influence of the metal will always be the predominant and so that, structures as the ones presented in this work can be used as temperature sensors.

In this section, a temperature sensor based on a gold nanoantenna is simulated. The model of the dielectric permittivity of the metal, used in these simulations, is on appendix A. Results are presented for five different temperatures, T, - $23\,^{\circ}$C, $100\,^{\circ}$C, $200\,^{\circ}$C, $250\,^{\circ}$C and $300\,^{\circ}$C -. It is possible to observe that the real part of the dielectric function is almost independent of the temperature until approximately a wavelength of $550\,\mathrm{nm}$. After it, the temperature dependence can be divided in two different regions. First, for each wavelength, as the temperature increase, the real part of the dielectric function becomes smaller until a critical temperature value, between $T = 200\,^{\circ}$C and $T = 250\,^{\circ}$C. Increasing the temperature above this critical point, the real part of the dielectric function becomes abruptly higher than the values for smaller temperatures. After that, as the temperature is increased, the real part of the dielectric function will be increased too. On the other hand, the imaginary part seems to have a temperature dependency along all the simulated range however, only above approximately a wavelength of $600\,\mathrm{nm}$ a strict rule seems to be established. Below it, the dependency is not well defined. Howsoever, the output optical response have to be verified, it is from the spectral response that the details about the sensor designing can be obtained.

On figure 5.3 the results are shown. There, it is observable that is possible to differentiate each temperature only using the maximum gain value. Moreover, until a certain temperature the peak value decreases as the temperature increases. As expected, the conclusion taken from the complex dielectric function analysis is reflected on the nanostructure response. It is quite impressive how the spectrum maintains the same shape and intensity values, except the peak region.

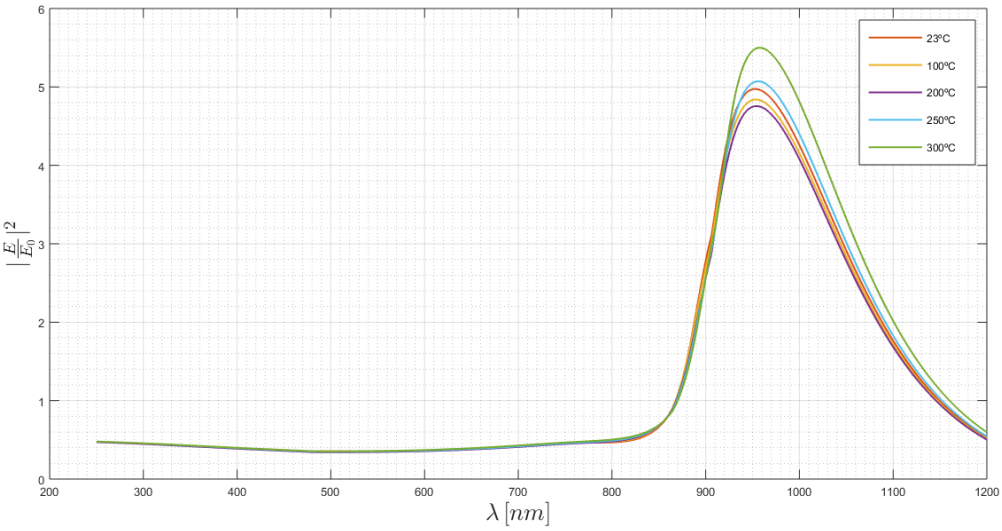

Figure 5.3: Gold nanostructure response for different temperatures.

In order to verify the peak variation, the spectra for the first work region is on figure 5.4 and for the second region is on 5.5, for a wavelength range between $900\,\mathrm{nm}$ and $1050\,\mathrm{nm}$.

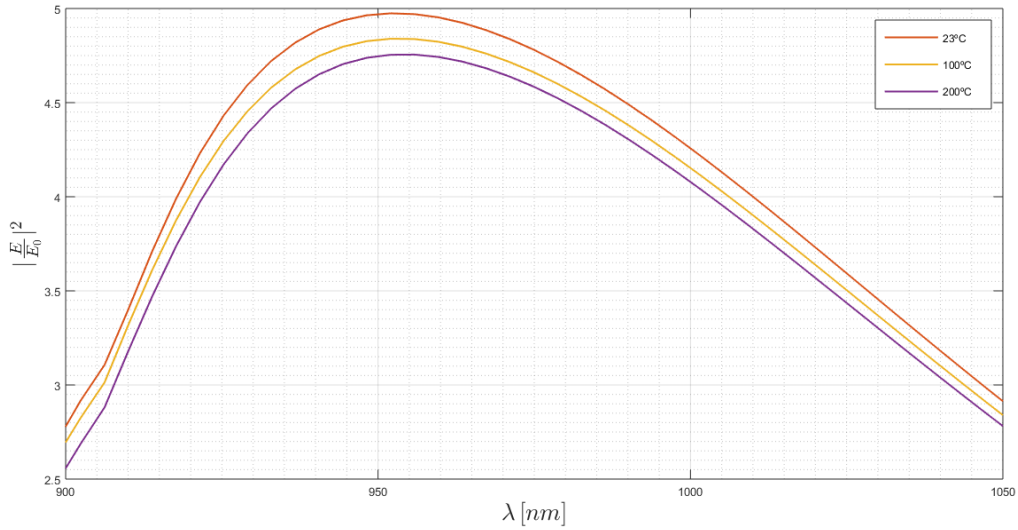

Figure 5.4: Gold nanostructure response for different temperatures, below the critical value.

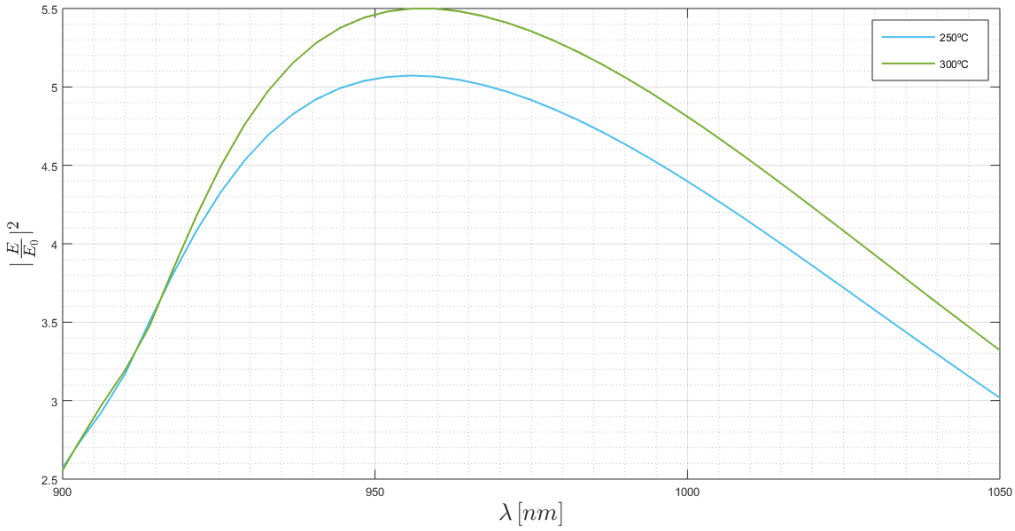

Figure 5.5: Gold nanostructure response for different temperatures, above the critical value.

These figures allow us to conclude that each temperature will generate a different nanostructure response, which is well defined. Thus, measuring the output spectrum at wavelengths near the peak one and knowing the critical temperature value, it is possible to determine what is the temperature around the nanostructure, since different temperatures produce different output electric field norms.

The peak wavelengths for curves below and above the critical temperature are different. Then, it is possible to determine the temperature measuring a single wavelength, without the necessity of go through all the range. If the peak value - and a uncertainty range -, is specify for each structure, it is possible to use only one wavelength measurements, since around the peak there are not equal values for different temperature.

Even more, due to the small differences in the peaks of the optical response curves, for large temperature variations, the sensors have small sensibilities. However, they can be used to detect temperature ranges, for example, to analyse the occurrence of certain chemical reactions.

Finally, the last conclusion considers the possibility to convert thermal to electrical energy. Around the room temperature the nanostructure has already optical gain however, after a certain temperature, the gain will increase as the temperature increases. Then, heating the sensor, it is possible increase the energy of the light beam and generate electrical energy.

5.4 Tissues Detection Sensor

In this section, it will be shown that is possible to detect biological tissues, using their optical properties. Four models were found - liver tissues, colon mucosa tissues, colon submucosa tissues and colon

serosa tissues -, and the main goal is to use the gold and the aluminium nanostructures in order to detect the tissue over the nanoantenna. As illustrated on figure 5.6, the structure is based on the one described at the beginning of this chapter. However, the tissues are placed between the dielectric and the nanoantenna. Thus, the nanoantenna holes will be covered by those tissues instead of the dielectric. The tissue medium has a thickness of $200\,\mathrm{nm}$, but only $150\,\mathrm{nm}$ are visible on the figure, since the remaining is the nanoantenna thickness. The dielectric has also a thickness of $150\,\mathrm{nm}$. The models for the tissues' complex dielectric function are presented on appendix A. Due to the models' wavelength range, the following simulations were done between $450\,\mathrm{nm}$ and $1200\,\mathrm{nm}$.

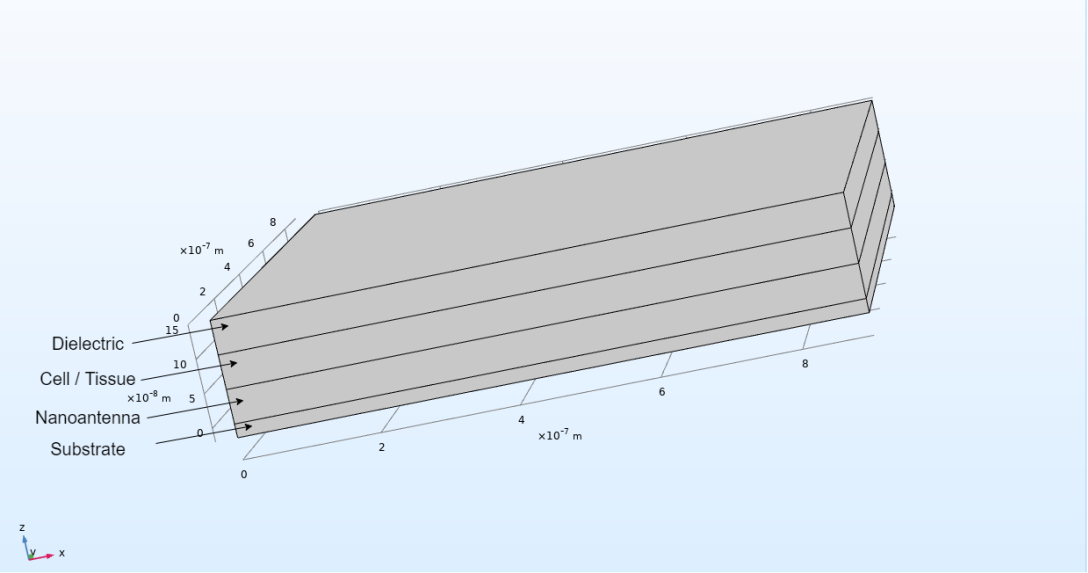

Figure 5.6: Typology of the simulated sensor structure (axis framework on lower left corner).

First, the gold made nanostructure is simulated considering the aforementioned tissues and its results are presented on figure 5.7. The optical response of all tissues is similar. It is noticeable that different tissues produce different spectra. In this case, it is possible to distinguish liver and the three types of colon tissues. As expected, the difference among colon tissues is smaller than the difference between any colon tissue and the liver one.

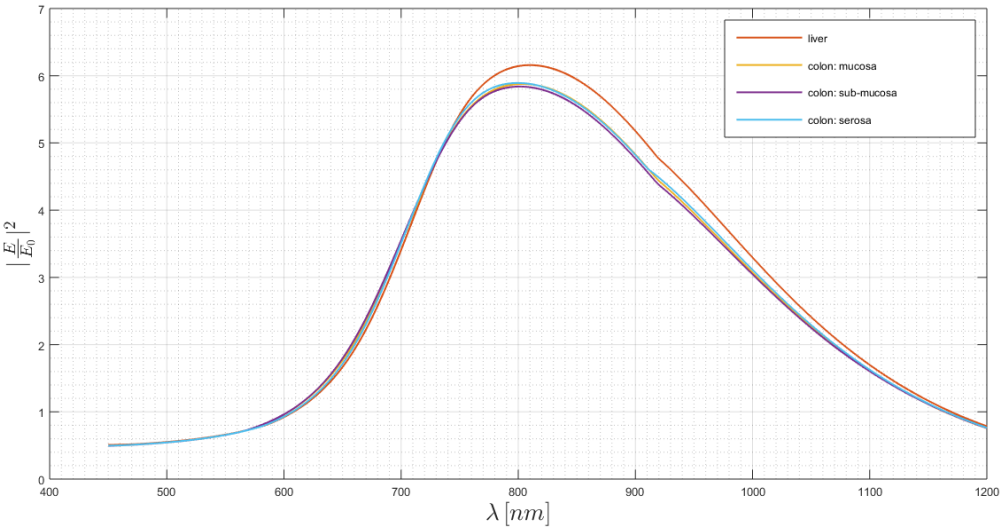

Figure 5.7: Gold nanostructure response for different human body tissues.

However, analysing the spectral region near the peak, it is possible to observe that even the colon tissues can be differentiated among them, as illustrated on figure 5.8, for different wavelengths.

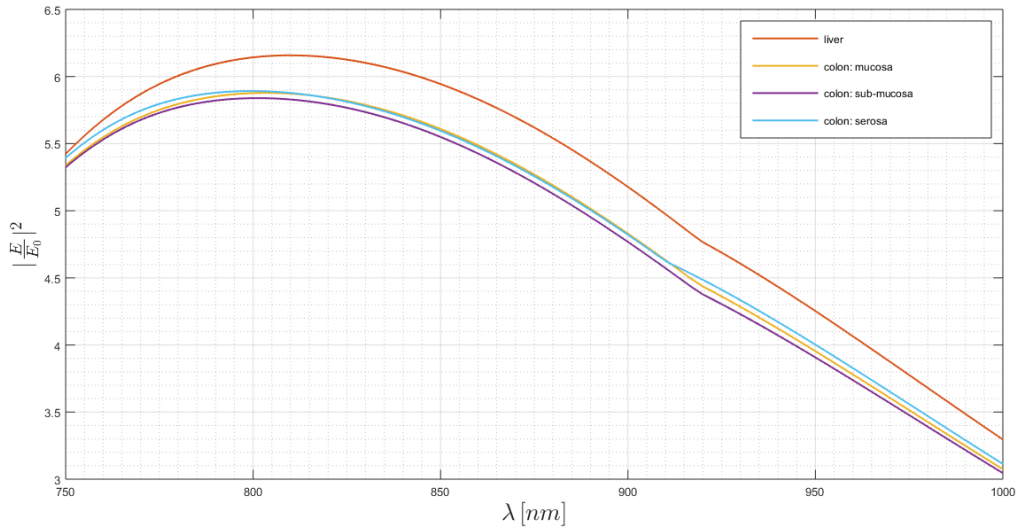

Figure 5.8: Gold nanostructure response for different human body tissues (zoom).

The same simulations were done using the aluminium nanoantenna, which results are presented on figure 5.9. There, although all the responses are very similar at higher wavelengths, the region around $500\,\mathrm{nm}$, that is in focus on figure 5.10, allows the detection of each tissue. Once again, the liver can be easily differentiated from the colon cells. However, it can be possible to distinguish similar tissues, as the colon ones.

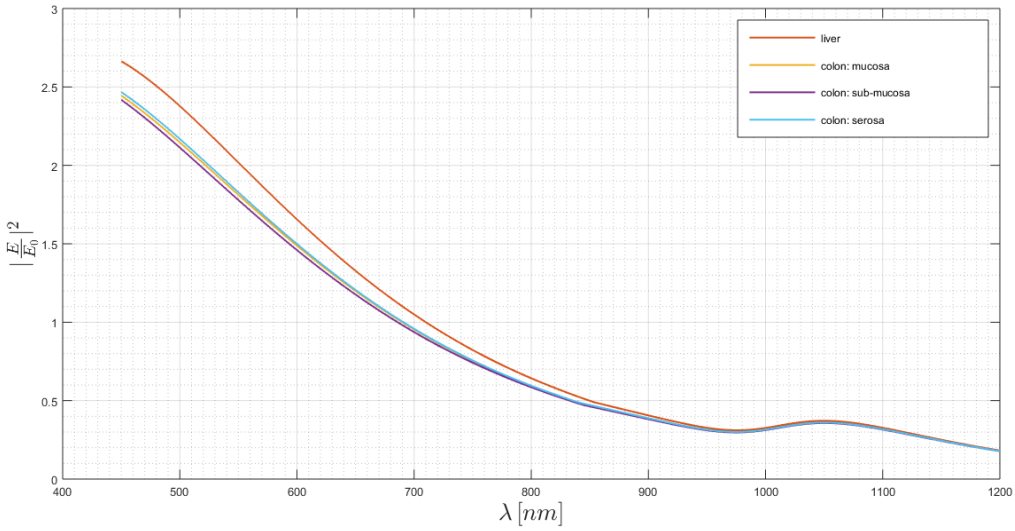

Figure 5.9: Aluminium nanostructure response for different human body tissues.

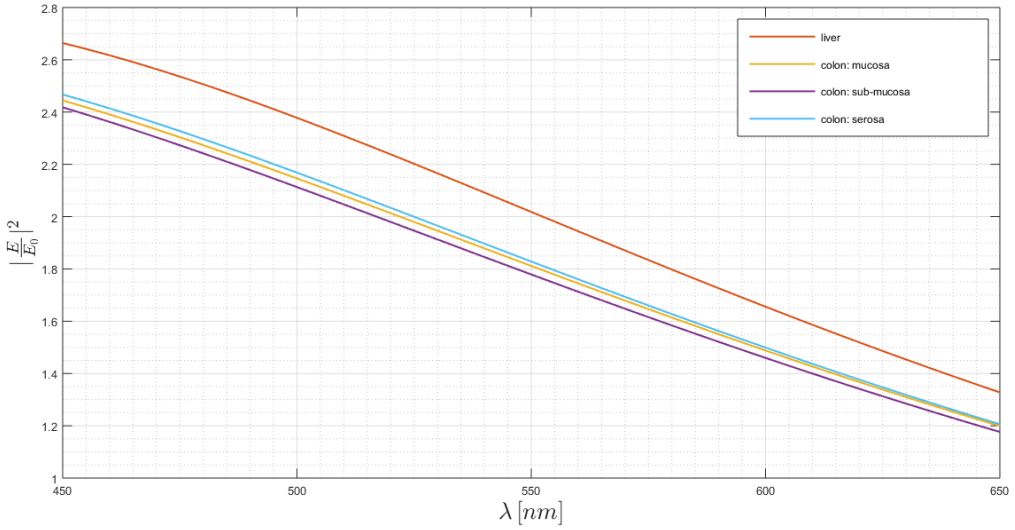

Figure 5.10: Aluminium nanostructure response for different human body tissues (zoom).

One way of distinguish similar characteristics is to do this analysis along all the spectrum. Nonetheless, based on which are the tissues to distinguish, it can be possible to use just one single wavelength. For example, to distinguish liver tissue from one of the colon tissue samples, it is possible to use just one wavelength. Nevertheless, to distinguish similar tissues, as the colon ones, it is much better to analyse all the wavelength range. Furthermore, to increase the accuracy of this method, several different structures can be used in order to have different responses to compare and decrease the error probability.

In addition, it can be possible to create a huge database of optical responses like these for each tissue. Some of them should be unhealthy tissues, for example cancer cells at different stages or cells affected by diseases as diabetes. There are already some studies reporting the variation of the optical properties with some diseases [42]. Then, the spectral response varies and it is possible to monitor cells and tissues in real time, *in vitro* or *in vivo*, in order to create a regular report of spectra. This method is useful to detect some diseases or to control substances levels. For instance, if the optical properties vary with the concentration of some substance, it is possible to take conclusions regarding the spectral analysis. It is the case of insulin levels - diabetes -, or, the blood pressure or oxygen in circulation [42–44]. Nonetheless, it is very important to have a huge database, in order to create a complex dielectric function model to use on these applications. These real models are not easily available.

5.5 Sensors Classification

A nanoantenna based sensor, as any other sensor or transducer, should be classified into, at least, four different categories regarding its energy source, its signal conditioning, the possibility of a reference value and its complexity [45–47].

In relation to its energy source, the device can be a self-generating sensor, when the energy needed to generate the output signal comes from the phenomenon/variation itself, otherwise it is called modulating or parametric device, because the energy comes from a power supply [45, 46]. A modulating sensor must have a characteristic parameter that changes with some phenomena occurrences. When the phenomenon occurs, that parameter changes and, consequently, the output signal varies too.

On the other hand, the device can be classified as active or passive, according to its signal conditioning. The biggest advantage of an active device is the possibility of having gain, but it requires an external energy source. The passive devices are characterised by generating an output signal from the surrounding environment, without the necessity of having an external power supply. Nonetheless, they must have powerful conditioning circuit to amplify the output signal that, usually, is a weak signal [45,46]. Thus, being passive is also a synonym of being self-generating.

Furthermore, sensors can be classified as absolute or relative, regarding the possibility of having their response referenced [45–47]. If the output response is independent of the measurement conditions, including input signals, output variations and power supplies, then it is an absolute device otherwise, it is relative.

The last category divides sensors according to their complexity. The way of measuring a sensor complexity is based on the number of energy transformation that occur on the sensor. It is considered a simple sensor if at most one energy transformation occurs, otherwise it is a complex sensor [45–47].

Sensors based on nanoantennas are not all characterised as the same, inside each category.

Mostly, sensors based on nanoantennas are modulating or parametric devices, since usually a well-defined signal is the input, allowing the polaritons propagation and the extraordinary optical transmission phenomenon. The structure parameter - after it is built -, that is dependent on physical or chemical variations is the complex dielectric function. Its variations create spectral modifications that can be analysed in order to determine what happens on the surrendering environment. However, it is not impossible to design a self-generating nanoantennas based sensor, inasmuch as there is radiation almost everywhere. Thus, it can be possible to filter it and design a sensor to use it, but the polaritons generation must be guaranteed. At the final, the output signal can be compared to the input one.

On the other hand, nanoantennas are active devices, because gain regions are allowed. Nonetheless, as previous seen, the design of the sensor, according to its specifications, is essential to define the type of sensor.

Moreover, this kind of sensors can be classified as absolute, when the optical properties models and the developed simulations are credible enough to present the output results for each case, or relative, if there is a reference spectrum and what is measured is the difference to the reference.

Finally, the sensors complexity is a bit tricky, because at first sight they seem to be simple, due to the fact that an optical signal is incident on the sensor and, consequently, the output signal should be also an optical signal when it is measured after the substrate with an optical spectrometer - band measurement -, or a regular photodetector - wavelength measurement -, or a electrical signal if the substrate allows it, measuring and analysing the behaviour of currents or voltages. However, the theoretical understanding of the sensors behaviour is decisive in defining the degree of complexity. Sensors that at a first are considered simple after a careful theoretical analysis are classified as complex ones. If an optical signal interacts with the structure and generates surface plasmons, which is the redistribution of the free metal electrical charges and, then one energy transformation happens. After it, if both energy and momentum are conserved, the surface plasmons can couple with the incident radiation, resulting on the polariton, which is essential to the resonant phenomenon and to the sensor designing. Consequently, the second conversion occurs, because electrical energy is converted to radiation - even that both are electromagnetic energy, they are two different energy types, mainly because their agents/particles are different: electrons and photons-. Thus, there are, at least, two different energy transformation and so that, the sensor should be classified as complex. Furthermore, a third transformation can occur if the substrate is linked to something that acts as an electrical circuit, in order to receive the electrical output signal. In this case, the substrate should allow the flux of electrons, being for instance a substrate made with a semiconductor.

The manufacture a sensor like this, demands a set of specifications and the design of the sensor, considering the factory technology and the available materials. Beyond the materials, the available technology imposes the minimum material dimensions, minimum drill diameter and minimum distance

between holes, and technological processes, for example how materials are deposited/implanted, which are the masks and which are the available protections/encapsulation.

The set of usual sensor specifications includes the sensitivity, the operation range and bandwidth, the resolution and accuracy, the possibility of having hysteresis in its response, the noise, the repeatability of measures and the possibility of having dead and saturation zones.

6

Conclusion

Contents

6.1 Conclusions

The discovery of the extraordinary optical transmission questioned all the classical theories of diffraction of the electromagnetic field. None of them explain the new phenomenology, because it is assumed the existence of ideal materials, namely metals. In doing so the generation and propagation of surface plasmon polaritons and of creeping waves is not considered and, consequently, the classical theories fail. The consideration of these effects demands the consideration of the electrical and optical properties of real materials, through a correct modelling of the dielectric function and refractive index. Then the propagation of surface plasmons polaritons can be theoretically analysed from Maxwell's equations. Their generation and propagation, combined with the propagation of creeping waves – specially out of the visible spectral region -, allow to describe the extraordinary optical transmission phenomenon. This phenomenon can be observed using nanoantennas. This kind of structures allow the concentration and amplification of electromagnetic energy.

Using *COMSOL Multiphysics* it was created a 3D simulation environment to model and simulate a nanoantenna, obtaining its optical response. The optical response is dependent on the used materials, on the nanoantenna and also in the surrounding materials.

Considering the air-metal-air structure and the simulated ranges, it is possible to verify that for the nanoantennas of silver and gold, when the structure periodicity increases, the maximum intensity value decreases. However, this conclusion is not valid for the nanoantennas of copper and aluminium. In this last case, the periodicity increases the flatness of the optical response in a wavelength region including the ultraviolet and visible radiation. With a subwavelength hole diameter, it is possible to verify that the larger the hole, the higher the intensity peak. Furthermore, this sweep creates a red-shift effect as the diameter increases. This effect can be compensated by varying the nanoantenna thickness. The increasing of the nanoantenna thickness leads to the decrease of the intensity peak, as well as to the occurrence of blue-shifts. These statements are not valid for the aluminium nanoantenna. In this case, the thicker the nanoantenna is, the flatter the optical response will be. Finally, when the number of holes in the nanoantenna changes, maintaining all the other parameters constant, it is concluded that the optical response of the gold and the aluminium nanoantennas is almost independent of the number of holes. Thus, it is possible to increase the structure dimensions – width and length -, and the number of holes, without having a trade-off that would affect the spectral response.

Considering the previous results, and the chemical stability of the analysed metals, gold and aluminium were chosen to continue the tests using the quartz solid substrate. Quartz is usually a good choice for these applications purposes. The wavelength associated with the quartz interband energy is much higher than the wavelengths used in the simulations, and so, it does not create another resonant peak on the optical responses. Thus, the substitution of air substrate by the quartz substrate will only increase losses, reducing the maximum intensity peak value.

Comparing the results from the air-metal-quartz structure with the air-metal-air one, similar conclusions can be taken. In addition, these new results lead to the idea of adjusting losses and consequently gains without changing the spectrum shape. The thicker the substrate is, the higher the losses are, keeping the optical response shape.

The simulations' results also lead to conclude that the spectral response can be tuned by varying the topology and the parameters of the structure. However, in order to create rigorous analytical models, a huge simulation database have to be created, requiring huge computational efforts. Furthermore, all the simulations show high amplification and concentration of the electromagnetic field near the interfaces. This is a clear evidence of the generation and propagation of surface plasmon polaritons.

The nanostructure of gold was simulated as a temperature sensor, using models for the complex dielectric function including the temperature. A nanostructure like this can behave as a temperature sensor with a critical temperature. Below this critical value the peak of the optical response decreases with the increase of temperature, but the corresponding wavelength remains almost constant. Above the critical value, the peak of the optical response increases with temperature and the peak wavelength is slightly shifted to a greater wavelength.

A sensor to distinguish human body tissues was also simulated using the gold and the aluminium nanostructure. The simulated structures can distinguish different tissues and even detect diseases. However, to detect diseases, it is very important to have a huge database in order to create models of the electrical permittivity – complex dielectric function -, of healthy and unhealthy tissues. The creation of good models for the different structures, and the creation of new structures, used to distinguish the human tissues and detect the diseases, is also very important.

To sum it up, some structures based on the occurrence of extraordinary optical transmission, were modelled and simulated. Several simulations were presented to discuss the influence of the materials and of the geometrical parameters on the optical response of the structures. The obtained results clearly point to the development of the project of miniaturised sensors, that could be used to detect and measure temperature variations, to distinguish different human tissues and, consequently, in some cases to detect diseases.

6.2 Future Work

There are different approaches to be followed on the future, depending on the application area. All of them are dependent on the possibility of developing models to analyse the influence of the parameters on the output spectrum. Equations are needed in order to describe it. These models can be developed using Monte Carlo simulations or neural networks. On both cases, a huge computational effort is required because it is needed to do a tremendous amount of simulations and after it, create that new

simulation method in order to reach model equations.

Several simulations lead to the conclusion that these structures can be use on communications, as antennas, in several applications from ultraviolet to the infrared regions, taking advantage of, at least, three great capabilities in just one miniaturised device: concentrate, amplify and filter electromagnetic energy. Thus, these capabilities can be used to improve devices specifications, for example on LED and LASER, to increase their gains and to tune their spectra. Also, on photodetectors, to improve their sensibility and to tune their response.

Other application area, where nanoantennas can be easily used is on solar cells, in order to increase the radiation that is incident on the active area and, consequently, produce more energy. On the other hand, these nanoantennas can be useful to produce energy, considering the surrounding environment radiation and some physical or chemical event - as the temperature variation -. If this event is considered necessary, *i.e.*, if the event is a secondary effect of the main necessity - in order to satisfy human needs, for example on the temperature case: oven temperature or car motor temperature -, this energy is produce without spend more money.

As sensors, which is the main goal of this work, it remains to have more optical models, both from metal temperature dependency and from molecular or diseases presence, in order to increase the number of simulations, despite the fact that this work concludes that nanoantennas can clearly work as sensors. After having the models for the parameters influence, a sensor project can be done, using real specifications.

Bibliography

[1] Deus, J.D., et al. Princípio de Huygens. *Introdução à Física*; Escolar Editora: Lisboa, Portugal, 2014; pp. 68-88.

[2] Hecht, E. *Óptica*; Fundação Calouste Gulbenkian: Lisboa, Portugal, 2012; pp. 495-578.

[3] Gomes, R.D.F.R., Martins, M.J., Baptista, A. et al. Study of an Optical Antenna for Intersatellite Communications. *Opt Quant Electron* **2017**, *49*, 135.

[4] Bethe, H. A. Theory of diffraction by small holes. *JPhysical review* **1944**, *66.7-8*, 163.

[5] Bouwkamp, C. J. On Bethe's Theory of Diffraction by Small Holes. *Philips Research Reports* **1950**, *5*, 321-332.

[6] Bouwkamp, C. J. Diffraction Theory. *Rep. Prog. Phys* **1954**, *17*, 35.

[7] Ritchie, R. H. Plasma losses by fast electrons in thin films. *Physical review* **1957**, *106.5*, 874.

[8] Ritchie, R. H., et al. Surface-plasmon resonance effect in grating diffraction. *Physical Review Letters* **1968**, *21.22*, 1530.

[9] Raether, H. Surface plasmons on smooth surfaces. In *Surface plasmons on smooth and rough surfaces and on gratings.*; Springer: Heidelberg, Berlin, Germany, 1988; pp. 4-39.

[10] Sharma, N., et al. Fuchs Sondheimer–Drude Lorentz model and Drude model in the study of SPR based optical sensors: A theoretical study. *Optics Communications* **2015**, *357*, 120-126.

[11] Barchiesi, D. and Grosges, T. Fitting the optical constants of gold, silver, chromium, titanium, and aluminum in the visible bandwidth. *Journal of Nanophotonics*, **2014** *8.1*, 083097.

[12] John, P. A Drude-Time Derivative Lorentz Model for the Optical Properties of Gold. 2015.

[13] Majedi, A. H. Theoretical investigations on THz and optical superconductive surface plasmon interface. *IEEE Transactions on Applied Superconductivity* **2009**, *19.3*, 907-910.

[14] Tsiatmas, A. et al. Superconducting plasmonics and extraordinary transmission. *Applied Physics Letters* **2010**, *97.11*, 111106.

[15] Biagioni, P., et al. Nanoantennas for visible and infrared radiation. *Reports on Progress in Physics* **2012**, *75*, 024402.

[16] Mohammadi, A., Sandoghdar, V., and Agio, M. Gold, copper, silver and aluminum nanoantennas to enhance spontaneous emission. *Journal of Computational and Theoretical Nanoscience* **2009**, *6.9*, 2024-2030.

[17] Ebbesen, T. W., et al. Extraordinary optical transmission through sub-wavelength hole arrays. *Nature* **1998**, *391*, 667.

[18] Lezec, H. J. and Thio, T. Diffracted evanescent wave model for enhanced and suppressed optical transmission through subwavelength hole arrays.*Optics Express* **2004**, *12*, 3629-3651.

[19] Gay, G., et al. The optical response of nanostructured surfaces and the composite diffracted evanescent wave model. *Nature Physics* **2006**, *2.4*, 262.

[20] Lalanne, Ph., Hugonin, J. P. Interaction between optical nano-objects at metallo-dielectric interfaces. *Nature Physics* **2006**, *2.8*, 551.

[21] Novotny, L. and Niek, V. H. Antennas for light. *Nature photonics* **2011**, *5.2*, 83.

[22] Brolo, A.G., et al. Surface Plasmon Sensor Based on the Enhanced Light Transmission Through Arrays of Nanoholes in Gold Films. *Langmuir* **2004**, *20(12)*, 4813-4815.

[23] Unser, S., et al. Localized surface plasmon resonance biosensing: current challenges and approaches. *Sensors* **2015**, *15.7*, 15684-15716.

[24] Gordon, R. Extraordinary optical transmission for surface-plasmon-resonance-based sensing. *Nanophotonics* **2008**, *2*, 206.

[25] Gordon, R., et al. A new generation of sensors based on extraordinary optical transmission. *Accounts of chemical research* **2008**, *41.8*, 1049-1057.

[26] Gu, Y., et al. Color generation via subwavelength plasmonic nanostructures. *Nanoscale* **2015**, *7.15*, 6409-6419.

[27] Thio, T., et al. Surface-plasmon-enhanced transmission through hole arrays in Cr films. *JOSA B* **1999**, *16.10*, 1743-1748.

[28] Wu, S., et al. Dielectric thickness detection sensor based on metallic nanohole arrays. *The Journal of Physical Chemistry C* **2011**, *115.31*, 15205-15209.

[29] Sen, M. A. Design and development of calorimetric biosensors using extraordinary optical transmission through nanohole arrays. **2012**.

[30] Kowalski, G.J., et al. Fast Temperature Sensing Using Changes in Extraordinary Transmission Through an Array of Subwavelength Apertures. *Optical Engineering* **2009**, *48.10*, 104402.

[31] Yang, J.C., et al. Metallic Nanohole Arrays on Fluoropolymer Substrates as Small Label-Free Real-Time Bioprobes. *Nano Letters* **2008**, *8(9)*, 2718-2724.

[32] Hill, R. T. Plasmonic biosensors. *Wiley Interdisciplinary Reviews: Nanomedicine and Nanobiotechnology* **2015**, *7.2*, 152-168.

[33] Etezadi, D., et al. Nanoplasmonic mid-infrared biosensor for in vitro protein secondary structure detection. *Light: Science & Applications* **2017** *6.8*, e17029.

[34] Sangwan, A., et al. Increasing the Communication Distance Between Nano-Biosensing Implants and Wearable Devices. *2018 IEEE 19th International Workshop on Signal Processing Advances in Wireless Communications (SPAWC)*, **2018**.

[35] Ji, J., et al. High-Throughput Nanohole Array Based System To Monitor Multiple Binding Events in Real Time. *Analytical Chemistry* **2008**, *80(7)*, 2491-2498.

[36] Wissert, M. D., et al. Nanoengineering and characterization of gold dipole nanoantennas with enhanced integrated scattering properties. *Nanotechnology* **2009**, *20.42*, 425203.

[37] Li, J.Y., et al. Influence of hole geometry and lattice constant on extraordinary optical transmission through subwavelength hole arrays in metal films. *Journal of Applied Physics* **2010**, *107.7*, 073101.

[38] Krishnan, A., et al. Evanescently coupled resonance in surface plasmon enhanced transmission. *Optics communications* **2001**, *200.1-6*, 1-7.

[39] Degiron, A., et al. Optical Tranmission Properties of a Single Subwavelength Aperture in a Real Metals. *Optics Communications* **2004**, *239*, 61-66.

[40] Degiron, A., et al. Effects of Hole Depth on Enhanced Light Transmission Through Subwavelength Hole Arrays. *Applied Physics Letters* **2002**, *81(23)*, 4327-4329.

[41] Koerkamp, K.J., et al. Strong Influence of Hole Shape on Extraordinary Transmission through Periodic Arrays of Subwavelength Holes. *Physical Review* **2004**, *92(18)*, 183901.

[42] Grigorev, R., Kuzikova, A., Demchenko, P., Senyuk, A., Svechkova, A., Khamid, A., and Khodzitskiy, M. Investigation of Fresh Gastric Normal and Cancer Tissues Using Terahertz Time-Domain Spectroscopy. *Materials* **2020**, *13(1)*, 85.

[43] Rakhshani, M. R., and Mansouri-Birjandi, M. A. High sensitivity plasmonic refractive index sensing and its application for human blood group identification. *Sensors and Actuators B: Chemical* **2017**, *249*, 168-176.

[44] Wolf, M., Gulich, R., Lunkenheimer, P., and Loidl, A. Broadband dielectric spectroscopy on human blood. *Biochimica et Biophysica Acta (BBA)-General Subjects* **2011**, *1810(8)*, 727-740.

[45] Yurish, S. Y., and Gomes, M. T. (editors). *Smart Sensors and MEMS: Proceedings of the NATO Adavanced Study Institute on Smart Sensors and MEMS Portugal 8-19 September 2003*; Springer Science & Business Media: Povoa de Varzim, 2005: Vol. 181.

[46] Kirianaki, N. V., Yurish, S. Y., Shpak, N. O., and Deynega, V. P. *Data acquisition and signal processing for smart sensors*; Wiley: Chichester, England, 2002; pp. 72-78.

[47] Webster, J. G. and Fox, S. (editors), *Measurement, Instrumentation and Sensors Handbook*, Springer Science & Business Media, 1999.

[48] Refractive index database - refractive index. Available online: https://refractiveindex.info/ (last access on 17 April 2020).

[49] Reddy, H., Guler, U., Kildishev, A. V., Boltasseva, A., and Shalaev, V. M. Temperature-dependent optical properties of gold thin films. *Optical Materials Express* **2016**, *6(9)*, 2776-2802.

A

Complex Dielectric Functions

In this appendix are provided the complex dielectric function characteristics for each material used on simulations. It is divided in three sections, presenting the frequency behaviour of the dielectric, the metals and the solid substrate used on simulations.

Actually, what is usually available is the refractive index, n, and the extinction factor, k. However, for this purpose it is better to analyse the complex dielectric function variation, which appears directly on Maxwell's equations. The complex dielectric function is related to the complex refractive index function by $\bar{\epsilon} = \epsilon' + j\epsilon'' = \bar{n}^2 = (n + ik)^2$, such as $\epsilon' = n^2 - k^2$ and $\epsilon'' = 2nk$.

The models used for each material are detailed, using the data compiled on an online database [48], which have the same models implemented and available on *COMSOL Multiphysics*. A condition that is crucial to select a material for the structure is the fact that its model is defined at least on the simulated wavelength range *i.e.*, $[250\,;\,1200]\,\text{nm}$. Although most of them have a larger range, it is only presented the simulation range, in order to adjust the window plot to the values that influence the simulations. On the other hand, as there is a huge lack of available optical models for tissues, it is used the ones that are available. In this case, the used wavelength range is $[450\,;\,1200]\,\text{nm}$.

A.1 Dielectric

To model the dielectric medium is used the 1996 Ciddor model, which models "standard air" conditions [48]. The complex dielectric function of air is illustrated on figure A.1, where it is possible to verify a null imaginary part, because its extinction factor is also null, since air is not a lossy medium.

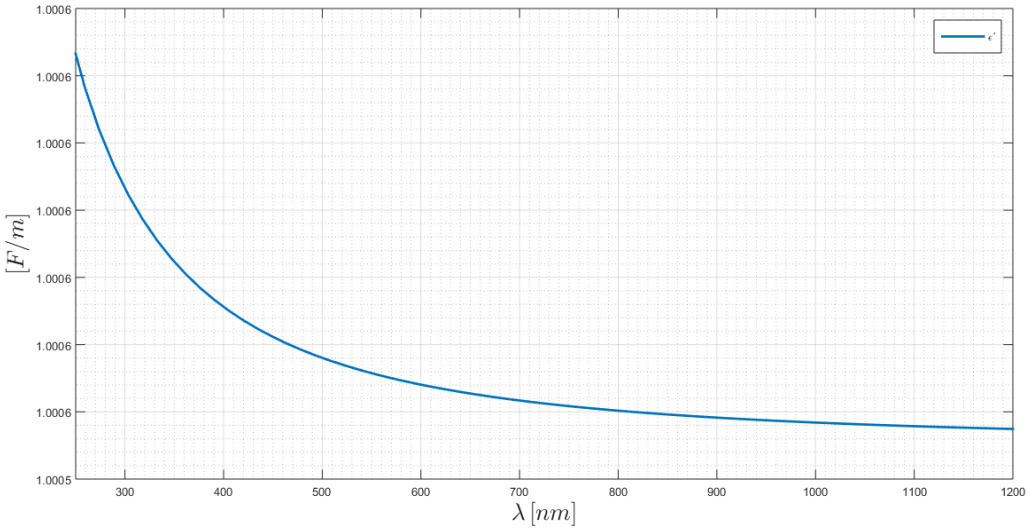

Figure A.1: Air complex dielectric function from the 1996 Ciddor model.

A.2 Metal/Plasma

The silver model is the Rakic, which is a Drude-Lorentz fitting of several sources of experimental data [48]. On figure A.2 is illustrated the silver complex dielectric function, where it is possible to observe that its interband wavelength region is below 400nm.

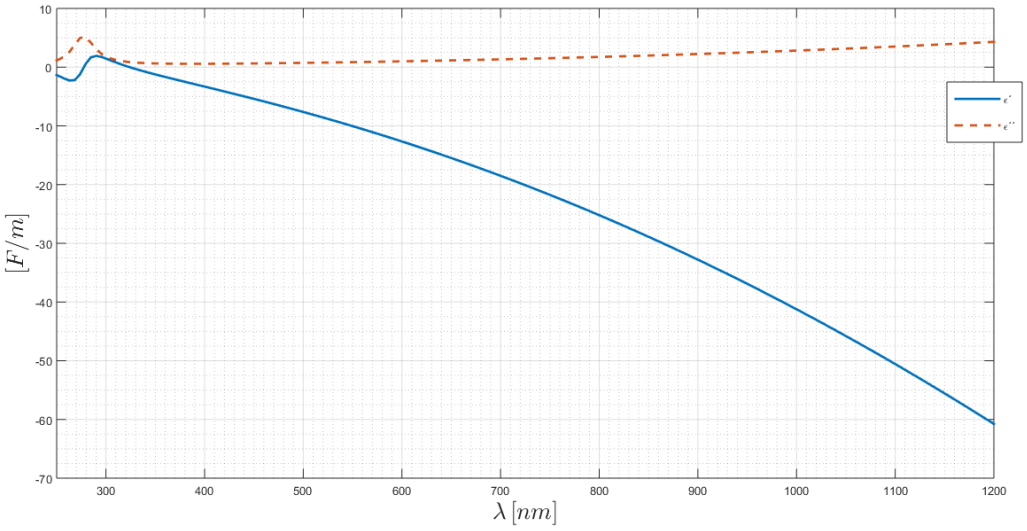

Figure A.2: Silver complex dielectric function from Rakic's Drude-Lorentz fitting.

Further, a Rakic model is also used to describe gold. As well as silver, the complex dielectric function, which is presented on figure A.3, is also a Drude-Lorentz fitting of several sources of experimental data.

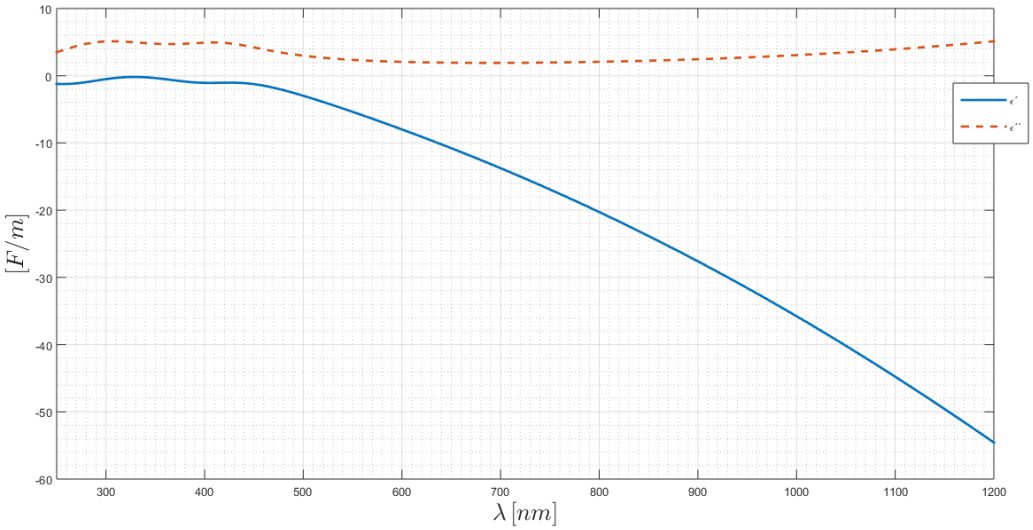

Figure A.3: Gold complex dielectric function from Rakic's Drude-Lorentz fitting.

The gold transition between Drude and interband regimes is around $530 \sim 600\text{nm}$, which is clearly observed on figures A.4 and A.5, that are respectively the real and the imaginary part of the complex dielectric function. On these figures, the temperature dependence of gold is revealed for five different temperatures, in order to simulate a temperature sensor, using Reddy data fitting [49].

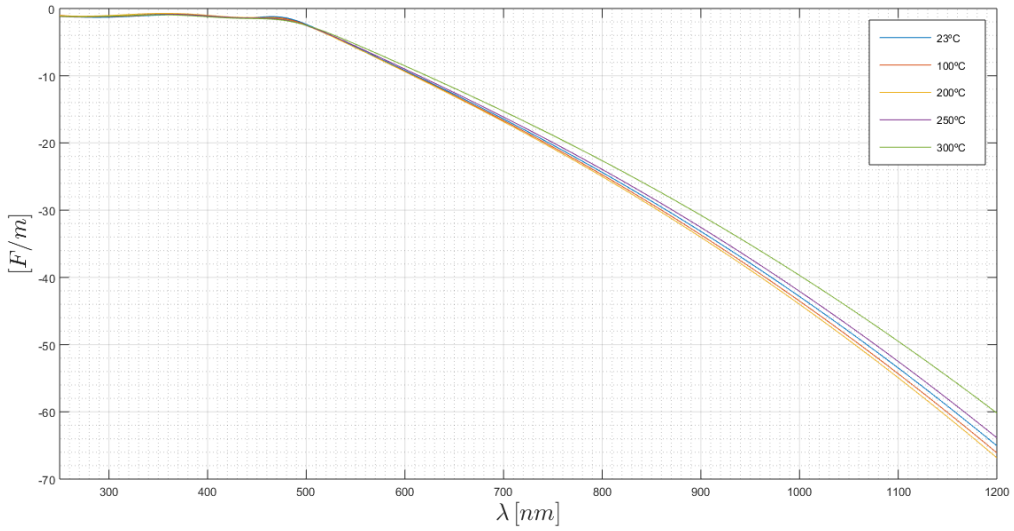

Figure A.4: Reddy fitting of the gold real part of complex dielectric function with temperature dependency.

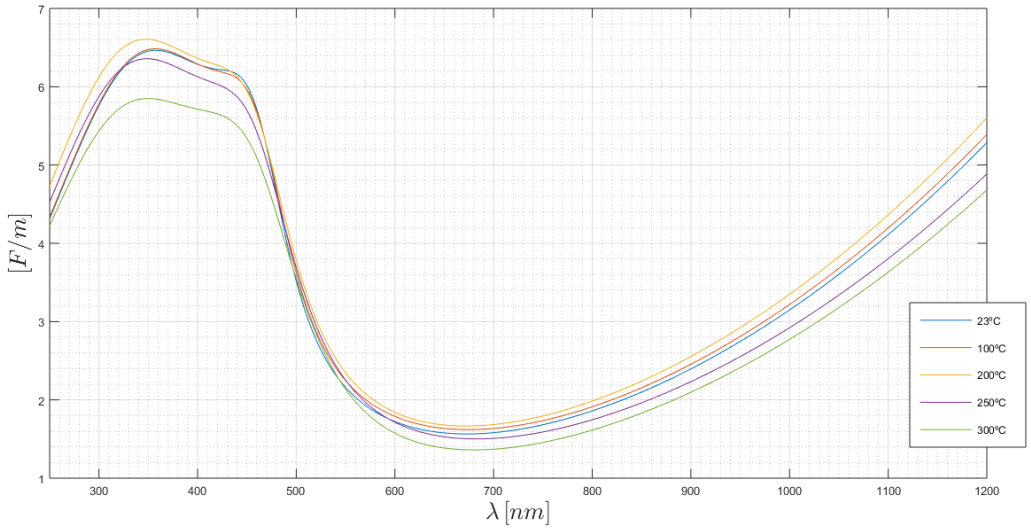

Figure A.5: Reddy fitting of the gold imaginary part of complex dielectric function with temperature dependency.

On figure A.6 is presented the copper complex dielectric function, which is also modelled by a Rakic Drude-Lorentz fitting, [48]. This complex function is very similar to the gold one and, consequently, both

optical responses will be identical.

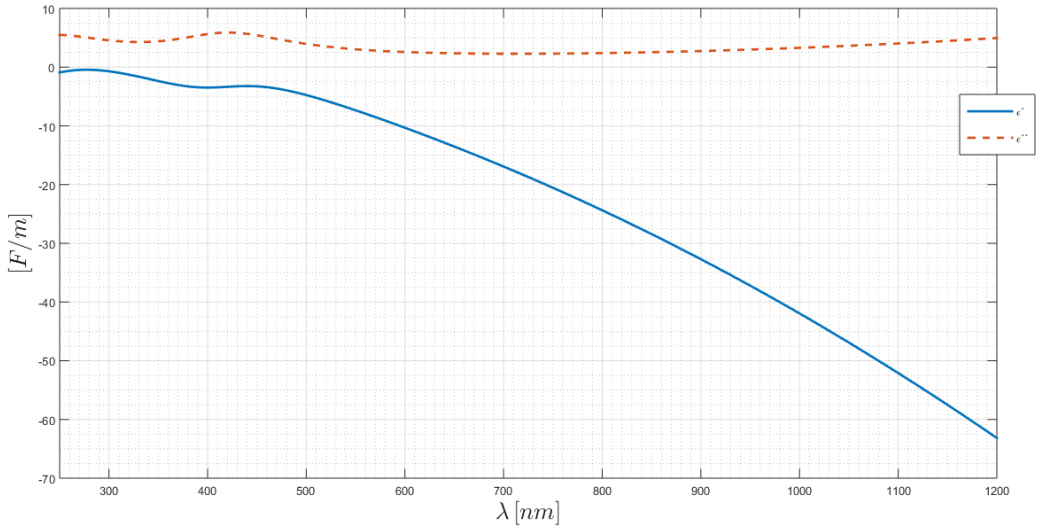

Figure A.6: Copper complex dielectric function from Rakic's Drude-Lorentz fitting.

A completely different complex dieletric function is the aluminium one, that is presented on figure A.7. It is also a Rakic's Drude-Lorentz fitting. Aluminium has a small imaginary part of the dielectric function until a wavelength around $500\mathrm{nm}$ and it has a maximum around $800\mathrm{nm}$. This maximum is responsible to high losses and, consequently, aluminium is not a good choice to red or near-infrared applications.

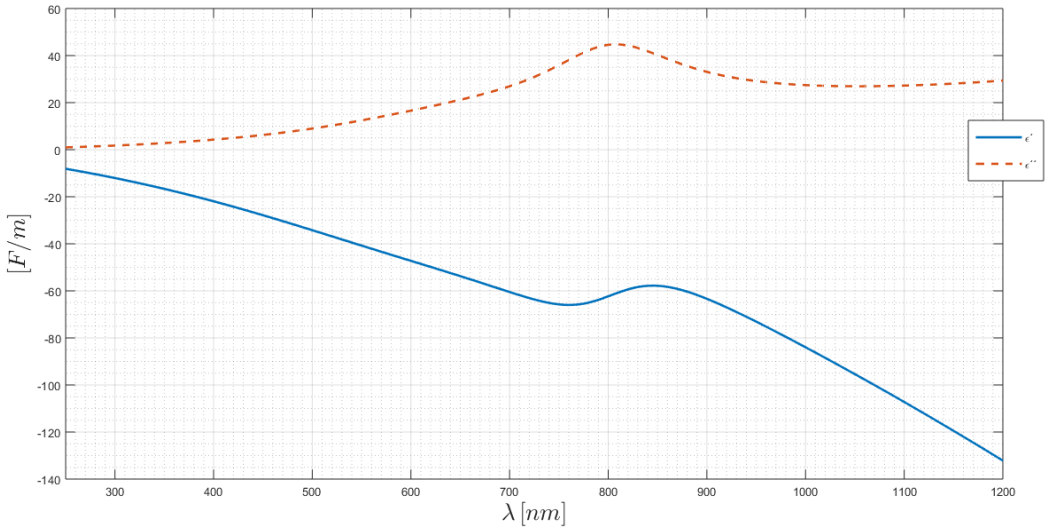

Figure A.7: Aluminium complex dielectric function from Rakic's Drude-Lorentz fitting.

A.3 Solid Substrate

The chosen solid substrate is quartz, whose complex dielectric function is presented on figure A.8 according to the complex refractive index reported by Gao [48]. It is possible to verify that its imaginary part is null and that the interband region does not appear along this wavelength range.

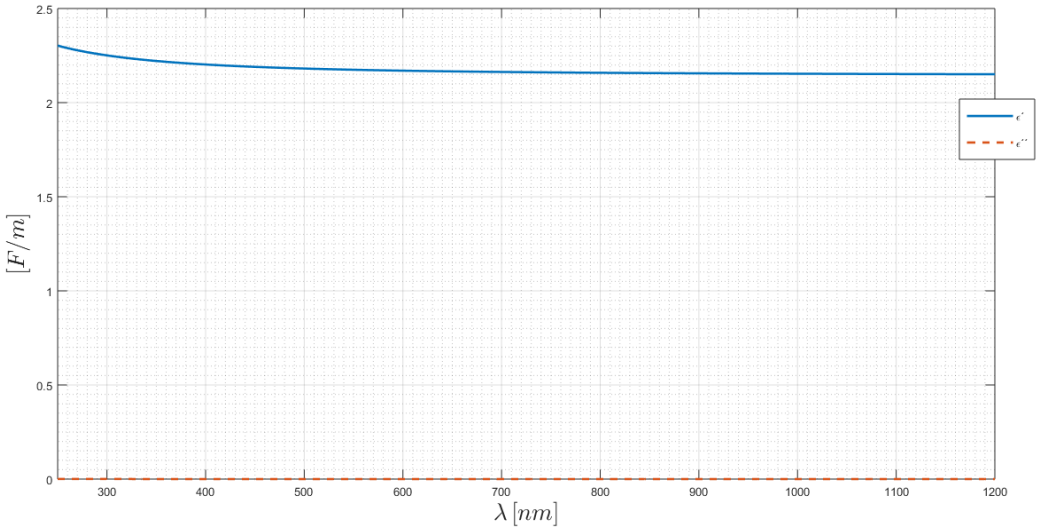

Figure A.8: Gao fitting of the quartz complex dielectric function.

A.4 Tissues

In order to test the tissue detection sensor, it is necessary the optical models for each tissue. On figure A.9 is presented the complex dielectric function of liver tissues, whereas on figures A.10, A.11 and A.12 are respectively presented the colon functions for the mucosa, submucosa and serosa tissues.

The imaginary part of the dielectric function of this tissues is almost zero along all the range and it is possible to analyse that colon tissues have similar functions. However, they are not the same and it is possible to differentiate them. In addition, the liver tissues present quite distinct values when comparing with any of the colon tissues.

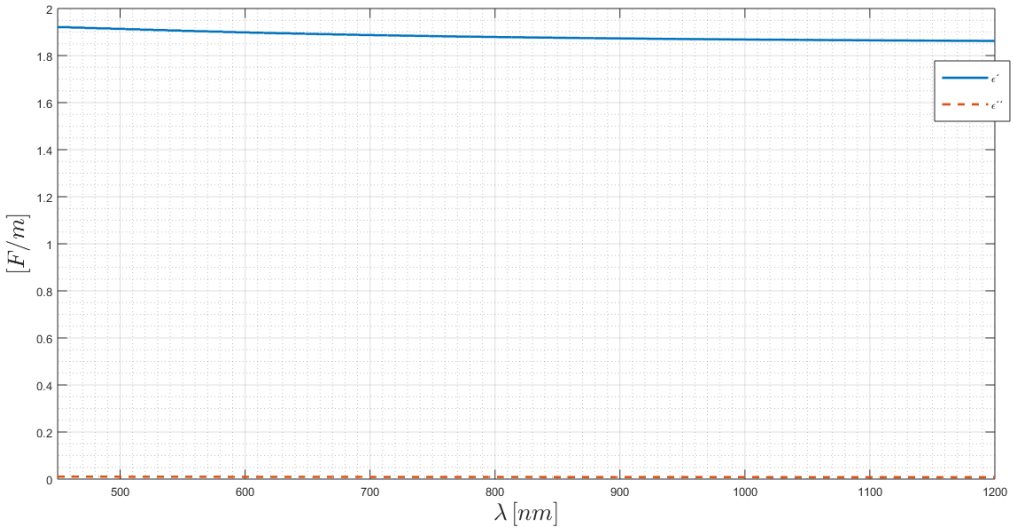

Figure A.9: Liver complex dielectric function.

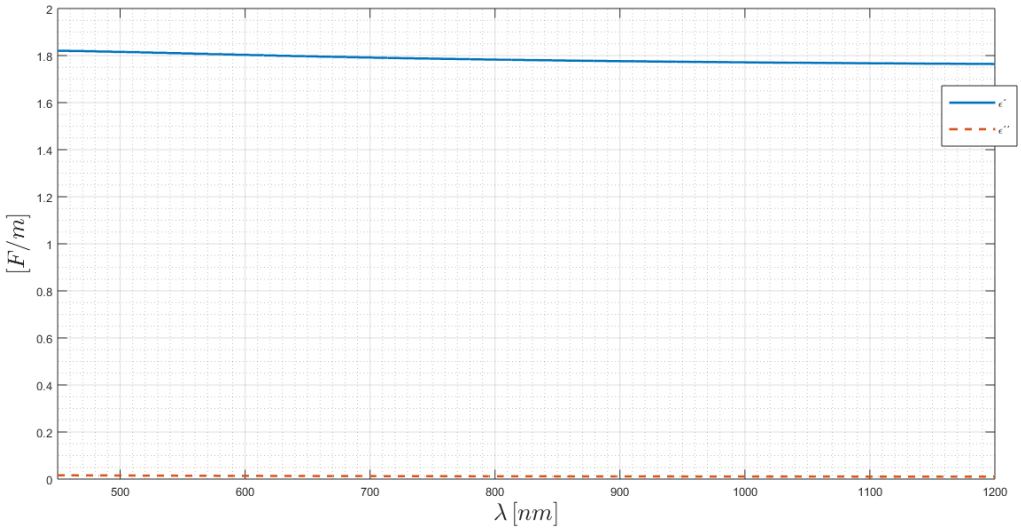

Figure A.10: Colon mucosa complex dielectric function.

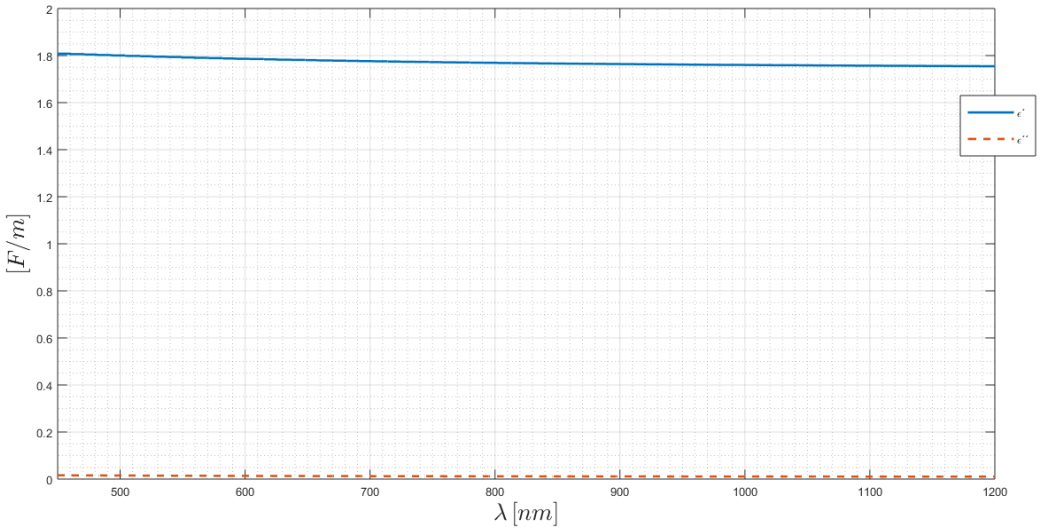

Figure A.11: Colon submucosa complex dielectric function.

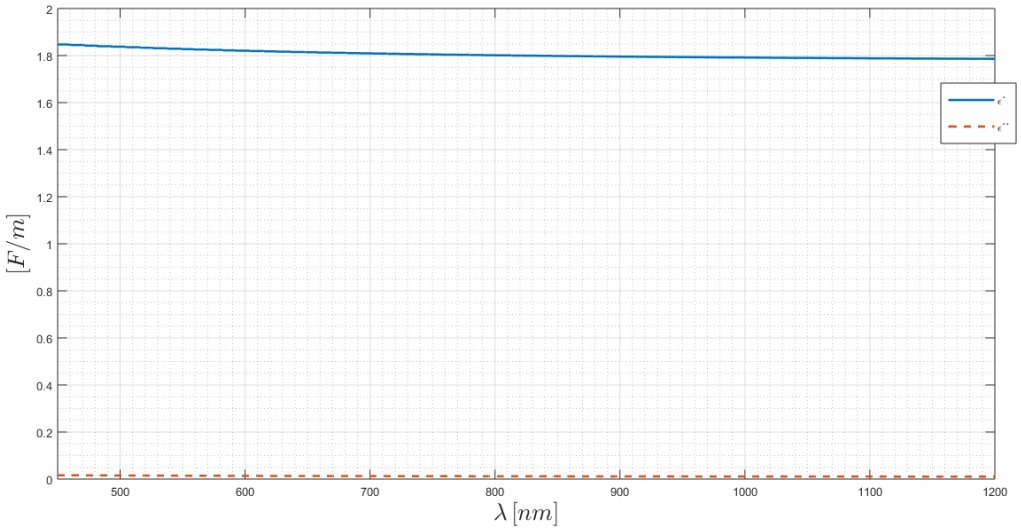

Figure A.12: Colon serosa complex dielectric function.